Geochemical Applications of Stable Rhenium and Mercury Isotopes

by

Daniel Louis Sullivan

A Dissertation Presented in Partial Fulfillment
of the Requirements for the Degree
Doctor of Philosophy

Approved July 2023 by the
Graduate Supervisory Committee:

Ariel Anbar, Chair
Gwyneth Gordon
Hilairy Hartnett
Richard Hervig
Wang Zheng

ARIZONA STATE UNIVERSITY

December 2023

ABSTRACT

Studying natural variations in the isotopic composition of oxygen-sensitive elements in ancient marine sediments is a powerful way to study the geochemical evolution of Earth's environments in the past. My dissertation focused on two broad aspects of isotope geochemistry: 1) the development of rhenium (Re) isotopes as a paleoredox and nuclear forensics tool, and 2) the application of mercury (Hg) isotopes as a tool to trace Hg mobility in the environment and what this movement means for isotopic changes in sedimentary rocks used to study Earth's past.

Chapter 2 is the first examination of Re isotopes in sedimentary rocks that formed ~2.5 billion years ago during a period of ocean and atmospheric oxygenation prior to the Great Oxidation Event. The data show variations in Re isotope ratios coincide with evidence for changes in oceanic and atmospheric oxygenation, supporting the use of Re isotopes as a tool to track paleoredox conditions throughout Earth's history.

Another application of rhenium isotopes is explored in the third chapter on nuclear forensics. Rhenium isotopes in uranium ore concentrates (UOC) from known production locations revealed more than double the range of isotope fractionation previously reported for any natural geologic samples so far. These first Re isotope ratio data indicate that Re is a promising new tool for provenance assessment of UOCs.

Chapter 4 focuses on geochemical applications of Hg isotopes. Mercury isotopes in shales are a geochemical tool that can be utilized to study the prevalence of global volcanism and detect oxygen-depleted conditions in the photic zone of ancient oceans. I measured Hg isotope ratio data from a Devonian shale bed in a road cut with varying degrees of weathering that has been well characterized for variations in elemental

concentrations and other isotopic ratios. I found significant variation in mass-dependent and mass-independent Hg isotope fractionation in weathered samples. Surprisingly, however, I observed both loss and gain of Hg, when only significant loss was expected based on prior weathering studies. These findings improve the understanding of Hg mobility in nature and indicate that mass-independent fractionation can be modified after deposition in surprising ways.

DEDICATION

For my father.

“Beneath the surface there are rocks, dirt, sediment, sand. That’s the planet’s memory, the picture of its history.”

-Frank Herbert, Children of Dune

“Shun no toil to make yourself remarkable by some talent or other; yet do not devote yourself to one branch exclusively. Strive to get clear notions about all. Give up no science entirely; for science is but one.”

-Seneca, Roman Stoic philosopher and statesman

“If you go into a project, it’s got to be a scientific problem that has rooms that continue into other rooms.”

-Harold Urey, Nobel Prize winner in chemistry, said to one of his graduate students

ACKNOWLEDGMENTS

This dissertation marks the end of a six-year quest where I have had the pleasure of meeting many wonderful people. Here, I thank some of those that have been with me along the way.

- My advisor: Ariel Anbar. Thank you for giving me the opportunity to pursue a Ph.D. and for all I have learned from you.
- The members of my committee – past and present: Gwyneth Gordon, Craig Hardgrove, Hilairy Hartnett, Richard Hervig, Cara Thompson, Wang Zheng. Thank you for your guidance and insistence on high standards and objectivity. The advice I have received has improved the quality of this dissertation.
- Mentors: Alan Brandon, Greg Brennecka, Steve Romaniello. Thank you for teaching me more in the lab in a few months than I could have learned alone in a few years. Your support in pushing forward projects, paper drafts, proposals, and ideas has been invaluable.
- Lab members: Aaron, Aleisha, Alyssa, Brandon, Catherine, Chad, Ethan, Feifei, Geoff, Julianne, Katy, Logan, Pilar, Sydney, Xinming, Yi. Thank you for the support, collaboration, and adventures throughout my time at ASU.
- Support Staff at ASU: Tyler Goepfert, Trevor Martin, Elizabeth McHugh, Jeffrey Schatzki. Thank you for your friendship and all the work you do on the back end.
- My family: Parents – Jill and Terry. Brothers - Derek and Pat. Thank you for your love, support, and counsel throughout this seemingly never-ending journey.
- Special thanks to Katy Rico: for consistently being there on short notice and providing invaluable feedback.
- Last but not least, my friends: Aisha, Alice, Jake, Julianne, Krishna, Lotfi, Lucia, Miles, Nael, Sean, Spencer, Tyler.

TABLE OF CONTENTS

Page

CHAPTER Page

CHAPTER Page

LIST OF TABLES

LIST OF FIGURES

CHAPTER 1

INTRODUCTION

1.1 Motivation to Study Earth History

Since the Earth formed ~4.5 billion years ago it has undergone many transformations. One of the transformations I have spent the most time studying is changes in the chemical composition of the ocean and atmosphere through time. This might sound dull to a layman, but it is critically important to answering questions about the habitability of Earth and the evolution of life. One of the most striking changes in Earth history is shifts in the amount of free O_2 in the ocean and atmosphere through time (Fig. 1.1).

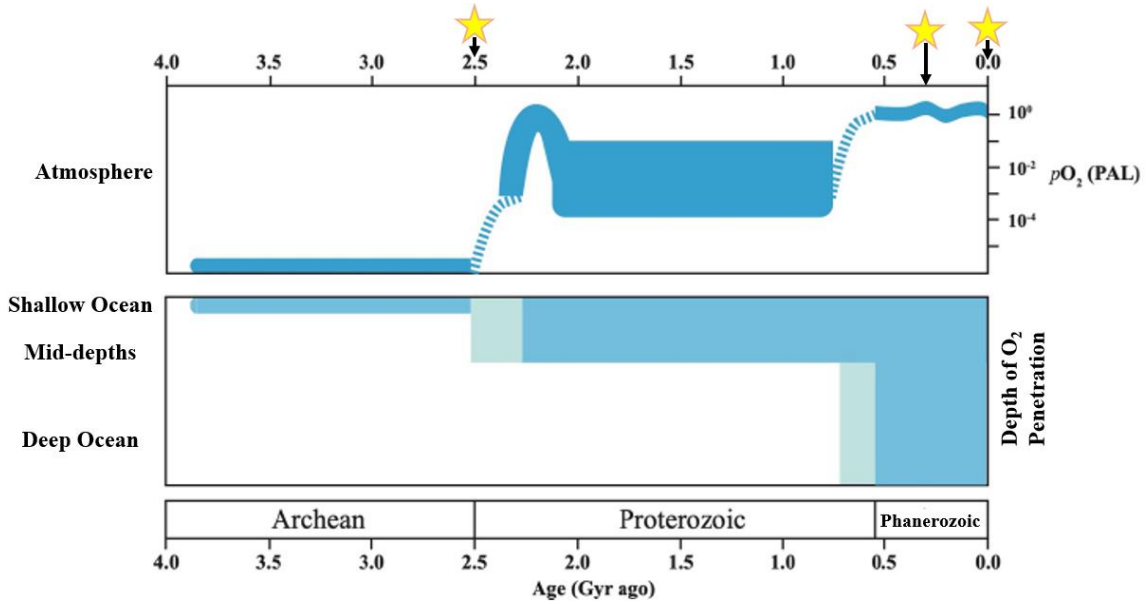

Fig. 1.1 General Oxygenation History of the Atmosphere and Ocean. Top panel: Amount of O_2 in the atmosphere through time on a logarithmic scale. The thickness of the curve indicates the likely range in O_2 at a given time. Dashed lines indicate a best guess at O_2 levels in the past. PAL = present atmospheric level. Yellow stars indicate time periods I have studied. Bottom panel: oxygenation of the shallow, mid-depth, and deep oceans through time. Light blue regions indicate possible first appearance. Modified from Ostrander (2020), who modified the top panel from Lyons et al. (2014) and bottom panel from Lowenstein et al. (2013).

In the Archean Eon 4.0 – 2.5 billion years ago (Ga), the Earth was much different than we know it today. There was an ocean, but there was no persistent free O_2 in the ocean and atmosphere (see Lyons et al., 2014 and references therein), nor were there plants or animals. There were subaerial land masses, but their size and distribution are unknown (Van Kranendonk, 2010). For humans, it was an uninhabitable world. However, there was life on Earth. How and when life initially arose is unknown and is an active area of research (e.g., Oró et al., 1990; Catling, 2013; Goldman and Kacar, 2021). Nevertheless, sometime in the Archean, microbes (likely in shallow ocean environments or lakes) become capable of oxygenic photosynthesis – the ability to use sunlight, CO_2, and H_2O to produce free O_2. This metabolism is common today, but in the Archean, it helped set the stage for the first permanent rise in atmospheric O_2 at ~2.45 – 2.2 Ga known as the Great Oxidation Event (GOE).

How do we know this? Much of what is known about ancient Earth history comes from geochemical data found in rocks that formed billions to millions of years ago. I focus on sedimentary rocks that formed in the ocean. In particular, rocks that are likely to record the chemical composition of redox (reduction-oxidation) sensitive metals (RSM) in seawater at the time of deposition. Studying RSMs can provide information about the oxygenation of the ocean and the sources of these elements to seawater. Geochemists use RSMs to study past environmental oxygenation because ancient oxygen levels cannot be measured directly: O_2 gas is not preserved in ancient sediments. RSMs, typically soluble under oxidizing conditions and less soluble under reducing conditions, are a ‘proxy’ to estimate the level of oxygenation of the ocean and atmosphere in the past.

Studying the isotope ratios of these RSMs provides much more nuanced and powerful data than abundance measurements alone. Natural processes introduce detectable isotopic fractionation that can be measured in geologic materials. Discussion of these ideas will begin from a high level to provide background on isotope ratio measurements for the general reader and will then transition into more detail as the elements studied in this dissertation are discussed.

1.2 What is Isotope Geochemistry?

Isotope geochemistry is a field of science that aims to understand processes in the Universe by detecting transformations – some long-gone billions of years ago – that the physical world has gone through. To do this, the relative abundance of isotopes of elements are analyzed using mass spectrometry.

The field of isotope geochemistry is less than a century old (Urey 1947) but has grown rapidly as new applications have been developed, as the capabilities of mass spectrometers have improved with each iteration (somewhat paralleling improvements in computers), and as analysis of new elements has been unlocked. Innovation in isotope geochemistry methods creates new applications to study the universe around us (e.g., Hoefs, 1997; Eiler et al., 2014).

My dissertation focuses on two new applications for isotope geochemistry based on rhenium (Re) and mercury (Hg). A brief overview of the geochemistry of Re and Hg is provided in the following sections that provides useful context for understanding the data chapters to come**.**

1.2.1 Rhenium Geochemistry

The motivation to study Re isotope ratios comes from its potential to provide unique information about suboxic (≤10 μM O_2) redox conditions in the past. Detecting suboxic conditions is important because some aerobic organisms can live in extremely low-O_2 waters (down to ~10 nM O_2; Stolper et al. 2010). It is of great interest to know when the ocean first crossed from anoxic (no free O_2) to suboxic.

Rhenium is one of the least abundant naturally occurring elements at Earth's surface with a typical concentration in the upper continental crust of ~200 pg/g (Rudnick and Gao, 2003). It was the last stable element to be discovered (Noddack et al., 1925); the rarity of Re-specific minerals made it difficult to isolate enough Re to measure. Rhenium has two isotopes, ^{185}Re and ^{187}Re, that have average relative natural abundances of 37.4% and 62.6%, respectively. The isotope ^{185}Re is stable, whereas ^{187}Re is radioactive with a half-life of approximately 41.6 billion years (Smoliar et al., 1996; Fig. 1.2). The half-life of ^{187}Re is long enough to be treated as stable in geochemical tracer applications.

The first Re isotope study of geologic samples was published by Miller et al. (2015), just eight years ago. Since then, there have been four additional publications examining the isotopic composition of seawater (Dellinger et al., 2020; Dickson et al., 2020), of low Re abundance reference materials (Dellinger et al., 2020), of river and bed load sediments (Dellinger et al., 2021), and of Fe-meteorites (Liu et al., 2017). The Re isotope variability found in these five publications spans 1.06 ‰ (-0.97 to 0.09 ‰ based on the NIST 3143 standard as δ=0).

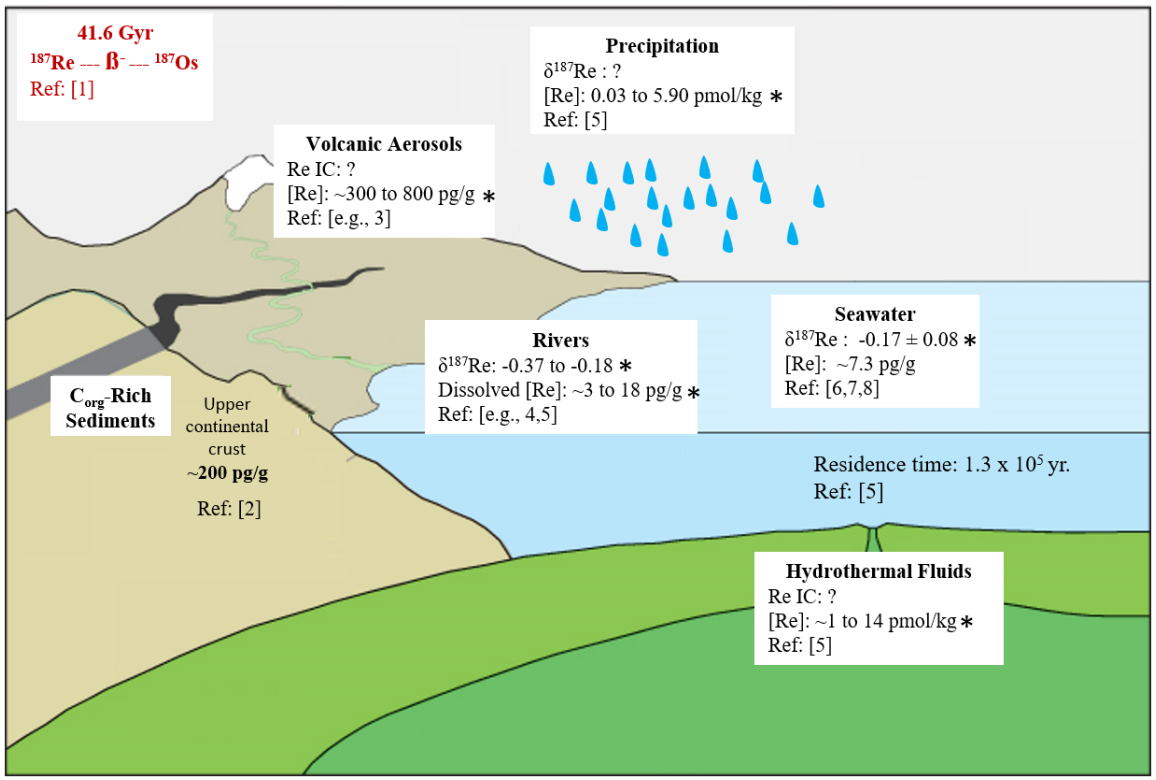

Figure 1.2 Current State of Knowledge of the Re Isotope System. Rhenium concentration ([Re]) and Re isotope ratio data ($\delta^{187}Re_{NIST\ 3143}$ (‰)) for Re reservoirs and environmental fluxes of Re to the ocean. Ocean residence time indicates pre-anthropogenic value. References: [1] Smoliar et al. (1996) Science, 271, 1099-1102. [2] Rudnick and Gao (2014) Treatise on Geochemistry, 3, 1−64. [3] Lassiter (2003). Earth and Planetary Science Letters, 214, 311–325. [4] Dellinger et al. (2021) Earth and Planetary Science Letters, 573, 117131. [5] Miller et al. (2011) Geochimica et Cosmochimica Acta, 75, 7146–7179. [6] Anbar et al. (1992) Geochimica et Cosmochimica Acta, 56, 4099–4103. [7] Dickson et al. (2020) Geochimica et Cosmochimica Acta, 287, 221–228. [8] Dellinger et al. (2020) Journal of Analytical Atomic Spectrometry, 35, 377–387. * indicates more data from additional locations will likely extend the range for the given parameter. Figure modified from Peucker-Ehrenbrink and Ravizza (2000).

Exploration of Re isotope ratios has been limited for two primary reasons:

1. Rhenium has an extremely low abundance in most natural samples. Consequently, it can be difficult to obtain enough material for a sufficiently precise Re isotope

measurement. With improvements in the detection capabilities of modern mass spectrometers, precise measurement of low abundance Re samples for isotopic measurements can now be achieved.

2. Rhenium only has two isotopes, making "double spiking"—a technique widely used to correct for mass-dependent fractionation during sample purification—impossible because it requires a minimum of four stable or long half-life radioactive isotopes. Without "double spiking", an "element spike" must be used to correct for instrumental mass bias (e.g., Peel et al., 2008). As such, the recovery of Re through the sample processing steps must be > ~75% to avoid isotopic fractionation (Miller et al., 2015; Dellinger et al., 2020).

The ability of Re isotopes to track suboxic conditions comes from Re's geochemical behavior (Fig 1.3). Under oxic conditions, Re exists primarily as the perrhenate ($Re^{VII}O_4^-$) anion that is highly unreactive and therefore accumulates int seawater (e.g., Koide et al., 1986; Colodner et al., 1993). Under low-O_2 conditions, Re^{VII} is reduced to Re^{IV} (potentially as ReO_2 or ReS_2 (e.g., Yamashita et al., 2007)), which becomes particle-reactive and can be efficiently removed from seawater, likely coupled to organic carbon or sulfide, typically at or below the sediment/water interface (Colodner et al., 1993; Kendall et al., 2010; Morford et al., 2012). However, Re geochemical behavior is not completely understood. For example, the mechanism(s) for Re reduction from Re^{VII} to Re^{IV} is unknown (Miller et al., 2015). Future work examining how Re is reduced and captured into sediments will improve our understanding of the utility of Re as a geochemical tool.

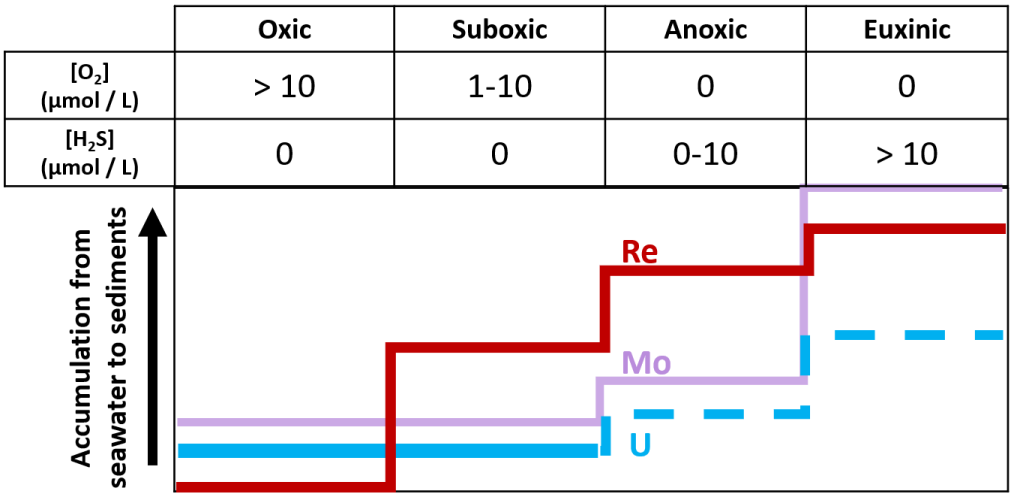

Figure 1.3 Redox Properties of Re Compared to the Common Redox Proxies Mo and U. The figure shows distribution coefficients (i.e., how efficiently elemental removal occurs from seawater into sediments) of redox sensitive metals into sediments under different redox conditions. Figure highlights the unreactive behavior of Re in oxic waters and its high reactivity under suboxic to euxinic conditions.

In this dissertation I examine the first paleoredox application of Re isotopes in an ancient sedimentary sequence that formed during a time of changing ocean and atmospheric oxygenation (Chapter 2). This is the first examination of Re isotopes in an ancient sedimentary sequence deposited during a time of changing environmental redox conditions. I then examine the first application of Re isotopes as a nuclear forensics tool (Chapter 3) to see if Re isotope ratios can be helpful in forensic investigations that aim to assess the provenance of nuclear materials found outside regulatory control.

1.2.2 Mercury Geochemistry

Mercury is a powerful geochemical tool with unique properties and sensitivities to photochemical reactions. Mercury is naturally occurring at the surface of the Earth and has seven stable isotopes (^{196}Hg, ^{198}Hg, ^{199}Hg, ^{200}Hg, ^{201}Hg, ^{202}Hg, and ^{204}Hg). The primary natural sources of Hg are volcanism and hydrothermal systems that deliver Hg to

surface environments (e.g., Nriagu and Becker, 2003; Selin, 2009). Mercury in the atmosphere can be oxidized and can be found in plants, soil, sediments, and seawater (Fig. 1.4). Mercury can be returned to the atmosphere as Hg(0) through biotic and abiotic chemical species transformations (Blum et al., 2014).

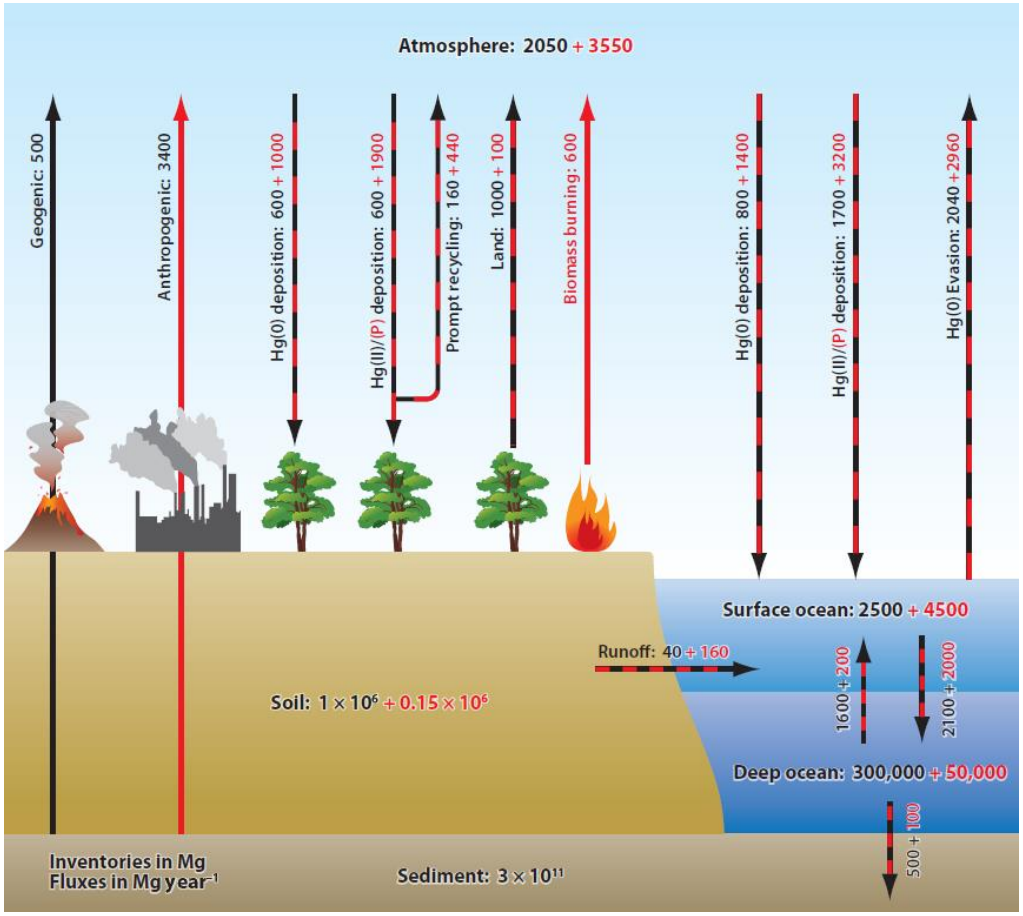

Figure 1.4 Mercury Global Cycling. Natural (black) and anthropogenic (red) fluxes and inventories for Hg. Red and black lines indicate natural sources combined with terrestrial emissions. Fluxes in megagram (Mg)/year and inventories are in Mg. Figure from Selin (2009). References used to create the figure: Mason et al. (1994), Lamborg et al. (2002), Mason and Sheu, (2002), Sunderland and Mason, (2007), Selin et al. (2008). A pre-Phanerozoic Hg cycle can be envisioned by removing plants and anthropogenic emissions from the figure.

The isotopes of Hg can undergo mass-dependent fractionation (MDF) and mass-independent fractionation (MIF). Mass-dependent fractionation can be caused by biotic

and abiotic mechanisms and can be utilized to understand the processes that influence Hg distribution and bioaccumulation in natural systems. Mass-dependent fractionation occurs during redox transformations, adsorption reactions, volatilization, and biologic cycling (Blum et al., 2014). Mass-independent fractionation occurs from a broadly different set of controls from MDF, mainly photochemical reactions in the photic zone of a body of water and in the atmosphere (e.g., Blum et al., 2014; Zheng et al., 2018). MIF is an unusual type of isotopic fractionation that is not present in many elements. For Hg, MIF is caused by nuclear volume (e.g., Schauble, 2007) and magnetic isotope effects (e.g., Motta et al., 2020), but the exact causes of Hg MIF are still under study. Examining MIF and MDF of Hg in geologic materials provides information from two decoupled isotope fractionation pathways in one element, allowing interpretations that are more specific than systems with only MDF or MIF.

Studies of Hg isotope ratios in ancient sediments have helped trace events throughout Earth history such as volcanism (e.g., Thibodeau et al. 2016; Meixnerová et al., 2021) and photic zone euxinia (PZE) – a condition where anoxic and sulfidic waters occur in the photic zone (Zheng et al., 2018; Sun et al., 2023; Wu et al., 2023). However, to date no studies have examined Hg behavior during oxidative weathering of black shales, which are commonly examined in paleoenvironmental Hg studies to trace these processes. If chemical weathering of shales compromises the fidelity of the Hg isotope records they contain, interpretations of Earth's past may be inaccurate.

In Chapter 4, I examined Hg abundances and isotope ratios in a black shale bed that ranges from heavily weathered to well-preserved. This is done to examine the behavior of Hg during weathering to examine the chemical impact of weathering on Hg

abundance and isotope ratios in the sediments. This is the first investigation of Hg isotopes in black shales during alteration by infiltration of fluids and oxidative weathering. I found significant isotopic fraction related to weathering which can lead to erroneous conclusions in ancient Earth studies if weathering processes are not detected.

1.2.3 How Re and Hg Geochemical Data are Complementary

Rhenium and Hg are both redox sensitive elements that can be emitted as volatiles from volcanic emissions (e.g., Korzhinsky et al., 1994 ; Zambardi et al., 2009), and both are known to be removed from the ocean into organic material or sulfides under reducing conditions; which often forms organic rich shales known as black shales. Therefore, both elements can be measured in black shales to investigate paleoenvironmental conditions throughout Earth history related to paleoredox changes and volcanism.

Black shales deposited in the ocean during periods of large-scale volcanism – known as large igneous province (LIP) events – can record Re and Hg geochemical signatures from the volcanic material that can be measured and used as proxies for LIP activity. However, Hg and Re are sensitive to a different set of geochemical processes, so the paired application of both isotope proxies can provide more information than measuring either proxy alone. For example, Hg is influenced by evaporation, photochemical reactions, and adsorption to iron-manganese oxides that can all introduce isotopic fractionation, whereas Re is not sensitive to these processes. Therefore, the combined signal of volcanism from both Re and Hg isotope and abundance data in a black shale can provide a more robust indicator of volcanic activity.

Furthermore, as noted in section 1.2.1, studies of Re isotope ratios of sediments that record the isotopic composition of seawater have the potential to track suboxic conditions in the past. The extent of suboxic sedimentation in an ancient ocean would likely be altered during times when PZE occurred – a change in ocean chemistry that alters Hg MDF and MIF (Zheng et al., 2018; Sun et al., 2023; Wu et al., 2023). The occurrence of PZE would likely reduce the extent of suboxic zones in the ocean, reducing the amount of Re being removed to suboxic sediments. If there is Re isotopic fractionation related to removal to sediments under suboxic conditions, changing the extent of suboxic sedimentation would alter the Re isotopic composition of seawater. Therefore, covariation of Re and Hg isotopes in a sample deposited during times of PZE could support that their respective variations are due to redox changes. Thus, pairing the two isotope systems is beneficial for the application of both proxies.

References

Anbar, A.D., Creaser, R.A., Papanastassiou, D.A., Wasserburg, G.J. (1992) Rhenium in seawater: Confirmation of generally conservative behavior. Geochimica et Cosmochimica Acta, 56, 4099–4103.

Blum, J.D., Sherman, L.S., Johnson, M.W. (2014) Mercury Isotopes in Earth and Environmental Sciences. Annual Review of Earth and Planetary Sciences, 42, 249–269.

Catling, D.C. (2013) Astrobiology: A Very Short Introduction. Oxford University Press, l, 1–161.

Colodner, D., Sachs, J., Ravizza, G., Turekian, K., Edmond, J., Boyle, E. (1993) The geochemical cycle of rhenium: a reconnaissance. Earth and Planetary Science letters, 117, 205–221.

Dellinger, M., Hilton, R.G., Nowell, G.M. (2020) Measurements of rhenium isotopic composition in low-abundance samples. Journal of Analytical Atomic Spectrometry, 35, 377–387.

Dellinger, M., Hilton, R.G., Nowell, G.M. (2021) Fractionation of rhenium isotopes in the Mackenzie River basin during oxidative weathering. Earth and Planetary Science Letters, 573, 117131.

Dickson, A.J., Hsieh, Y., Bryan, A. (2020) The rhenium isotope composition of Atlantic Ocean seawater. Geochimica et Cosmochimica Acta, 287, 221–228.

Eiler, J.M., Bergquist, B., Bourg, I., Cartigny, P., Farquhar, J., Gagnon, A., Guo, W., Halevy, I., Hofmann, A., Larson, T.E., Levin, N., Schauble, E.A., Stolper, D. (2014) Frontiers of stable isotope geoscience. Chemical Geology, 372, 119–143.

Goldman, A.D. and Kacar, B. (2021) Cofactors are Remnants of Life's Origin and Early Evolution. Journal of Molecular Evolution, 89, 127–133.

Hoefs, J. (1997) Stable isotope geochemistry. Book (4th edition). Berlin: Springer Verlag.

Kendall, B., Reinhard, C.T., Lyons, T.W., Kaufman, A.J., Poulton, S.W., Anbar, A.D. (2010) Pervasive oxygenation along late Archaean ocean margins. Nature Geoscience, 3, 647–652.

Koide, M., Hodge, V.F., Yang, J.S., Stallard, M., Goldberg, E.G., Calhoun, J., Bertine, K.K. (1986) Some comparative marine chemistries of rhenium, gold, silver and molybdenum. Applied Geochemistry, 1, 705–714.

Korzhinsky, M.A., Tkachenko, S.I., Shmulovich, K.I., Taran, Y.A., Steinberg, G.S. (1994) Discovery of a pure rhenium mineral at Kudriavy volcano. Nature, 369, 51–52.

Lamborg, C.H., Fitzgerald, W.F., Damman, A.W.H., Benoit, J.M., Balcom, P.H., Engstrom D.R. (2002) Modern and historic atmospheric mercury fluxes in both hemispheres: Global and regional mercury cycling implications: Modern and historic fluxes of atmospheric mercury. Global Biogeochemical Cycles, 16, 51-1–51–11.

Lyons, T.W., Reinhard, C.T., Planavsky, N.J. (2014) The rise of oxygen in Earth's early ocean and atmosphere. Nature, 506, 307–315.

Lowenstein, T.K., Kendall, B., Anbar, A.D. (2013) The geologic history of seawater. In Treatise on Geochemistry: Second Edition, 8, 569–622.

Mason, R.P., Fitzgerald, W.F., Morel, F.M.M. (1994) The biogeochemical cycling of elemental mercury: Anthropogenic influences. Geochimica et Cosmochimica Acta, 58, 3191–3198.

Mason, R.P. and Sheu, G.-R. (2002) Role of the ocean in the global mercury cycle. Global Biogeochemical Cycles, 16, 1–14.

Meixnerová, J., Blum, J.D., Johnson, M.W., Stüeken, E.E., Kipp, M.A., Anbar, A.D., and Buick, R. (2021) Mercury abundance and isotopic composition indicate subaerial volcanism prior to the end-Archean "whiff" of oxygen. Proceedings of the National Academy of Sciences, 118, 1–6.

Miller, C.A., Peucker-Ehrenbrink, B., Schauble, E.A. (2015) Theoretical modeling of rhenium isotope fractionation, natural variations across a black shale weathering profile, and potential as a paleoredox proxy. Earth and Planetary Science letters, 430, 339–348.

Miller, C.A., Peucker-Ehrenbrink, B., Walker, B.D., Marcantonio, F. (2011) Re-assessing the surface cycling of molybdenum and rhenium. Geochimica et Cosmochimica Acta, 75, 7146–7179.

Morford, J.L., Martin, W.R., Carney, C.M. (2012) Rhenium geochemical cycling: Insights from continental margins. Chemical Geology, 325, 73–86.

Motta, L.C., Chien, A.D., Rask, A.E., Zimmerman, P.M. (2020) Mercury Magnetic Isotope Effect: A Plausible Photochemical Mechanism. Journal of Physical Chemistry A, 124, 3711–3719.

Noddack, W., Tacke, I., Berg, O. (1925) Zwei neue Elemente der Mangangruppe. Sitzung der physikalisch-mathematischen Klasse, 11, 400–409.

Nriagu, J. and Becker, C. (2003) Volcanic emissions of mercury to the atmosphere: Global and regional inventories. Science of the Total Environment, 304, 3–12.

Oró., J., Miller, S.L., Lazcano, A. (1990) The origin and early evolution of life on earth. Annual Review of Earth and Planetary Science, 18, 317–356.

Ostrander, C.M. (2020) Refining Earth's Ocean Oxygenation History using Molybdenum and Thallium Isotopes. Dissertation. Arizona State University. 1–275.

Peucker-Ehrenbrink, B. and Ravizza, G. (2000) The marine osmium isotope record. Terra Nova, 12, 205−219.

Rudnick, R.L. and Gao, S. (2003) Composition of the Continental Crust. Treatise on Geochemistry, 3, 1−64.

Schauble, E.A. (2007) Role of nuclear volume in driving equilibrium stable isotope fractionation of mercury, thallium, and other very heavy elements. Geochimica et Cosmochimica Acta, 71, 2170–2189.

Selin, N.E. (2009) Global Biogeochemical Cycling of Mercury: A Review. Annual Review of Environmental and Resources, 34, 43–63.

Selin, N.E., Jacob, D.J., Yantosca, R.M., Strode, S., Jaeglé, L., Sunderland, E.M. (2008) Global 3-D land-ocean-atmosphere model for mercury: Present-day versus preindustrial cycles and anthropogenic enrichment factors for deposition. Global Biogeochemical Cycles, 22, 1–13.

Smoliar, M.I., Walker, R.J., Morgan, J.W. (1996) Re-Os Ages of Group IIA, IIIA, IVA, and IVB Iron Meteorites. Science, 271, 1099–1102.

Stolper, D.A., Revsbech, N.,P., Canfield, D.E. (2010) Aerobic growth at nanomolar oxygen concentrations. Proceedings of the National Academy of Science, 107, 18755–18760.

Sun, R., Liu, Y., Sonke, J.E., Feifei, Z., Zhao, Y., Zhang, Y., Chen, J., Liu, C.-Q., Shen, S., Anbar, A.D., Zheng, W. (2023) Mercury isotope evidence for marine photic zone euxinia across the end-Permian mass extinction. Communications Earth and Environment, 4, 1–11.

Sunderland, E.M. and Mason, R.P. (2007) Human impacts on open ocean mercury concentrations. Global Biogeochemical Cycles, 21, 1–15.

Thibodeau, A. T., Ritterbush, K., Yager, J. A., West, A. J., Ibarra, Y., Bottjer, D. J., Berelson, W. M., Bergquist, B. A., and Corsetti, F. A. (2016) Mercury anomalies and the timing of biotic recovery following the end-Triassic mass extinction. Nature Comm., *7*, 1−8.

Van Kranendonk, M.J. (2010) Two types of Archean continental crust: Plume and plate tectonics on early Earth. American Journal of Science, 310, 1187–1209.

Wu, Y., Tian, H., Yin, R., Chen, D., Grasby, S. E., Shen, J., Li, T., Ji, S., Peng, P. (2023) Highly fractionated Hg isotope evidence for dynamic euxinia in shallow waters of the Mesoproterozoic ocean. Earth and Planetary Science Letters, 616, 118211.

Zambardi, T., Sonke, J. E., Toutain, J. P., Sortino, F., Shinohara, H. (2009) Mercury emissions and stable isotopic compositions at Vulcano Island (Italy). Earth and Planetary Science Letters, 277 (1–2), 236–243.

Zheng, W., Gilleaudeau, G. J., Kah, L.C., Anbar, A. D. (2018) Mercury isotope signatures record photic zone euxinia in the Mesoproterozoic ocean. Proceedings of the National Academy of Sciences, 115, 10594−10599.

CHAPTER 2

RHENIUM ISOTOPE INVESTIGATION OF ORGANIC-RICH SEDIMENTS FROM PRIOR TO THE GREAT OXIDATION EVENT IN THE MT. MCRAE SHALE

2.1 Abstract

In the Archean eon, the Great Oxidation Event (GOE; ~2.45 – 2.2 Ga) marked a rise in atmospheric O_2 that radically altered the chemistry and habitability of surficial environments. Prior to the GOE, geochemical evidence from sedimentary rocks suggests there were short-term accumulations of O_2 in the atmosphere (aka a 'whiff' of O_2; Anbar et al., 2007) and in the oceans along continental margins (e.g., Anbar et al., 2007; Kendall et al., 2015; Ostrander et al., 2019; Johnson et al., 2019). However, this is still an active field of research with much uncertainty surrounding the extent and timing of oxygenation. Recently, Slotznick et al. (2022) challenged the idea of a 'whiff' of O_2 before the GOE. In particular, Slotznick et al. (2022) contend that enrichments of the redox sensitive metal rhenium (Re) in the Mt. McRae Shale, viewed as evidence of oxidative weathering by Anbar et al. (2007), were instead derived from volcanic emissions of volatile Re. In this study, I present the first examination of Re isotope ratios in the ~2.5 Ga Mount McRae Shale to test the volcanic source idea. To do this, I compare new Re isotope ratio data to recently published Hg abundance and isotope ratio data in the Mt. McRae Shale. Mercury is emitted from volcanic material as a volatile and Hg enrichments and paired isotope ratio data are commonly used to determine if a LIP eruption occurred in a subaerial or submarine environment in Earth's past. Mercury data from the lower section of the Mt. McRae (deposited before the contested 'whiff' interval)

has shown evidence for subaerial volcanism, detected by positive odd-mass-independent fraction (MIF). Positive MIF indicates photooxidation of Hg in the atmosphere interpreted as evidence of subaerial volcanism. By pairing Re and Hg geochemical data from the lower section where subaerial volcanism was detected, I obtain expected geochemical signatures for subaerial volcanism which was compared to the upper section that contains the contested 'whiff' interval. In the lower section, Hg isotopes have consistently positive MIF values. Rhenium enrichments are low with minimal variation, and the Re isotopic composition of a sample deposited under anoxic and sulfidic (aka euxinic) conditions has a heavy isotopic composition. In contrast, in the upper section containing the 'whiff' interval that was deposited under euxinic conditions, there is no Hg MIF, Re abundances increase significantly relative to the lower section, and Re isotope ratios shift to lighter values as Re abundances increase at the beginning of the 'whiff' interval. Therefore, the Re and Hg geochemical signatures in the upper section are inconsistent with subaerial volcanism. The Re isotope ratio variations occur coincident with other proxies that have been interpreted to indicate changes in environmental oxygenation (e.g., Mo, Tl, Se, Os, U). These new Re isotope ratio data are most parsimoniously explained by changes in environmental oxygenation rather than volcanic activity.

2.2 Introduction

The Great Oxidation Event (GOE) at ~2.45 to 2.2 billion years ago (Ga) marks the transition to the sustained presence of atmospheric O_2 being > 0.1% of the atmosphere (Lyons et al., 2014; Luo et al., 2016; Gumsley et al., 2017; Philipot et al., 2018). This

important event had major consequences for the early evolution and expansion of aerobic life. Prior to this event, the Earth was dominantly not habitable for aerobes. Before the GOE, multiple lines of evidence suggest trace amounts of free O_2 were present in shallow waters along continental margins (e.g., Kendall et al., 2010; Ostrander et al., 2019) and in the atmosphere (e.g., Anbar et al., 2007; Johnson et al., 2019) for short periods of time known as the 'whiff' hypothesis. However, there is still much uncertainty surrounding how interactions between the coevolving geosphere, biosphere, and atmosphere of ancient Earth led to the GOE.

Much of what is known about ancient Earth history comes from geochemical data found in rocks deposited billions to millions of years ago. Interpretation of geochemical from ancient sediments requires a sophisticated examination of how well preserved the elements are since deposition. There are many post-depositional influences that can alter the original geochemical signatures of a rock, leading to erroneous conclusions. For example, the introduction of fluids through cracks or pore spaces (e.g., Miller et al., 2015), and heating under pressure can create changes in the original chemical signatures of a rock (e.g., Liu et al., 2022). Some of these processes are easily identified visually by changes in coloration or inclusion of secondary minerals. However, other alteration processes are more difficult to determine visually (e.g., initial fluid alteration) and require laboratory examination to detect.

Recently, Slotznick et al. (2002) suggested the geochemical data recorded in the 2.5 Ga Mt. McRae shale has been influenced by volcanic and postdepositional processes and, therefore, do not represent the original chemical composition of the sediments at the time of deposition (Slotznick et al., 2022). Prior to Slotznick et al. (2022), many

researcher groups had analyzed multiple isotopes systems from this sequence (e.g., Anbar et al., 2007; Kaufman et al., 2007; Garvin et al., 2009; Duan et al., 2010; Kendall et al., 2015; Ostrander et al., 2019). These authors unanimously concluded that the geochemical signatures are well-preserved and reveal changes in environmental oxygenation conditions before the GOE. Slotznick et al. (2022) examined spatially resolved petrogenic data and concluded the chemical signatures were largely caused by alteration and influenced by volcanic activity. Slotznick et al. (2022) contend there was no oxygenation of the ocean and atmosphere at the time of deposition, and suggest two elements in particular, rhenium (Re) and molybdenum (Mo), are a result of volcanism and alteration. In this interpretation, Re is thought to be derived from volcanic outgassing, which will be referred to as the 'volcanogenic' hypothesis. However, this interpretation has been rebutted by Anbar et al. (2023).

Recently published Hg isotope ratio and abundance data from the lower member of the Mt. McRae (deposited before the contested 'whiff' interval) has provided evidence for continuous subaerial volcanism that is likely related to a large igneous province event (Meixnerová et al., 2021). Similar to Re, the element mercury (Hg) can be emitted as a volatile during volcanism. Subaerial volcanism was detected by continuous positive Hg odd-mass-independent fractionation (odd MIF, hereafter MIF) values in the lower section of the Mt. McRae, which are indicative of photooxidation of Hg in the atmosphere delivered from subaerial volcanic emissions. Volcanic emissions are the primary natural source of Hg to Earth's surface environment (Selin, 2009), and Hg enrichments in black shales are commonly used as a proxy for volcanic activity (e.g., Grasby et al., 2013;

Thibodeau et al., 2016; Charbonnier & Föllmi, 2017; Charbonnier et al., 2020; Park et al., 2022).

In this paper, I combine Re isotope ratio and abundance data to recently published Hg abundance and isotope ratio data (Meixnerová et al., 2021) from the lower and upper sections of the Mt. McRae Shale. The Re isotope ratio data was collected with a new method that was developed for purifying Re from black shale samples that have low Re abundances and require large sample sizes (~ 1 g). This work was done to determine if the geochemical signatures found in the upper shale are most parsimoniously explained by a subaerial volcanic signature or by changes in environmental oxygenation.

2.3 Samples and Methods

2.3.1 Sample Background

I analyzed sedimentary rocks from the Mt. McRae Shale in Western Australia. This drill core, obtained as part of the Deep Time Drilling Project of the Astrobiology Drilling Program of the NASA Astrobiology Institute, has been extensively studied (e.g., Anbar et al., 2007; Kaufman et al., 2007; Garvin et al., 2009; Duan et al., 2010; Kendall et al., 2015; Ostrander et al., 2019). The lithology present in the analyzed sections is primarily black laminated shales with banded iron formations (BIF) present in the lower sections, grey carbonate/marl couplets, and one breccia occurrence. The black shale and BIF sections are interpreted to have been deposited in deep water below the wave base and the carbonate facies deposited in comparatively shallow water (Krapež et al., 2003; Barley et al., 2005; Anbar et al., 2007). The rocks have experienced low-grade metamorphism and minimal deformation (Anbar et al., 2007).

The Mt. McRae Shale is commonly divided into “upper” and “lower” members. The upper member (125 – 155 m) was likely deposited under predominantly euxinic conditions (Reinhard et al., 2009), over a period of approximately 11 Myr (Anbar et al., 2007). The lower member (170 – 190 m) was deposited under predominantly anoxic/ferruginous conditions, with short periods of euxinic conditions throughout, spanning ~2-4 Myr (Trendall et al., 2004).

The upper member contains evidence for postdepositional processes that could alter the distributions of redox-sensitive metals, such as formation of secondary sulfide nodules and laminae. Therefore, during sampling of the core for geochemical analyses, careful attention was paid to targeting the fine-grained carbonaceous matrix that hosts authigenic trace metals while excluding secondary sulfide nodules, veins, and other laminae which were influenced by alteration (Anbar et al., 2007).

2.3.2 Sample Preparation

2.3.2.1 Sample Digestion

Sample purification was carried out in a metal-free, class 100, clean room with a HEPA-filtered air supply and laminar flow benches. Trace metal grade acids were used throughout dissolution, sample preparation, and processing. All dilutions were made using high purity Milli-Q® water (18.2 MΩ x cm).

Samples were digested in glass Carius tubes (CT) using inverse aqua regia following procedures from Sullivan et al. (2020). Carius tubes were cleaned by being stood up in a large glass beaker, filled with 50% HNO_3, covered with a mirror glass, and heated on a hot plate at 140° C for ~24 hours. The 50% HNO_3 was drained and the CTs

were rinsed with Milli-Q®. Then, each CT was again stood up in a large glass beaker, filled with Milli-Q®, covered with a mirror glass, and heated on a hot plate at 140° C for ~24 hours. This step was repeated twice. Finally, the CTs were placed in an oven at 220° C for ~2 hours to remove any residual liquid and were ready for use.

Carius tubes were used for sample digestion to ensure quantitative removal of Re from the black shales, which I found difficult with beaker and hot plate digestions. Briefly, 0.21 to 0.72 g of previously powdered samples (see supplement from Anbar et al., 2007 for powdering details) were weighed and added to the CTs. The CTs were placed in a cold dry-ice/ethanol bath to inhibit reactions, and 9 ml nitric acid and 3 ml hydrochloric acid was added. The CTs were sealed using a hydrogen-oxygen torch and heated in an oven at 220° C for 48 hours. The CTs were removed from the oven, opened, and the supernatant decanted into Teflon beakers. The samples were then dried down and reconstituted in 5 ml of 0.5 M HCl.

To validate that Re is quantitatively transferred to solution with this digestion method, I tested the abundance of the USGS black shale standard SDO-1 with this digestion technique. The average Re abundance for SDO-1 with this method is 79 ± 3 ppb (2SD, n = 4) determined using isotope dilution (ID) and measured on a Thermo iCAP Q ICP-MS. Published Re abundances for SDO-1 = 77 ± 12 ppb (2SD, n = 16; Du Vivier et al., 2014, 2015), 76 ± 5 ppb (2SD, n = 6; Ishikawa et al., 2014), and 77 ± 1 (2SD, n = 6; Finlay et al., 2012). Thus, the Re abundance data agrees with published values.

In SDO-1, a published Re abundance determination of 93 ± 140 % ppb (n = 1) reported by Meisel and Moser (2004) is slightly outside the range of the measured

uncertainty. Meisel and Moser (2004) digested SDO-1 with a high pressure asher for 3 hours, after which they measured the Re abundance on an ICP-MS using isotope dilution. The small but significant difference between the abundance determined by Meisel and Moser (2004) and determinations in other studies may be due to incomplete sample/spike equilibration or incomplete sample digestion due to the short digestion time, as suggested by Finlay et al. (2012).

2.3.2.2 Purifying Re with Column Chromatography

Re purification was completed using a new column chromatography protocol using Biorad® AG 1-X8 (100-200 mesh) and 1 ml Eichrom® N,N,N'N' tetraoctyl-1,5-diglycolamide (TODGA; hereafter DGA) resin cartridges. A new method was developed to ensure sufficient removal of matrix elements from large sample sizes (~1 g) needed for low Re abundance samples while maintaining high recoveries of Re. Additionally, DGA resin is compatible with the Elemental Scientific® prepFAST automated inline dilution system that can automatically perform column chemistry procedures. Thus, development of a protocol utilizing DGA resin sets the foundation for the development of a fully automated Re purification procedure, though development of a prepFAST method was not part of this work.

Rhenium was loaded onto 1 ml Biorad AG 1-X8 100-200 mesh anion exchange resin in polypropylene chromatography columns (9 cm high and conical 0.8 cm x 4 cm). Prior to use, the resin was cleaned with successive rinses of 12 M HCl, 3M HNO_3, 10 M HNO_3, 100% ethanol, and Milli-Q®; the resin was washed with Milli-Q® between each

cleaning step to remove the previous reagent from the resin before addition of the next reagent.

Rhenium was purified following the protocol in table 2.1. After AG 1-X8 column chemistry, the samples were dried down and picked up in 0.7 ml concentrated HNO_3 and 0.2 ml hydrogen peroxide, then capped and heated at ~100 °C for ~ 3 hours. This was done to digest organic material from the resin that otherwise makes it difficult to fully reconstitute in dilute acids. The solutions were then fully dried and reconstituted in 10 ml 0.5 N HCl to be loaded onto DGA resin cartridges in a vacuum box at a flow rate of ~1.5 ml/min. After Re was eluted following the DGA protocol in Table 2.1, the samples were fully dried, and again reconstituted in 0.7 ml HNO_3 and 0.2 ml hydrogen peroxide, then capped and heated at ~100 °C for ~ 3 hours. After this digestion the samples were fully dried and reconstituted in 2% HNO_3 at 4 ppb Re in preparation for isotopic analysis.

Table 2.1 Re Purification Column Chemistry Protocol. Two-stage column chemistry protocol utilizing AG 1-X8 (100-200) mesh resin into a DGA column chemistry purification.

AG 1-X8 (100-200 mesh)				
Description	**Volume (ml)**	**Acid Normality**	**Acid Type**	**Increments (ml)**
Wash Resin	10	10	HNO_3	5
Condition Resin	5	0.5	HCl	5
Load Sample	5	0.5	HCl	-
Matrix Removal	50	0.5	HCl	5
	30	0.5	HNO_3	5
Elute Re	12	10	HNO_3	5

DGA				
Description	**Volume (ml)**	**Acid Normality**	**Acid Type**	**Increments (ml)**
Condition Resin	5	0.5	HCl	5
Load Sample	5	0.5	HCl	-
Matrix Removal	20	0.5	HCl	5
	7	0.1	HNO_3	5, 2
Elute Re	10	10	HNO_3	5

Rhenium abundances were measured using isotope dilution on a Thermo Scientific iCAP-Q inductively coupled plasma mass spectrometer (ICP-MS) at the METAL (Metals, Environmental and Terrestrial Analytical Laboratory) facility, part of the Eyring Materials Center core facility at Arizona State University. The Re recovery after the chromatographic procedures was calculated by taking an aliquot of Re from the eluted solution and compared to the amount of Re loaded on the column. The yield for each of the twelve Mt. McRae Shale samples was > 80%, and averaged ~94% . There was no correlation between Re yield and amount of sample digested. Previous method development using AG 1-X8 showed there is no measurable Re isotopic fractionation when yield is >75% (Dellinger et al., 2020). The minimum yield to detect no isotopic

fractionation for the DGA resin has not been determined, but it is assumed to be similar to AG 1-X8. Importantly, it has been found that Ca and Sr do not have isotopic fractionation associated with poor recovery on DGA resin (Romaniello et al., 2015).

The Re blank for the method, from digestion through column chemistry protocols, is < 20 pg (n = 1). This is less than 1% of the Re in each sample and is therefore negligible. This value was determined by running the blank on the iCAP Q in 4 ml 2% HNO_3.

2.3.3 Isotope Ratio Analyses

Rhenium isotope ratios were measured on a Thermo Scientific Neptune multi collector inductively coupled plasma mass spectrometer (MC-ICP-MS) at Arizona State University (ASU) in low resolution mode. Samples were prepared at a concentration of 4 ng/g Re in 0.32 N HNO_3 and introduced via self-aspiration at a flow rate of 100 µl/min with a glass nebulizer into an Apex-Q desolvating nebulizer (ESI, Omaha, NE, USA).

2.3.3.1 Nomenclature and Instrument Parameters

The isotopic compositions of Re are reported in delta (δ) notation in equation (2.1):

$$\delta^{187}\text{Re}\ (‰) = [(^{187}\text{Re}/^{185}\text{Re})_{\text{sample}} / (^{187}\text{Re}/^{185}\text{Re})_{\text{NIST 3143}} - 1] * 1000 \qquad (2.1)$$

NIST 3143 was used as the reference standard, following Dickson et al. (2020). δ^{187}Re data are reported as the average of two runs for each sample. Each individual run included 20 cycles and the signal intensity on ^{187}Re ranged from 0.9 – 1.4 V for the 4

ng/g Re sample solutions. The signal intensity obtained on ^{186}W ranged from 0.7 – 1.0 V for the 7 ng/g W in sample solution used for machine mass bias correction discussed in the following section. All detectors were 10^{-11} Ω and ^{182}W, ^{184}W, ^{186}W, ^{185}Re, ^{187}Re, ^{189}Os, ^{191}Ir, and ^{193}Ir were monitored.

2.3.3.2 Mass Bias Corrections with W and Ir

Since Re has only two isotopes, correction for instrumental mass bias employs an element spike rather than an isotope double spike (Anbar et al., 2001). Tungsten (W) and iridium (Ir) have similar masses and ionization efficiencies to Re, and thus are good candidates as element spikes. Tungsten has been used as an element spike in all Re isotopic publications thus far (Miller et al., 2015; Liu et al., 2017; Dickson et al., 2020; Dellinger et al., 2020, 2021). No studies have explored the use of Ir, which when paired with W, could provide more confidence in the accuracy of the Re isotope data by having agreement between two independent mass bias corrections.

A $\delta^{187}Re$ mass bias correction was tested with 4 ppb Re and 7 ppb W and Ir standards (in the same sample) with the Re standards NIST 3143 and NIST 989. The precision and accuracy of $\delta^{187}Re$ data were similar whether correcting for mass bias using the W or Ir spikes (Fig 2.1). When measuring the isotopic composition of NIST 3143 against NIST 989, I found $\delta^{187}Re$ = -0.27 ± 0.05 ‰ (2SD, n = 33) and -0.28 ± 0.05 ‰ (2SD, n = 33) when using W or Ir, respectively. These values agree with published values for the offset of NIST 3143 compared to NIST 989 of ≈ -0.28 ‰ (Miller et al., 2015; Liu et al., 2017; Dickson et al., 2020; Dellinger et al., 2020, 2021).

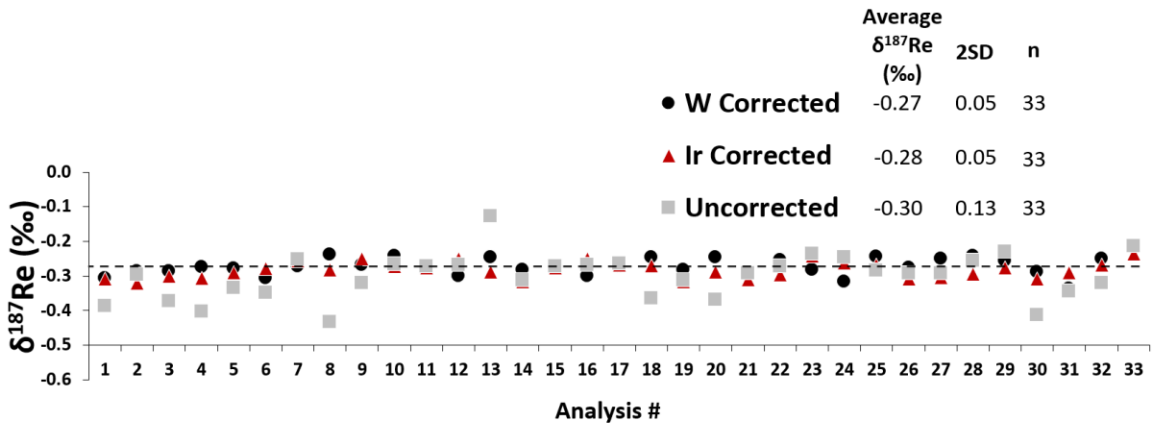

Figure 2.1 Re Standard Isotope Ratio Data. Rhenium standard δ^{187}Re data for the Re standards NIST 3143 compared to the Re standard NIST 989. Both standards were run at 4 ppb Re and 7 ppb W and Ir each. This figure compares δ^{187}Re accuracy and precision using W and Ir spikes to correct for mass bias, or no mass bias correction (uncorrected). The expected δ^{187}Re value of NIST 3143 against NIST 989 using W for the mass-bias correction ≈ -0.28 ‰, indicated by the dashed line. n represents the number of analyses. 2SD is calculated from the 33 analyses for each variable.

I utilized the black shale standard SDO-1 to test the effectiveness of W and Ir element spikes in a sample derived from a complex matrix. The W and Ir spikes were added after Re purification, immediately prior to isotope ratio measurements on the MC-ICP-MS. To perform these tests, I extracted Re from SDO-1 using the protocols outlined in section 2.3. To measure δ^{187}Re in SDO-1, two Re purification procedures were employed: Procedure 1) three separate SDO-1 digestions analyzed twice each (only two analyses each due to limitation in the amount of sample digested) using the AG 1-X8 chemistry only, and Procedure 2) three separate SDO-1 digestions analyzed twice each using both AG 1-X8 and DGA column chemistry protocols. These separate tests were run to determine how much matrix removal was necessary for accurate and precise Re isotope ratio analyses.

I found that the W-corrected δ^{187}Re obtained from samples subjected to procedure 1 was -0.22 ± 0.09 ‰ (2SD, n = 6). For samples subjected to procedure 2, the W-corrected δ^{187}Re = -0.26 ± 0.05 ‰ (2SD, n = 6). These values are identical within error.

The consistency of the data indicates the reproducibility of both procedures. The precision was better for procedure 2, perhaps due to the additional removal of matrix elements by the DGA step.

In contrast, when using an Ir-based bias correction for the three samples, δ^{187}Re data for procedure 1 were enriched in the light isotope ^{185}Re and less precise with a measured δ^{187}Re of -1.61 ± 1.11 ‰ (2SD, n = 6). However, the Ir-corrected data for procedure 2 yielded δ^{187}Re = -0.18 ± 0.04 ‰ (2SD, n = 6). The consistency of the Ir-spike data from procedure 2 samples with the W-spiked samples described above, suggests that discrepancy in the Ir-spiked procedure 1 data is caused by an interference(s) on the light Ir isotope (^{191}Ir) that is removed when the DGA resin step is employed. Hence, for black shales, W is a more robust choice for the mass bias correction. Likely possibilities for an interference on ^{191}Ir include native Ir remaining in the samples after Re purification, ^{151}Eu + ^{40}Ar, ^{175}Lu + ^{16}O, and ^{177}Hf + ^{14}N.

Since all Mt. McRae Shale samples underwent AG 1-X8 and DGA purifications (which had accurate W and Ir corrected data when both columns were used on SDO-1), both W and Ir were used for the mass bias correction. I found that the results for W and Ir spikes were identical within uncertainty for eight of the twelve samples. The other four out of twelve samples had Ir-corrected δ^{187}Re values that were lighter than the W-corrected δ^{187}Re values, as well as had poor precision (Table 2.2). Light δ^{187}Re values and poor precision were also found during the SDO-1 tests; again, likely indicating a matrix interference(s) present for ^{191}Ir that was not fully removed during the purification procedures. Therefore, the Mt. McRae Shale W-corrected δ^{187}Re data is used for data interpretations and figures.

Table 2.2 Mt. McRae Ir-corrected Re Isotope Data. Upper and lower member Mt. McRae Shale δ^{187}Re (‰) data using Ir as the mass bias correction and sample standard bracketing. Each sample was analyzed twice indicated by analysis 1 and 2. δ^{187}Re in red indicates a >15 ‰ difference between the measured isotope ratios of analysis 1 and 2.

		δ^{187}Re (‰) (Ir corrected)		
	Depth (m)	Analysis 1	Analysis 2	Mean
Upper	133.97	-0.31	-0.33	-0.32
	136.15	-0.52	-0.79	-0.66
	139.01	-0.23	-0.27	-0.25
	140.95	-0.41	-0.39	-0.40
	143.45	-0.40	-0.42	-0.41
	145.61	-0.44	-0.49	-0.47
	147.30	-0.52	-0.46	-0.49
	148.27	-0.56	-0.58	-0.57
	149.30	-0.60	-0.79	-0.70
	150.24	-0.63	-0.81	-0.72
Lower	178.61	-0.59	-0.78	-0.69
	189.39	-0.44	-0.49	-0.47

2.3.3.3 Accuracy and Precision of Re Isotope Measurements

In addition to using a W spike during Re isotopic measurements, standard-sample-standard bracketing (e.g., Peel et al., 2008) was utilized during all analytical sessions. The accuracy and precision of the Re isotope measurements was assessed by regularly analyzing the offset between NIST 989 against NIST 3143. The bracketing standards were introduced to the MC-ICP-MS in the same acid type, acid molarity, [Re], [W], and [Ir] as all samples. The repeated analysis of NIST 989 relative to NIST 3134 throughout the analytical session had a δ^{187}Re of -0.28 ± 0.07 ‰ (2SD, n = 15). This value agrees well with previous studies (Miller et al., 2015; Liu et al., 2017; Dickson et al., 2020; Dellinger et al., 2020, 2021).

To evaluate the optimal range, accuracy, and precision of W/Re and Ir/Re ratios, variable doping series tests were conducted. To do this, the abundance of W and Ir external standards was held constant and added to each sample together at 10 ppb each, while the abundance of Re from NIST 3143 varied from 1- 10 ppb – Re abundances tested included 1, 2, 3, 4, 5, and 10 ppb (Fig. 2.2). Thus, the [Re] to [W] and [Ir] ratios tested were 0.1, 0.2, 0.3, 0.4, 0.5, and 1, with n = 17 for each concentration range. Sample standard bracketing was used, and the samples from each concentration range were bracketed against themselves. Thus, the samples and bracketing standards had the same [Re]/[W] and [Re]/[Ir] ratios for each concentration range. We observed similar precision and accuracy in [Re]/[W] and [Re]/[Ir] ratios from 0.2 to 1 (Fig. 2.2). In this study, a [Re]/[W] and [Re]/[Ir] value of 0.57 (4 ppb Re and 7 ppb W and Ir) was selected for all black shale samples and standards.

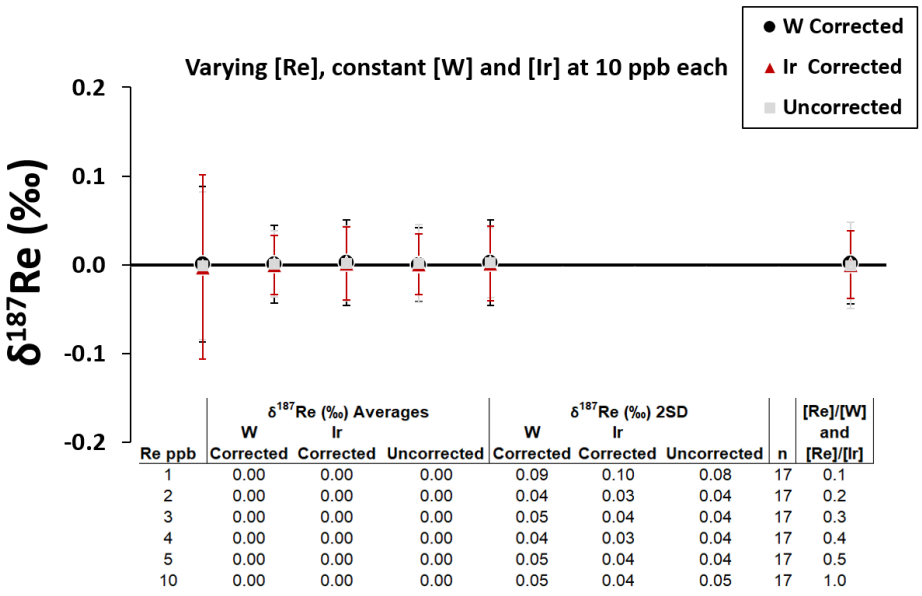

Re ppb	δ187Re (‰) Averages W Corrected	Ir Corrected	Uncorrected	δ187Re (‰) 2SD W Corrected	Ir Corrected	Uncorrected	n	[Re]/[W] and [Re]/[Ir]
1	0.00	0.00	0.00	0.09	0.10	0.08	17	0.1
2	0.00	0.00	0.00	0.04	0.03	0.04	17	0.2
3	0.00	0.00	0.00	0.05	0.04	0.04	17	0.3
4	0.00	0.00	0.00	0.04	0.03	0.04	17	0.4
5	0.00	0.00	0.00	0.05	0.04	0.04	17	0.5
10	0.00	0.00	0.00	0.05	0.04	0.05	17	1.0

Figure 2.2 Testing Optimal [Re]/[W] and [Re]/[Ir] Range. Rhenium abundances varied at 1, 2, 3, 4, 5, and 10 ppb while W and Ir abundances were held constant at 10 ppb in each sample. Rhenium, W, and Ir were added to each sample. This data was used to determine the optimal [Re]/[W] and [Re]/[Ir] ranges to measure accurate and precise data δ^{187}Re data. Horizontal black line represents the expected δ^{187}Re value of 0 ‰. Data reported as W corrected isotope ratios, Ir corrected isotope ratios, and the uncorrected isotope ratios. Error bars represent the 2SD of replicate measurements (n = 17 for each).

Our measured SDO-1 post-DGA column W-corrected δ^{187}Re of -0.26 ± 0.05 ‰ (2SD, n = 6) does not agree within uncertainty with the published values, -0.09 ± 0.05 ‰ (2SD, n = 2) and -0.07 ± 0.13 ‰ (2SD, n = 5) from Dellinger et al. (2020) and Miller et al. (2009), respectively. The accuracy of my δ^{187}Re values is supported by the quantitative release of Re by the digestion method, the high yield of the purification protocol, and low blank contribution throughout sample processing. I note that Dellinger et al. (2020) reported a low blank of ~14 ± 4 ppg (n = 9, 1sd) and yields > 80%, while Miller et al. (2009) does not list the recovery or blank of the method. Both Dellinger et al. (2020) and Miller et al. (2009) used W for the mass bias correction and sample standard bracketing. It is possible my SDO-1 W-corrected δ^{187}Re value does not agree with these

studies due to differences in the abundance of matrix elements between studies. This study has a two column (AG 1-X8 and DGA) Re purification protocol, while Dellinger et al. (2020) and Miller et al. (2009) both used AG 1-X8 resin only. Alternatively, differences in digestion methods could be the cause for the difference in δ^{187}Re values. This study utilized CT digestions using inverse aqua regia, while Miller et al. (2009) and Dellinger et al. (2020) utilized beaker digestions which included concentrated HCl, HNO_3, and HF. Hydrofluoric acid is known to break down silicates which may contain trace amount of Re, while inverse aqua regia does not. Thus, the difference in isotope ratios may be due to this study not digesting silicates, while the other studies did.

Error bars for the averages of Mt. McRae Shale samples use SDO-1 as a representative error bar (± 0.05 ‰). This is done because there are only two analyses each for the Mt. McRae Shale samples. SDO-1 has a similar matrix to the samples and was put through AG 1-X8 and DGA purification procedures. The higher Re abundance of SDO-1 (~78 ng/g Re) compared to the Mt. McRae Shale samples (ranging from 7 – 48 ng / g Re) means less SDO-1 material needed to be digested, leading to fewer matrix elements than Mt. McRae Shale samples. However, the precision for measured W-corrected Re isotope ratio data was similar for all samples, indicating any possible differences in the measurement of Re isotope ratios were abated by the Re purification protocol.

Table 2.3: Mt. McRae Re Geochemical Data. Mt. McRae Shale data from the lower and upper shale members including Re abundance, Re enrichment factor (EF) = $(Re/Al)_{sample}$ / $(Re/Al)_{Upper\_crust}$, and $\delta^{187}Re$ using W mass bias correction. Rhenium (EF) data and indication of secondary pyrite inclusion during sampling taken from Anbar et al. (2007).

				δ^{187}Re (‰) (W corrected)		
	Depth (m)	Re (ng/g)	Re (EF)	Analysis 1	Analysis 2	Mean
Upper	133.97	28	28	-0.35	-0.33	-0.34
	136.15	23	26	-0.32	-0.32	-0.32
	139.01	33	48	-0.31	-0.31	-0.31
	140.95	48	56	-0.44	-0.40	-0.42
	143.45	31	80	-0.45	-0.45	-0.45
	145.61	32	48	-0.47	-0.50	-0.49
	147.30	20	35	-0.46	-0.39	-0.43
	148.27	15	22	-0.44	-0.44	-0.44
	149.30	32	43	-0.35	-0.41	-0.38
	150.24	14	22	-0.44	-0.43	-0.44
Lower	178.61	7	9	-0.29	-0.24	-0.27
	189.39	10	20	-0.41	-0.40	-0.41

2.4 Results and Discussion

Prior studies of the Mt. McRae Shale provided evidence for a transient increase (or 'whiff') of atmospheric and shallow-water oxygenation prior to the GOE (e.g., Anbar et al., 2007; Kaufman et al., 2007; Garvin et al., 2009; Duan et al., 2010; Kendall et al., 2015; Ostrander et al., 2019). The enrichment of Re and Mo is interpreted to reflect increased delivery of these metals to the ocean from oxidative weathering of subaerial sulfides (Anbar et al., 2007; Johnson et al., 2019). However, a recent study challenged the idea of transient oxygenation before the GOE, suggesting the observed geochemical shifts in Mo, U, Se, N, S, Hg, Os, etc. are due to volcanic activity (Slotznick et al., 2022). This idea was rebutted by Anbar et al. (2023) based on existing data.

Rhenium isotopes provide a new way to explore the 'volcanogenic' hypothesis. Here, data from the lower shale member of the Mt. McRae Shale – where persistent

volcanic activity has been interpreted based on Hg geochemical data (Meixnerová et al., 2021) – are compared to the upper shale where the 'whiff' hypothesis is challenged by Slotznick et al. (2022).

2.4.1 Volcanic Volatiles? To Be or Not to Be

Volatilization of Re during volcanism is well-documented (Korzhinsky et al., 1994; Sun et al., 2003; Lassiter, 2003; Norman et al., 2004; Tessalina et al., 2008; Yudovskaya et al., 2008; Pitcher et al., 2009). Vapor-phase Re can be deposited in nearby sulfide minerals (Korzhinsky et al., 1994), or form Re-oxides or Re-sulfides (Yudovskaya et al., 2008). The Re-oxides are soluble, while Re-sulfides are stable as precipitates. The location of eruptions has been found to influence Re volatility. Subaerial eruptions can emit up to ~80% of the original Re as a volatile, while submarine eruptions exhibit decreased emission of Re as a volatile due to more limited outgassing (Lassiter et al., 2003). Rhenium abundances in mid-ocean ridge basalt and undegassed basaltic glass have been found to be ~0.9 ± 0.5 ppb, whereas outgassed melts have Re abundances of ~200 – 800 ppt (Norman et al., 2004). These differences indicate volatile loss of Re that is close to 1 ppb (Norman et al., 2004). Thus, volcanic vapor-phase Re delivery to the oceans could possibly explain the whole-rock Re enrichments of up to ~ 50 ppb observed in the upper unit of the Mt. McRae Shale, though it would require significant volumes of volcanic material erupted to the surface.

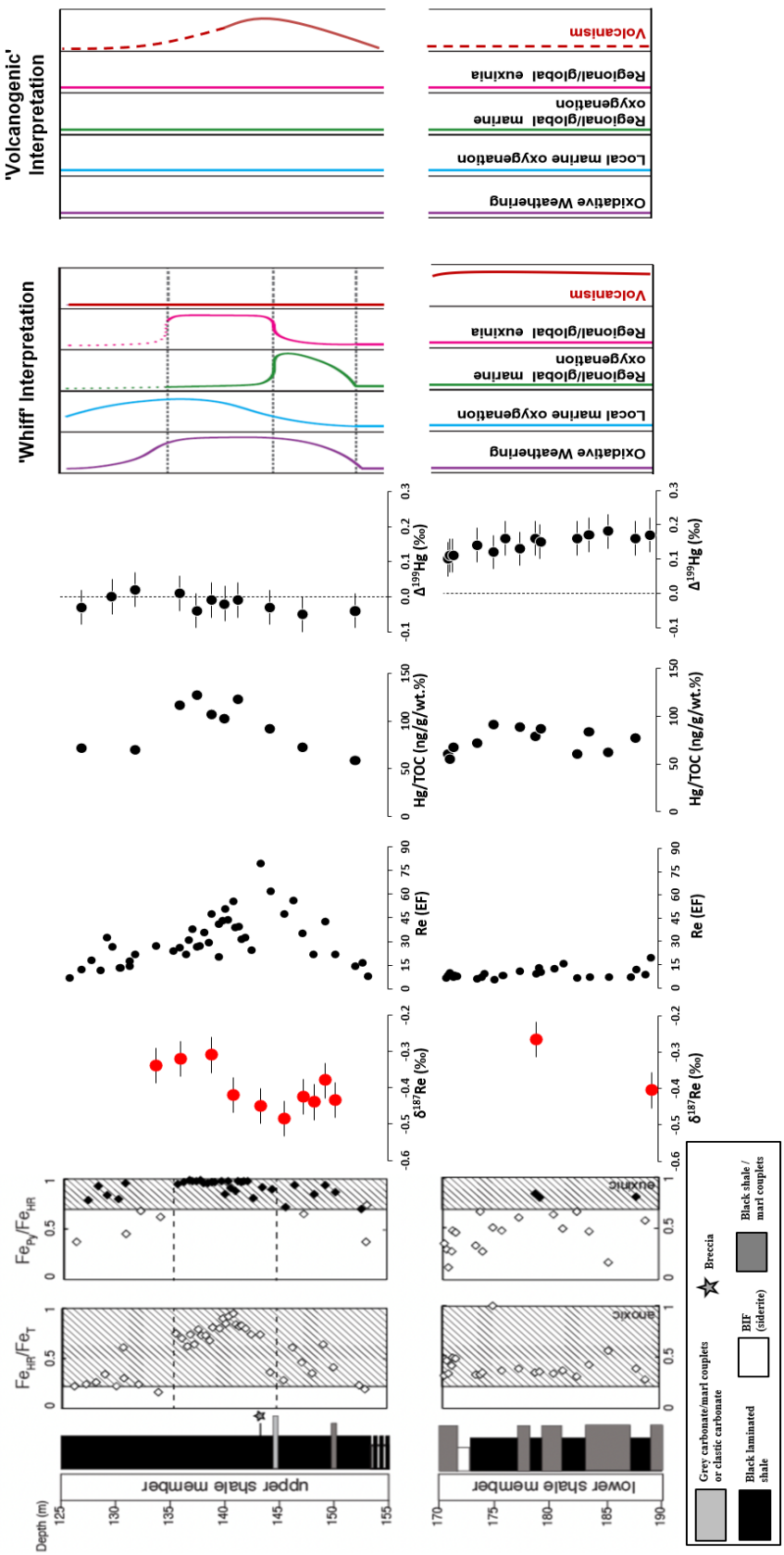

Fig. 2.3 Re and Hg Geochemical Data and Interpretations. $\delta^{187}Re$, Re enrichment factor (EF), Hg/TOC (ng/g/wt.%), and $\Delta^{199}Hg$ data. Total organic carbon data is from Anbar et al. (2007), and Hg abundance and isotope ratio data is from (Meixnerová et al., 2021). Inferred redox conditions are modified from Ostrander et al. (2021) and are based on Re and Mo abundances (Anbar et al., 2007), Mo isotope ratios (Duan et al., 2010; Ostrander et al., 2019), N isotope ratios (Garvin et al., 2009), U and Os isotope ratios (Kendall et al., 2013), and Se isotope ratios (Stüeken et al., 2015). Volcanic interpretations based on Meixnerová et al. (2021) and Slotznick et al. (2022). Dashed lines indicate a best guess due to uncertainty. Error bars on $\delta^{187}Re$ data represent the 2SD of replicate measurements of the black shale standard SDO-1. Error bars on $\Delta^{199}Hg$ data represent the error of repeat measurements of standards from Meixnerová et al. (2021).

The new δ^{187}Re data can be paired with Hg abundance and isotope ratio data to test whether the source of the Re (and other trace metals) enrichment is due to volcanism or to oxidative weathering. Mercury and Re are both removed from seawater to organic matter and sulfides under reducing conditions, indicating they can share similar input and output pathways in the ocean (Blum et al., 2014). Mercury is primarily delivered to the surface from volcanism as a volatile, making it an excellent proxy for volcanism.

The lower shale member hosts evidence for subaerial volcanism (Fig. 2.3), in the form of Hg enrichments and a positive shift in odd-mass-independent fractionation (odd-MIF: Δ^{199}Hg, hereafter MIF; Fig. 2.3) that are indicative of photooxidation of Hg(0) in the atmosphere (Meixnerová et al., 2021). These positive MIF values data indicate persistent subaerial volcanism (likely related to a large igneous province (LIP) event) throughout deposition of the entirety of the lower shale member from 170 m – 190 m (Fig. 2.3). The sample at 178.61 m is the only lower shale member sample deposited under euxinic conditions which is the same depositional redox conditions at the samples in the 'whiff' interval (Fig. 2.3). There are two data points with δ^{187}Re data in the lower shale, 189.39 m and 178.61 m, that were deposited under ferruginous (anoxic and Fe-rich) and euxinic (anoxic and sulfidic) conditions, respectively (Reinhard et al., 2009). The δ^{187}Re values for these samples are -0.41 ± 0.05 ‰ and -0.27 ± 0.05 ‰ for 189.39 m and 178.61 m, respectively. Rhenium removal from seawater is more effective as bottom water conditions become more reducing. Therefore, the sample deposited under euxinic conditions at 178.61 m is most likely to record the isotopic composition of seawater. However, I note there have been no studies that have examined if euxinic conditions are capable of recording the isotopic composition of seawater to date. Based on the

geochemical signatures of subaerial volcanism from Re and Hg geochemical data in the lower shale member, I expect subaerial volcanic signatures represented in euxinic sediments to have positive Δ^{199}Hg values and δ^{187}Re values that are close to -0.27 ± 0.05 ‰ with low Re enrichments (~9-20 Re EF).

Between ~153 m and 145 m, the beginning of the Re enrichment in the contested 'whiff' interval, there is a shift to lighter δ^{187}Re values, with Δ^{199}Hg ≈ 0 ‰. The Δ^{199}Hg ≈ 0 ‰ values indicate the Hg recorded in this section of the Mt. McRae Shale has likely not been influenced by photochemical reactions. If the Re and Hg were derived from volcanic activity, a shift to heavy Re isotope compositions and Δ^{199}Hg values of ~0.1 to 0.2 would be expected based on geochemical signatures from the lower unit. Thus, the paired geochemical signatures of Re and Hg abundance and isotope data are inconsistent with subaerial volcanism. At ~143- 138 m, there is a shift to heavier Re isotopic compositions while Δ^{199}Hg remains ≈ 0 ‰. Again, this is not the expected trend for paired Hg and Re isotope ratio data for a subaerial volcanic signature.

If volcanism is the source of Re enrichments in the 'whiff' interval, then I would expect that Re and Hg enrichments would occur simultaneously, as these elements are both delivered in a vapor phase during volcanism (e.g., Sun et al., 2003; Zambardi et al., 2009). Importantly, an initial study of Re delivery from hydrothermal vents indicates that Re abundances from hydrothermal fluids are very low at < 14 pmol / kg (Miller et al., 2011), indicating hydrothermal fluids are likely a negligible source of Re to seawater. Hydrothermal alteration of volcanic rocks is another possible source of Re to seawater, though this is unlikely in an Archean ocean that was likely dominantly anoxic. Rhenium removal from hydrothermal alteration of volcanic rocks would require the oxidizing

fluids to oxidize Re to the soluble oxidized Re species perrhenate. Thus, volcanic emissions of Re as a volatile is the most likely volcanic source of Re at high enough abundances to reach ~50 ppb seen in the upper shale unit. At ~153 m – ~143 m there is a gradual shift in Re (EF) from ~15 - ~85, where there is a consistent increase in Hg/TOC from ~50 - ~100. However, Re EF begins to decrease after ~143 m while Hg/TOC continues to increase to ~145 at ~135 m, then begins to decrease.

However, a possibility to support volcanism in the upper shale member is a submarine eruption (underwater, likely somewhere in the ocean) rather than a subaerial eruption. A submarine eruption could explain the $\Delta^{199}Hg \approx 0$ ‰ by inputting Hg into the ocean that has not been influenced by photochemical reactions. It is possible a submarine eruption more efficiently delivered vapor-phase Re to seawater compared to subaerial volcanism, explaining the differences in Re enrichments of the upper and lower sections as well. However, this is unlikely as the consistent maintenance of $\Delta^{199}Hg \approx 0$ ‰ throughout the upper shale would require Hg to be sourced deep underwater outside the photic zone of the ocean, as Hg in the atmosphere or photic zone can have a MIF signature imprinted by interacting with light (e.g., Blum et al., 2014). Studies of volcanic delivery of Re to the ocean indicate the deeper the eruption, the less Re is emitted as a volatile due to a reduction in outgassing (Lassiter et al., 2003). Therefore, maintaining $\Delta^{199}Hg \approx 0$ ‰ with high Re enrichments is unlikely from a deep submarine eruption. Another aspect of the 'volcanogenic' hypothesis that is difficult to explain is the shift to light $\delta^{187}Re$ values (-0.38 to -0.49 ‰ from ~153 to 145 m) and then heavy $\delta^{187}Re$ values (-0.41 to -0.31 ‰ from 143 to 137 m) seen in the upper member. Perhaps there was redox-related fractionation during Re reduction from Re^{VII} to Re^{IV} and subsequent

removal to sediments. If so, a continuous shift to heavy values would be expected from ~137 to 133. However, the δ^{187}Re values are mostly invariable in this section, inconsistent with redox-related removal from a source with an unchanging isotopic composition.

The 'volcanogenic' hypothesis is also not supported by previously published geochemical data from the upper member of the Mt. McRae Shale. Iron isotope data from Ostrander et al. (2022) indicates hydrothermal inputs did not dominate the trace metal supply in the upper member, making a submarine eruption unlikely. Furthermore, a radiogenic $^{187}Os/^{188}Os_{initial}$ (hereafter Os_i) value of 0.34 ± 0.19 from samples at 145.2 m – 148.3 m (Kendall et al., 2015) indicates oxidative weathering of continental material and disputes subaerial or submarine volcanism. Osmium isotope ratios can distinguish between continental weathering and volcanic/extraterrestrial sources of Os to the ocean. The Os_i value of a mantle (or extraterrestrial) source of Os to the ocean ≈ 0.12 (e.g., Peucker-Ehrenbrink and Ravizza, 2000), which is approximately the nucleosynthetic ratio of $^{187}Os/^{188}Os$ value. On the other hand, weathering of continental material has Os_i values ≈ ≥ 0.2 due to radioactive decay of ^{187}Re leading to enrichments in amount of ^{187}Os in continental material. Thus, the radiogenic Os_i value indicates volcanism was not the source of the trace metals to the ocean. Taken together, the geochemical data in the upper and lower members of the Mt. McRae Shale are most parsimoniously explained by changes in oceanic and atmospheric oxygenation.

2.4.2 Re Interpretations from an Environmental Oxygenation Perspective

There is a shift toward lighter δ^{187}Re values (from ~ -0.38 to -0.49 ‰) in the upper shale, beginning at ~150 m to ~145 m (Fig. 2.3; Table 2.3). This shift is coincident with Re enrichments that occur with other redox sensitive metal enrichments (e.g., Mo; Anbar et al., 2007). If the Re enrichments are a result of oxidative weathering of continental material, then the shift to more negative δ^{187}Re values may indicate the isotopic composition of Re delivered from weathering was heavier than seawater. The shift in Re isotopic compositions and abundances due to oxidative weathering would provide information about changing sources of Re to the ocean with different isotopic compositions.

An alternative – or possibly supplemental – explanation for the shift toward lighter isotopic compositions is related to mass-dependent fractionation of Re isotopes in seawater during reduction of the oxidized Re species perrhenate ($Re^{VII}O_4^-$). Perrhenate is largely unreactive with no significant oxic sink, thus accumulates in seawater (e.g., Yamashita et al., 2007). In low-O_2 conditions, Re^{VII} is reduced to Re^{IV}, leading to efficient removal from seawater coupled to organic carbon burial at the sediment/water interface, evidenced by a strong correlation between Re and total organic carbon abundances (Colodner et al., 1993,1995; Kendall et al., 2010; Morford et al., 2005, 2012). Thus, fractionation during removal from seawater related to redox changes is expected, which could have led to the observed δ^{187}Re variations in the Mt. McRae Shale. However, we note the isotopic behavior of Re is not well characterized and will benefit from additional investigations.

2.5. Future Directions

2.5.1 Re as a Paleoenvironmental Proxy

Re isotope ratios have the potential to provide unique information about past suboxic redox conditions. There are currently indicators of ocean-basin-scale oxic and anoxic (0 μM O_2) conditions. But, at present there is no global-scale geochemical tool to determine when large parts of the oceans were in a low-O_2, but not anoxic, condition termed 'suboxic' (i.e., ≤10 μM O_2). Detecting suboxic conditions is important because some aerobic organisms can live in extremely low-O_2 waters (down to ~10 nM O_2; Stolper et al. 2010). It will be of great interest to know when the majority of the ocean first crossed from anoxic conditions to suboxic conditions.

There are three possible interpretations for the observed changes in the Mt. McRae Shale δ^{187}Re values in the 'whiff' interval. Option 1) euxinic sediments record the Re isotopic composition of seawater and variations are due to redox effects. Option 2) euxinic sediments do not record the Re isotopic composition of seawater, and variations are due to local fractionation during Re incorporation to sediments. Option 3) there are changes in the input fluxes of Re to the ocean throughout the 'whiff' interval. Some combination of these options is also possible.

If option one is the case, then Re isotope mass balance models may provide information about the extent of suboxic conditions in the past. Furthermore, characterization of the isotopic compositions of sources of Re to seawater (e.g., volcanic emissions, oxidative weathering of continental material) can be used in models to constrain to the balance between input fluxes of Re to the ocean. This will unlock a

powerful tool and provide new information about the ancient conditions relevant to the evolution of life on Earth.

If option two is the case, then more work is needed to determine what the sedimentary fractionation is and to determine if a fractionation factor can be applied to correct for it. Other rock types (e.g., carbonates) could be examined for their Re isotopic composition to see if they record the isotopic composition of seawater.

Option three is possible in both cases one and two. To distinguish between these options, future work in modern environments is needed to constrain Re isotope behavior. By studying Re isotope ratios and abundances in modern environments, the isotopic fractionation, if any, that is recorded in sediments can be detected and this information can be applied to studies of ancient Earth.

2.5.2 Future Work to Develop the Re Paleoenvironmental Proxy

There have only been a handful of papers at this point in the development of the Re isotope proxy. The research thus far has examined the potential to use Re as a paleoredox tool (Miller et al., 2015), track oxidative weathering through time (Dellinger et al., 2021) measure low Re abundance geologic samples (Dickson et al., 2020; Dellinger et al., 2020), and understand processes influencing Fe-meteorites (Liu et al., 2017). The variability found to date spans 1.06 ‰ (from -0.97 to 0.09 ‰ using NIST 3143 as δ=0).

Additional research is required to advance the understanding of Re geochemical behavior in the modern environment and to further investigate its potential as a paleoredox proxy. One crucial aspect is the development of a robust mass balance model for Re. To achieve this, it is essential to determine the magnitudes and isotopic

compositions of modern inputs and outputs of Re to the ocean. This information will provide necessary constraints for the model, enabling us to accurately assess the Re budget and its implications for paleoredox reconstructions. It is also important to confirm the δ^{187}Re of Atlantic seawater reported by Dellinger et al. (2020) and Dickson et al. (2020) is homogenous throughout the ocean by sampling more locations.

Targeted investigations of modern locations are required to gain insights into the capability of euxinic sediments or other geologic materials to record seawater's Re isotopic composition. Measuring the δ^{187}Re of sediments, water, pore water, and suspended particles from modern analogs for ancient oceans is a good way to do this (e.g., Neubert et al., 2008; Weyer et al., 2008). The Black Sea is a well-studied modern location to investigate redox sensitive metal behavior in an environment that transitions from oxic to euxinic (e.g., Colodner et al., 1995; Neubert et al., 2008). Suboxic locations (e.g., the Benguela margin) will also be key to understanding Re isotope behavior, as it has been for U (e.g., Abshire et al., 2020). This knowledge is crucial for accurately interpreting Re isotope variations observed in ancient sediments and their connection to paleoredox conditions. This is because we assume the same conditions found today hold true to studies of the past when similar conditions were present. Another approach for studying Re isotope behavior is laboratory-based reduction experiments. These experiments will help determine factors influencing Re isotope fractionation and provide insight to reaction rates during controlled environments. Thus, to access the full potential of the Re isotope paleoredox proxy, it is imperative to address the gaps in our knowledge regarding its geochemical behavior in the modern environment.

2.6 Conclusions

I measured the first δ^{187}Re data from an ancient sedimentary sequence in the upper and lower sections of the Mt. McRae Shale. The lower section hosts evidence for significant volcanism, while the upper section has been reported to host evidence for volcanism (the 'volcanogenic' hypothesis) or changes in environmental oxygenation (the 'whiff' hypothesis). I found that samples had δ^{187}Re values that spanned from – 0.54 ‰ to – 0.22 ‰ for a total range of 0.32 ‰.

The evidence for volcanism in the lower section of the Mt. McRae Shale is defined by low Re enrichment factors (EF) of ~15 and isotopic compositions that trend toward heavy values of ~ -0.27 ‰. In the upper section of the Mt. McRae Shale at the contested 'whiff' or volcanic interval, Re EF values increase from ~15 at ~150 m to ~80 at ~143 m, paired with a shift to light δ^{187}Re values (from ~ -0.38 to -0.49 ‰). In this same interval, there are Os isotope ratio data indicating a radiogenic Os_i value of 0.34 ± 0.19 measured in samples from 145.2 m – 148.3 m. The unradiogenic Os_i values can only be explained by oxidative weathering of continental material, and further disputes volcanic activity, whether it be subaerial or submarine. Additionally, a Re-Os isochron age of 2495 ± 14 Ma (Anbar et al., 2007; Kendall et al., 2015) agrees with a U-Pb age of 2504 ± 5.0 Ma (Rasmussen et al., 2005), indicating Re in the Mt. McRae Shale is well preserved. When considering all the geochemical data from the Mt. McRae Shale, the most parsimonious explanation for the observed changes throughout deposition are changes in environmental oxygenation rather than volcanism.

Examining the δ^{187}Re through the lens of the 'whiff' hypothesis, I found shifts in the Re isotope ratios that are coincident with evidence for changes in ocean and

atmospheric oxygenation. Rhenium is uniquely sensitive to suboxic conditions in the ocean and these variations are a promising first detection of Re isotope variations in nature. Overall, these data highlight the potential for Re to be used as a paleoredox tool to improve our understanding of Earth's environmental oxygenation history. Future work constraining Re behavior in modern euxinic (e.g., Black Sea), suboxic (e.g., Benguela Margin), and ferruginous environments (e.g., Green Lake) will be a critical next step in the development of the Re isotope paleoredox proxy.

2.7 Acknowledgements

I thank Trevor Martin and Gwyn Gordon from the METAL lab at ASU for technical assistance. This work was supported by FESD Dynamics of Earth System Oxygenation (NSF EAR 1338810 to Anbar), and NASA Future Investigators in NASA Earth and Space Science and Technology Fellowship to Sullivan (19-PLANET20-0226).

2.8 References

Abshire, M.L., Romaniello, S.J., Kuzminov, A.M., Cofrancesco, J., Severmann, S., Riedinger, N. (2020) Uranium isotopes as a proxy for primary depositional redox conditions in organic-rich marine systems. Earth and Planetary Science Letters, 529, 115878.

Anbar, A.D., Buick, R., Gordon, G.W., Johnson, A.C., Kendall, B., Lyons, T.W., Ostrander, C.M., Planavsky, N.J., Reinhard, C.T., Stüeken, E.E. (2023) Technical comment on "Reexamination of 2.5-Ga 'whiff' of oxygen interval points to anoxic ocean before GOE." Science Advances, 9, eabq3736.

Anbar, A.D., Duan, Y., Lyons, T.W., Arnold, G.L., Kendall, B., Creaser, R.A., Kaufman, A.J., Gordon, G.W., Scott, C., Garvin, J., Buick, R. (2007) A Whiff of Oxygen Before the Great Oxidation Event? Science, 317, 1903–1906.

Barley, M.E., Bekker, A., Krapez, B. (2005) Late Archean to Early Paleoproterozoic global tectonics, environmental change and the rise of atmospheric oxygen. Earth and Planetary Science letters, 238, 156–171.

Blum, J.D., Sherman, L.S., Johnson, M.W. (2014) Mercury Isotopes in Earth and Environmental Sciences. Annual Review of Earth and Planetary Sciences, 42, 249–269.

Colodner, D., Edmond, J., Boyle, E. (1995) Rhenium in the Black Sea: comparison with molybdenum and uranium. Earth and Planetary Science Letters, 131, 1–15.

Colodner, D., Sachs, J., Ravizza, G., Turekian, K., Edmond, J., Boyle, E. (1993) The geochemical cycle of rhenium: a reconnaissance. Earth and Planetary Science letters, 117, 205–221.

Dellinger, M., Hilton, R.G., Nowell, G.M. (2020) Measurements of rhenium isotopic composition in low-abundance samples. Journal of Analytical Atomic Spectrometry, 35, 377–387.

Dellinger, M., Hilton, R.G., Nowell, G.M. (2021) Fractionation of rhenium isotopes in the Mackenzie River basin during oxidative weathering. Earth and Planetary Science Letters, 573, 117131.

Dickson, A.J., Hsieh, Y., Bryan, A. (2020) The rhenium isotope composition of Atlantic Ocean seawater. Geochimica et Cosmochimica Acta, 287, 221–228.

Du Vivier, A.D.C., Selby, D., Condon, D.J., Takashima, R., Nishi, H. (2015) Pacific 187Os/188Os isotope chemistry and U–Pb geochronology: Synchroneity of global Os isotope change across OAE 2. Earth and Planetary Science Letters, 428, 204–216.

Du Vivier, A.D.C., Selby, D., Sageman, B.B., Jarvis, I., Gröcke, D.R.,Voigt, S. (2014) Marine 187Os/188Os isotope stratigraphy reveals the interaction of volcanism and ocean circulation during Oceanic Anoxic Event 2. Earth and Planetary Science Letters, 389, 23–33.

Duan, Y., Anbar, A.D., Arnols, G.L., Lyons, T.W., Gordon, G.W., Kendall, B. (2010) Molybdenum isotope evidence for mild environmental oxygenation before the Great Oxidation Event. Geochimica et Cosmochimica Acta, 74, 6655–6668.

Finlay, A.J., Selby, D., Osborne M.J. (2012) Petroleum source rock identification of United Kingdom Atlantic Margin oil fields and the Western Canadian Oil Sands using Platinum, Palladium, Osmium and Rhenium: Implications for global petroleum systems. Earth and Planetary Science Letters, 313–314, 95–104.

Garvin, J., Buick, R., Anbar, A.D., Arnold, G.L., Kaufman, A.J. (2009) Isotopic evidence for an aerobic nitrogen cycle in the latest Archean. Science, 323, 1045–1048.

Gumsley, A.P., Chamberlain, K.R., Bleeker, W., Söderlund, U., De Kock, M.O., Larsson, E.R., Bekker, A. (2017) Timing and tempo of the Great Oxidation Event. Proceedings of the National Academy of Science, 114, 1811–1816.

Ishikawa, A., Senda, R., Suzuki, K., Dale, C.W., Meisel, T. (2014) Re-evaluating digestion methods for highly siderophile element and 187Os isotope analysis: Evidence from geological reference materials. Chemical Geology, 384, 27–46.

Johnson, A.C., Romaniello, S.J., Reinhard, C.T., Gregory, D.D., Garcia-Robledo, E., Revsbech, N.P., Canfield, D.E., Lyons, T.W., Anbar, A.D. (2019) Experimental determination of pyrite and molybdenite oxidation kinetics at nanomolar oxygen concentrations. Geochimica et Cosmochimica Acta, 249, 160–172.

Kaufman, A.J., Johnston, D.T., Farquhar, J., Masterson, A.L., Lyons, T.W., Bates, S., Anbar, A.D., Arnold, G.L., Garvin, J., Buick, R. (2007) Late Archean biospheric oxygenation and atmospheric evolution. Science, 317, 1900–1903.

Kendall, B., Brennecka, G.A., Weyer, S., Anbar, A.D. (2013) Uranium isotope fractionation suggests oxidative uranium mobilization at 2.50 Ga. Chemical Geology, 362, 105–114.

Kendall, B., Creaser, R.A., Reinhard, C.T., Lyons, T.W., Anbar, A.D. (2015) Transient episodes of mild environmental oxygenation and oxidative continental weathering during the late Archean. Science Advances, 1, 1–10.

Kendall, B., Reinhard, C.T., Lyons, T.W., Kaufman, A.J., Poulton, S.W., Anbar, A.D. (2010) Pervasive oxygenation along late Archaean ocean margins. Nature Geoscience, 3, 647–652.

Koide, M., Hodge, V.F., Yang, J.S., Stallard, M., Goldberg, E.G., Calhoun, J., Bertine, K.K. (1986) Some comparative marine chemistries of rhenium, gold, silver and molybdenum. Applied Geochemistry, 1, 705–714.

Korzhinsky, M.A., Tkachenko, S.I., Shmulovich, K.I., Taran, Y.A., Steinberg, G.S. (1994) Discovery of a pure rhenium mineral at Kudriavy volcano. Nature, 369, 51–52.

Krapež , B., Barley, M.E., Pickard, A.L. (2003) Hydrothermal and resedimented origins of the precursor sediments to banded iron formation: sedimentological evidence from the Early Palaeoproterozoic Brockman Supersequence of Western Australia: Resedimented origins of banded iron formation. Sedimentology. 50, 979–1011.

Lassiter, J.C. (2003) Rhenium volatility in subaerial lavas: constraints from subaerial and submarine portions of the HSDP-2 Mauna Kea drillcore. Earth and Planetary Science Letters, 214, 311–325.

Liu, R., Hu, L., Humayun, M. (2017) Natural variations in the rhenium isotopic composition of meteorites. Meteoritics and Planetary Science, 52, 479–492.

Liu Z., Tian H., Yin R., Chen D. and Gai H. (2022) Mercury loss and isotope fractionation during thermal maturation of organic-rich mudrocks. Chem. Geol. 612, 121144.

Luo, G., Ono, S., Beukes, N.J., Wang, D.T., Xie, S., Summons, R.E. (2016). Rapid oxygenation of Earth's atmosphere 2.33 billion years ago. Science Advances, 2(5), e1600134.

Lyons, T.W., Reinhard, C.T., Planavsky, N.J. (2014) The rise of oxygen in Earth's early ocean and atmosphere. Nature, 506, 307–315.

Meisel, T. and Moser, J. (2004) Platinum-Group Element and Rhenium Concentrations in Low Abundance Reference Materials. Geostandards abd Geoanalytical Research, 28, 233–250.

Meixnerová, J., Blum, J.D., Johnson, M.W., Stüeken, E.E., Kipp, M.A., Anbar, A.D., and Buick, R. (2021) Mercury abundance and isotopic composition indicate subaerial volcanism prior to the end-Archean "whiff" of oxygen. Proceedings of the National Academy of Sciences, 118, 1–6.

Miller, C.A., Peucker-Ehrenbrink, B., Ball, L. (2009) Precise determination of rhenium isotope composition by multi-collector inductively-coupled plasma mass spectrometry. Journal of Analytical Atomic Spectrometry, 24, 1069–1078.

Miller, C.A., Peucker-Ehrenbrink, B., Schauble, E.A. (2015) Theoretical modeling of rhenium isotope fractionation, natural variations across a black shale weathering profile, and potential as a paleoredox proxy. Earth and Planetary Science letters, 430, 339–348.

Miller, C.A., Peucker-Ehrenbrink, B., Walker, B.D., Marcantonio, F. (2011) Re-assessing the surface cycling of molybdenum and rhenium. Geochimica et Cosmochimica Acta, 75, 7146–7179.

Morford, J.L., Emerson, S.R., Breckel, E.J., Kim, S.H. (2005) Diagenesis of oxyanions (V, U, Re, and Mo) in pore waters and sediments from a continental margin. Geochimica et Cosmochimica Acta, 69, 5021–5032.

Morford, J.L., Martin, W.R., Carney, C.M. (2012) Rhenium geochemical cycling: Insights from continental margins. Chemical Geology, 325, 73–86.

Neubert, N., Nagler, T.F., Bottcher, M.E. (2008) Sulfidity controls molybdenum isotope fractionation into euxinic sediments: Evidence from the modern Black Sea. Geology, 35, 775–778.

Norman, M.D., Garcia, M.O., Bennett, V.C. (2004) Rhenium and chalcophile elements in basaltic glasses from Ko'olau and Moloka'I volcanoes: Magmatic outgassing and composition of the Hawaiian plume. Geochimica et Cosmochimica Acta, 68, 3761–3777.

Ostrander C.M., Johnson A.C., Anbar A.D. (2021) Earth's First Redox Revolution. Annual Reviews in Earth and Planetary Science, 49, 337–366.

Ostrander, C.M., Nielsen, S.G., Owens, J.D., Kendall, B., Gordon, G. W., Romaniello, S.J., Anbar A.D. (2019) Fully oxygenated water columns over continental shelves before the Great Oxidation Event. Nature Geoscience, 12, 186–191.

Ostrander, C.M., Severmann, S., Gordon, G.W., Kendall, B., Lyons, T.W., Zheng, W., Roy, M., Anbar A.D. (2022) Significance of ^{56}Fe depletions in late-Archean shales and pyrite. Geochimica et Cosmochimica Acta, 316, 87–104.

Peel, K., Weiss, D., Chapman, J., Arnold, T., Coles, B. (2008) A simple combined sample–standard bracketing and inter-element correction procedure for accurate mass bias correction and precise Zn and Cu isotope ratio measurements. Journal of Analytical Spectrometry, 23, 103–110.

Philippot, P., Ávila, J.N., Killingsworth, B.A., Tessalina, S., Baton, F., Caquineau, T., Muller, E., Pecoits, E., Cartigny, P., Lalonde, S.V., Ireland, T.R., Thomazo, C., Van Kranendonk, M.J., Busigny, V. (2018) Globally asynchronous sulphur isotope signals require re-definition of the Great Oxidation Event. Nature Communications, 9, 2245.

Pitcher, L., Helz, R.T., Walker, R.J., Piccoli, P. (2009) Fractionation of the platinum-group elements and Re during crystallization of basalt in Kilauea Iki Lava Lake, Hawaii. Chemical Geology, 260, 196–210.

Rasmussen, B., Blake, T.S., Fletcher, I.R. (2005) U–Pb zircon age constraints on the Hamersley spherule beds: evidence for a single 2.63 Ga Jeerinah–Carawine impact ejecta layer. Geology, 33(9), 725–728.

Reinhard, C.T., Raiswell, R., Scott, C., Anbar, A.D., and Lyons, T.W. (2009) A Late Archean Sulfidic Sea Stimulated by Early Oxidative Weathering of the Continents. Science, 326, 713–716.

Romaniello, S.J., Field, M.P., Smith, H.B., Gordon, G.W., Kim, M.H., Anbar, A.D. (2015) Fully automated chromatographic purification of Sr and Ca for isotopic analysis. Journal of Anaytical and Atomic Spectrometry, 30, 1906–1912.

Selin N.E. (2009) Global Biogeochemical Cycling of Mercury: A Review. Annual Review of Environmental and Resources, 34, 43–63.

Sheen, A.I., Kendall, B., Reinhard, C.T., Creaser, R.A., Lyons, T.W., Bekker, A., Poulton, S.W., Anbar, A.D. (2018) A model for the oceanic mass balance of rhenium and implications for the extent of Proterozoic ocean anoxia. Geochimica et Cosmochimica Acta, 227, 75–95.

Slotznick, S.P., Johnson, J.E., Rasmussen, B., Raub, T.D., Webb, S.M., Zi, J.-W., Kirschvink, J.L., Fischer, W.W. (2022) Reexamination of 2.5-Ga "whiff" of oxygen interval points to anoxic ocean before GOE. Science Advances, 8, 1–10.

Stolper, D.A., Revsbech, N.,P., Canfield, D.E. (2010) Aerobic growth at nanomolar oxygen concentrations. Proceedings of the National Academy of Science, 107, 18755–18760.

Stüeken, E.E., Buick, R., Anbar, A.D. (2015) Selenium isotopes support free O2 in the latest Archean. Geology, 43, 259–262.

Sullivan, D.L., Brandon, A.D., Eldrett, J., Bergman, S.C., Wright, S., Minisini, D. (2020) High resolution osmium data record three distinct pulses of magmatic activity during cretaceous Oceanic Anoxic Event 2 (OAE-2). Geochimica et Cosmochimica Acta, 285, 257–273.

Sun, W., Bennett, V.C., Eggins, S.M., Kamenetsky, V.S., Arculus, R.J. (2003) Enhanced mantle-to-crust rhenium transfer in undegassed arc magmas. Nature, 422, 294–297.

Tessalina. S.G., Yudovskaya. M.A., Chaplygin. I.V., Birck. J.L., Capmas. F. (2008) Sources of unique rhenium enrichment in fumaroles and sulphides at Kudryavy volcano. Geochimica et Cosmochimica Acta, 72, 889–909.

Trendall, A.F., Compston, W., Nelson, D.R., De Laeter, J.R., Bennett, V.C. (2004) SHRIMP zircon ages constraining the depositional chronology of the Hamersley Group, Western Australia*. Australian Journal of Earth Science, 51, 621–644.

Weyer, S., Anbar, A.D., Gerdes, A., Gordon, G.W., Algeo, T.J., Boyle, E.A. (2008) Natural fractionation of $^{238}U/^{235}U$. Geochimica et Cosmochimica Acta, 72, 345–359.

Yudovskaya, M., Tessalina, S., Distler, V., Chaplygin, I., Chugaev, A., Dikov Y. (2008) Behavior of highly-siderophile elements during magma degassing: A case study at the Kudryavy volcano. Chemical Geology, 248, 318–341.

Zambardi, T., Sonke, J. E., Toutain, J. P., Sortino, F., Shinohara, H. (2009) Mercury emissions and stable isotopic compositions at Vulcano Island (Italy). Earth and Planetary Science Letters, 277 (1–2), 236–243.

CHAPTER 3

RHENIUM ISOTOPE RECONNAISSANCE OF URANIUM ORE CONCENTRATES (UOC)

3.1 Abstract

Exploration of natural isotopic variations of the element rhenium (Re) is in its infancy, with initial studies exhibiting isotopic fractionation in a variety of geological materials. I am investigating Re isotope variations as a new geochemical tool, given its redox-sensitive properties and affinity for organic matter and sulfides. In this work, Re abundance and isotope ratio data were collected from uranium ore concentrates (UOCs) across a variety of depositional ages, locations, and geologic settings. Ore types from which the UOC were derived include sandstone, unconformity, and quartz-pebble (QP) conglomerate. To isolate Re from the U-rich matrix of UOCs, I developed a new purification method utilizing DGA ion exchange resin. I found that UOCs exhibit a wide range of Re isotope ratios, with sandstone ore-derived UOCs having the isotopically lightest values, QP conglomerate ore-derived UOCs having the heaviest, and unconformity ore-derived UOCs in between these (with some overlap with sandstone UOCs). The Re isotope ratio range observed in the UOC samples extends literature data by more than a factor of two. Industrial processing (e.g., incomplete recovery of Re from ore, contamination, fractionation during processing) may play a role in the isotopic variability in the UOCs. However, systematic differences between ore types suggest that the depositional setting may also play a role. I find that Re isotope ratios combined with isotope ratio data from other elements provide unique geochemical signatures that can aid in the provenance assessment of UOCs for forensic investigations. Regardless of the

cause of the wide range of Re isotope ratios in samples, these initial data indicate Re is a promising tool for nuclear forensics.

3.2 Introduction

In the past two decades, advances in mass spectrometry have led to the discovery of significant variations in naturally occurring isotope ratios across the periodic table that arise from isotope fractionation processes (see Teng et al. (2017) and references therein). For example, heavy elements (> atomic number 42) were previously not thought to exhibit significant isotopic fractionation due to the large number of nucleons in these elements and the relatively smaller variation in mass caused by a difference of up to ~10 neutrons. However, it has since been discovered that these heavy elements exhibit significant isotopic fractionation caused by mass-dependent and mass-independent processes. New areas of research in geochemistry and other fields have since been opened by these discoveries.

One element that has recently begun to be explored for its natural isotopic variation is rhenium (Re), a heavy transition metal sensitive to environmental oxygen with important industrial and scientific applications. Despite its significance, only a handful of studies have investigated Re isotopic compositions (Miller et al., 2015; Liu et al., 2017; Dickson et al., 2020; Dellinger et al., 2020, 2021).

Rhenium has two primary isotopes, ^{185}Re and ^{187}Re that have average relative natural abundances of 37.4% and 62.6%, respectively. The isotope ^{185}Re is stable, whereas ^{187}Re is radioactive with a half-life of approximately 41.6 billion years (Smoliar et al., 1996; Selby et al., 2007), although this long half-life makes it effectively stable for

purposes as a geochemical tracer. The β^- decay of ^{187}Re into ^{187}Os is the basis of the widely used Re-Os dating technique. It was not until recently that modern mass spectrometry techniques began resolving isotopic variations in Re. Therefore, Re isotope ratio data has only been collected from a limited variety of materials including standard reference materials (e.g., basalts, serpentinites), meteorites, and black shale samples (Fig. 3.1). Currently, the range of isotopic fractionation during Re reduction – which is thought to be the main process influencing natural variations in Re isotopes ratios – has not been examined experimentally.

I am particularly interested in the potential for Re isotope fractionation to provide insights into ancient ocean redox conditions. In oxidizing waters, compounds containing redox sensitive metals such as Re, Mo, and U often form oxyanions that are soluble and not readily removed from solution. Mo and U are removed from seawater under oxic conditions by adsorption to iron/manganese (Fe-Mn) oxides. This process has a distinct mass-dependent isotopic fractionation that changes the seawater isotopic composition of these elements (e.g., Barling and Anbar, 2004; Brennecka et al., 2011). In contrast, Re (as the oxyanion $Re^{VII}O_4^-$) is largely unaffected by this process (Yamashita et al., 2007) because of the highly unreactive and stable behavior of perrhenate under oxidizing conditions. However, under reducing conditions, the valence state of Re can be reduced from Re^{VII} to Re^{IV}, likely leading to isotopic fraction due to differences in the bond strength between isotopologues, though this is yet to be confirmed experimentally. The reduced chemical species of Re (as ReO_2 or ReS_2 (Yamashita et al., 2007)) becomes insoluble and reactive with organic matter or sulfides (Colodner et al., 1993,1995; Morford et al., 2012), removing Re from seawater into these sediments. Thus, oxic

removal is important to Mo and U oceanic mass balances; but this is not the case for Re. Therefore, analyses of Re isotopes in geologic materials formed in different redox conditions can provide a unique redox sensitive geochemical tool.

Rhenium has other properties that make it unique and useful in geochemical and commercial applications. Rhenium is one of the least abundant naturally occurring elements at Earth's surface with a typical upper continental crust concentration of ~200 pg / g (Rudnick and Gao, 2003). It was the last stable element to be discovered (Noddack et al., 1925) due to the rarity of Re-specific minerals. Rhenium is in demand in the aerospace and petroleum industries due to its refractory properties in alloys which allows the creation of extremely heat and corrosion resistant materials, and for its catalytic properties, respectively (USGS, 2021). The abundance of Re in rocks deposited under reducing conditions can be significantly elevated from continental crust values by more than a factor of 100 (e.g., Colodner et al., 1993, 1995), similar to the enrichment of uranium. Rhenium is not known to have a biological role, but elevated abundances in brown algae (Yang, 1991) and certain plants have been observed (e.g., Novo et al., 2015; Tzvetkova et al., 2021).

Recent studies of natural Re isotope fractionation to have explored the potential of the Re isotopic system to infer past paleoenvironmental conditions (Miller et al., 2015), trace the oxidative weathering flux of petrogenic organic carbon through time (Dellinger et al., 2020, 2021), and understand early Solar System processes (Liu et al., 2017). Rhenium isotope variation is reported as δ^{187}Re, where δ^{187}Re is the relative difference of the ^{185}Re/^{187}Re ratio between a sample and the standard reference material (NIST 3143). The variability found to date spans 1.06 ‰ (Fig. 3.1), from -0.97 to 0.09 ‰ (Miller et al.,

2015; Liu et al., 2017; Dickson et al., 2020; Dellinger et al., 2020, 2021). The lightest value is from a heavily weathered black shale (Miller et al., 2015) and the heaviest value is from an iron meteorite (Liu et al., 2017).

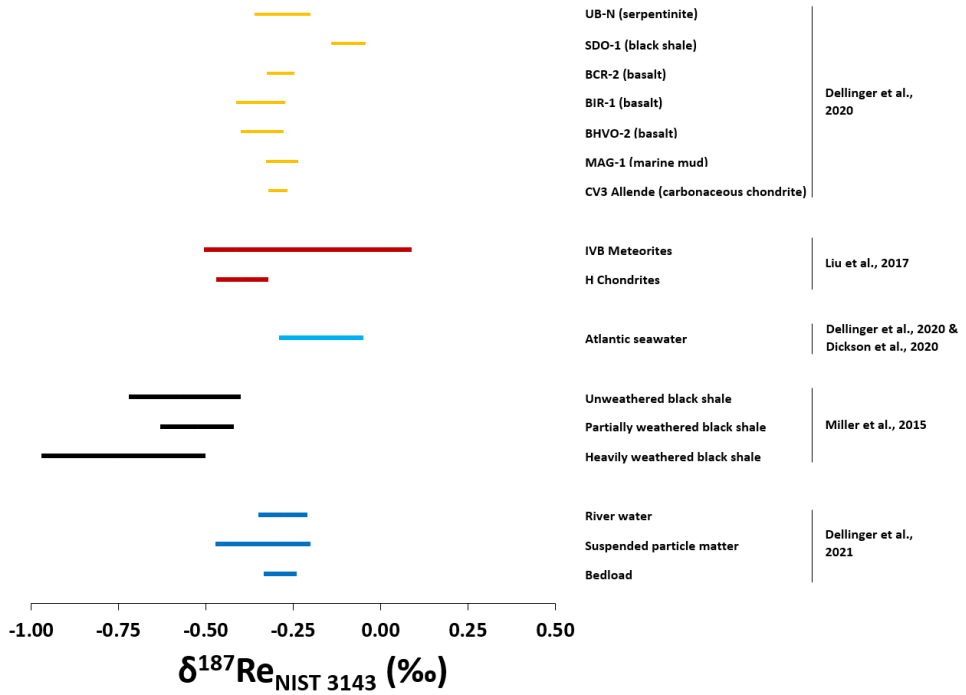

Figure 3.1 Compilation of Currently Published Re Isotope Ratio Data. δ^{187}Re data in the peer-reviewed literature, presented using NIST 3143 as the normalizing standard. Data are from Miller et al. (2015), Liu et al. (2017), Dickson et al. (2020), and Dellinger et al. (2020, 2021). Ranges for published data include 2sd error from the publications the data came from. One Fe-meteorite sample from Liu et al. (2017) with a very light δ^{187}Re value (-1.84 ± 0.03 ‰ 2SE), is excluded from this plot because a replicate analysis of the same sample with a value of -0.12 ± 0.03 ‰ 2SE was measured indicating the very light isotopic composition is an unreproducible outlier.

Re isotopic variations in uranium ore concentrate (UOC; also known as yellowcake), that can be significantly enriched in Re, have yet to be explored. UOCs are friable solids that contain a very high abundance of U, typically 60-80 wt. %. Uranium ore concentrates are made from mining natural U-rich deposits, followed by industrial processing to produce a U-rich concentrate. Exploration of elemental abundance and

isotope ratios (e.g., U, Mo, Sm, Nd, Pb) in UOCs has provided information about the natural behavior of these elements and have been found to be useful for nuclear forensics investigations (e.g., Brennecka et al., 2011; Varga et al., 2009, 2017, 2023; Rolison et al., 2019; Migeon et al., 2020; Shollenberger et al., 2021; Devlin McLoughlin et al., 2023).

UOCs are a globally regulated nuclear material that can be obtained on the open market. As diversion of nuclear material is a major concern for international governmental agencies due to the potential dangers from the material itself and the products that can be created (Kristo et al., 2016), UOC smuggling is a concerning issue. If UOC is found outside regulatory control, then it is important to be able to trace the source of the UOC to determine where it left the stream of legitimate transactions and where it may have originated. To provide tighter constraints and higher confidence in the provenance assessment of a sample, it is beneficial to increase the number of possible geochemical signatures that can be used. Signatures that are minimally modified during the milling process and exhibit a large range of isotope ratios are especially useful for identification purposes.

The geochemical signatures of the ore material can be retained or altered in the produced UOC. To create UOC, the mined U-rich ore is brought to a milling facility. At the mill, the ore is crushed and put through successive processes of extraction and purification of U followed by precipitation as a solid. The exact methods for U extraction vary based on the chemical composition of the ore material.

In this study I present the first δ^{187}Re data from UOC. The samples are derived from U-rich ore material including sandstone ore, unconformity ore, and quartz-pebble

(QP) ore. The results provide improved constraints on the range of Re isotope ratios that are possible and demonstrate the potential of Re isotopes as a nuclear forensics tool.

3.3 Samples and Methods

3.3.1 Sample U Ore Deposit Types

The International Atomic Energy Association (IAEA) categorizes U deposits chiefly by host rock and/or structure. Twelve total UOC samples in this study derive from sandstone, unconformity, and QP conglomerate deposits. The countries of origin and deposit types for the samples are taken from Brennecka et al. (2010), Krajkó et al. (2014), Reading et al. (2016), and Shollenberger et al., (2021).

Sandstone-type deposits form in low-temperature settings and refer to U accumulations from siliciclastic sedimentary rocks that were deposited in continental fluvial, lacustrine, or shallow-marine sedimentary environments. Uranium enrichments occur when low-temperature oxidized fluids (carrying soluble U^{VI}) interact with a reducing agent (e.g., sulfides, carbonaceous material, hydrocarbons) and precipitate U as U^{IV} (IAEA-TEC-DOC-328). While sandstone is not a major host of authigenic Re, organic-rich shale interbedding—which can host large amounts of Re—is a common geologic feature for these deposits. Therefore, the range of Re abundance in UOCs created from sandstone ore is likely to vary based on how much organic-rich shale material is included during the mining and milling process. Sandstone ore interbedded with black shales incorporated during mining will likely lead to UOCs with high Re abundances relative to UOCs derived from sandstone ore that does not include black shales.

Unconformity deposits form in high-temperature settings associated with metamorphic processes and include some of the largest and most abundant U deposits globally. Similar to sandstone deposits, this category includes U deposited via reduction of soluble U^{VI} to insoluble U^{IV}. The U ores often take the form of veins, breccias, and replacements. Since mining operations will target the veins, breccias, and replacements, Re abundances are expected to be low as these materials are likely not a major host for Re.

QP conglomerates are ancient U deposits formed during the Archean eon. There is ongoing debate if QP conglomerates have a detrital or hydrothermal origin (see Burron et al., 2018 and references therein). Regardless of the specific emplacement mechanism, QP conglomerates formed prior to the emergence of a widely oxygenated planet. The absence of oxygenation in the atmosphere and ocean would thus inhibit the release of Re. Therefore, the abundance of Re in QP conglomerate deposits is expected to be low.

3.3.2 Sample Preparation

3.3.2.1 Digesting UOC Samples

High-purity Seastar Baseline® concentrated nitric (HNO_3) and hydrochloric (HCl) acids were used throughout dissolution, sample preparation, and processing. High purity Milli-Q® water (18.2 MΩ x cm) was used for all dilutions. All sample processing was completed at Lawrence Livermore National Laboratory (LLNL) in a trace metal clean laboratory.

Powdered UOC samples (0.13 – 2.49 g) were weighed and placed into sealed Savillex® Teflon beakers with 4 N HNO_3 on a hotplate at 140° C for 72 hours. While this

process fully dissolved many of the samples, in some cases there was residual undissolved material. These samples were dried down and reconstituted in ~4 ml of concentrated HCl. These samples were then capped and heated at 140° C overnight, followed by drying and addition of 5 ml of aqua regia, capped and heated overnight at 140° C. This process was sufficient to fully dissolve all samples. Once all samples were in solution, they were dried and reconstituted in 10 ml 0.5 N HCl.

3.3.2.2 Purifying Re with Column Chromatography

Rhenium was purified from UOC samples using a DGA resin column chromatography protocol developed as part of this study. In preparation for column chromatography, all samples were transferred into 15 ml centrifuge tubes and centrifuged at 3000 RPM for 5 minutes. This was done to isolate any particles, visible or not, in the samples. The supernatant was decanted into new beakers. These decanted samples were then loaded onto 1 ml Eichrom DGA resin cartridges in a vacuum box (at a flow rate of ~1.5 ml/min) and purified following the protocol in Table 3.1. The column chemistry protocol was based on elemental partition coefficients from Pourmand and Dauphas (2010) for DGA resin. To minimize blank contributions during column chromatography, all materials were acid cleaned using 0.32 N HNO_3 + 0.1% hydrofluoric acid (HF) prior to use. The DGA resin cartridges were washed, conditioned with 0.5 N HCl (the loading acid), then the samples were loaded in 10 ml 0.5 N HCl (Table 3.1). These matrix removal steps were loaded in 5 ml increments which were allowed to pass through the column completely before the next volume was added. Rhenium was eluted into Savellix® beakers with 12 ml of 10 N HNO_3 in increments of 2 ml, 4 ml, 4 ml, 2 ml.

Table 3.1 Column Chemistry Protocol to Purify Re from UOCs

Description	Volume (ml)	Acid Normality	Acid Type
Wash Resin	5	10	HNO_3
	5	0.1	HNO_3
	5	0.5	HNO_3
	5	0.5	HCl
Condition Resin	10	0.5	HCl
Load Sample	10	0.5	HCl
Matrix Removal	15	0.5	HCl
	10	0.5	HNO_3
	5	0.1	HNO_3
Elute Re	12	10	HNO_3

To remove any organic material present in the Re elution solutions from the column chemistry protocol (seen as brownish coloration to the dried down samples), the samples were fluxed and dried down in ~200 µl of aqua regia in Savillex® beakers (uncapped) at 140-150° C. The samples took approximately 20 minutes to reach dryness after the addition of aqua regia. This procedure was repeated until the samples were visibly colorless when dissolved in ~1 – 2 ml of dilute nitric acid which indicated near complete removal of organic material from the samples.

3.3.3 Elemental Concentration Analyses

Rhenium abundances were measured with a Thermo Scientific iCAP-Q at Arizona State University. An aliquot representing ~1% of the post-column chromatography Re elution solution was taken from each sample and diluted with 0.32 N HNO_3. Due to the extreme matrix effects from U in unadulterated UOCs, Re

concentrations are shown from aliquots of solution collected following the first round of column chemistry.

Samples were analyzed in the same analytical session using multi-element calibration standards. An internal standard containing Sc, Ge, Y, In, and Bi was introduced to the instrument in parallel with all samples and standards to correct for signal drift. A check standard containing all the elements in the calibration standards was analyzed after every 5 samples to assess accuracy and precision throughout the analytical session. The relative standard deviation of each analyte in the check standard was typically less than 2%, and the uncertainty associated with each abundance measurement is ± 10%.

The UOC standard CUP-2 has a reference Re abundance of 24 ± 8 (2SD) ng/g (Denton et al., 2022). CUP-2 was included in this study and, post-chemistry, was determined to have a Re abundance of 19 ± 2 ng/g (2SD). This agreement in pre- and post-chemistry indicates that the chemical separation process successfully extracted the majority Re from the samples with minimal loss of Re. Additionally, 100 ng of the Re standard NIST 989 was put through the column chemistry procedure and a recovery of 100 ± 6 % was calculated between the post- and pre-chemistry samples.

3.3.4 Isotope Ratio Analyses

Rhenium isotope ratios were measured on a Thermo Scientific Neptune Plus multi collector inductively coupled plasma mass spectrometer (MC-ICP-MS) at LLNL in low resolution mode. Samples were prepared in 0.32 N HNO_3 and introduced to an Apex 2 IR desolvating nebulizer. Samples were run at 20 ng/g Re. The ion beam intensity of each

sample was confirmed to match the intensity of the standard by ± 10%. This was done via concentration checks on the MC-ICP-MS prior to isotopic analysis.

3.3.4.1 Use of Tungsten for Mass Bias Correction

Since Re has only two isotopes, an element spike with a similar mass and ionization efficiency is used to correct for internal mass bias during the analytical session. Due to its similar mass and ionization efficiency, the element tungsten (W) represents a good analog for Re and has been used as a monitor for instrumental mass bias in previous Re isotopic publications (Miller et al., 2015; Liu et al., 2017; Dickson et al., 2020; Dellinger et al., 2020, 2021). The element spike approach has been applied to other elements such as Mo before a double spike was created and commonly used (Anbar et al., 2001).

Since W is used as a monitor for mass bias, it is crucial to quantitatively remove native W from the samples to blank levels in the chemical separation process prior to W addition. After the first round of column chemistry, there was detectable W present in some of the samples. To ensure no detectable W remained, all samples were put through the column chemistry protocol a second time to further remove the natural W, as well as any other remaining matrix elements. Prior to isotopic analysis, all samples were determined to have near-blank intensities of native W and U abundances. Following this confirmation, a W standard was added to each sample to reach 35 ng/g W. The appropriate abundance of W was confirmed with concentration checks on the MC-ICP-MS for each sample. In this process, the signal intensity on ^{186}W was checked to confirm that the samples and standards matched within ± 10%, and that the Re/W ratios of the

samples were within 10% of that of the standard. Instrumental mass bias was corrected using standard-sample-standard bracketing with NIST 3143 and the added W.

Importantly for preparing MC-ICP-MS solutions, W is only stable in solution for weeks to months in dilute nitric acid without HF. Therefore, the W standard bottle used contained ~1% HF and 1% HNO_3, whereas the Re standard and samples with W added did not include additional HF. Adding dilute HF to the samples would have increased the hazard of the chemistry and potentially altered the behavior of Re or other elements during MC-ICP-MS analysis. Therefore, all samples and standards in this study were analyzed within hours to days after the addition of W.

3.3.4.2 Nomenclature and Instrument Parameters

The isotopic compositions of Re are reported in delta (δ) notation shown in equation (3.1).

$$\delta^{187}\text{Re}\ (‰) = [(^{187}\text{Re}/^{185}\text{Re})_{\text{sample}} / (^{187}\text{Re}/^{185}\text{Re})_{\text{NIST 3143}} - 1] \times 1000 \qquad (3.1)$$

δ^{187}Re data are reported as an average of multiple runs, except for one sample (Enusa) which was run only once due to the low abundance of Re in the sample. Uncertainties are listed as the 2SD of replicate analyses of samples when $n \geq 3$, or the uncertainty of replicate standard analyses of NIST 989 (± 0.05 ‰ 2SD, n = 22), whichever is higher.

Each individual run included 50 cycles with an integration time per cycle of 8.4 s. A jet sample cone and an H skimmer cone were used. An Apex 2 IR was used with a N gas flow rate of 2.41 – 2.5 mL/min, and a 50 µl/min nebulizer was used to uptake samples via aspiration. The signal intensity obtained on ^{187}Re for a 20 ng/g Re solution ranged from 1.15 – 1.35 V. The signal intensity obtained on ^{186}W for a 35 ng/g W

solution ranged from 0.85 – 1.00 V. All detectors were 10^{-11} Ω and signals at ^{182}W, ^{184}W, ^{186}W, ^{185}Re, ^{187}Re, and ^{190}Os were monitored.

3.3.4.3 Accuracy and Precision of Re Isotope Measurements

In addition to using W-doping during Re isotopic measurements, standard-sample-standard bracketing was utilized throughout all analytical sessions. The accuracy and precision of the Re isotope measurements was assessed by regularly analyzing the Re standard NIST 989 compared to the Re standard NIST 3143. These materials were introduced to the MC-ICP-MS in 0.32 N HNO_3, the same acid and molarity as all samples. The repeated analysis of NIST 989 yielded $\delta^{187}Re$ = -0.28 ± 0.05 ‰ (2SD, *n* = 22) (table 2). This value agrees with previous studies (Miller et al., 2015; Liu et al., 2017; Dickson et al., 2020; Dellinger et al., 2020, 2021). As NIST 989 is out of production, I used the Re standard NIST 3143 for the δ=0 value, as in Dickson et al. (2020).

Table 3.2 UOC Quality Control Tests. $\delta^{187/185}Re$ and [Re] from replicate UOC samples and standards using NIST 3143 as δ=0 and W mass bias correction. n indicates the number of replicate analytical measurements. *Denotes replicate samples that were put through individual Re purification procedures. Errors represent the 2SD of replicate analyses or the 2SD of the error on standards, whichever is higher.

Label	Description	$\delta^{187}Re$ (‰)	2SD	n
Re Standards	SRM 989	-0.28	0.05	22
	Processed SRM 989	-0.32	0.04	4
Replicate Samples	Union Carbide #1*	-0.49	0.07	8
	Union Carbide #2*	-0.49	0.10	8
Replicate Samples	Somair (20 ppb Re)	0.18	0.07	3
	Somair (40 ppb Re)	0.16	0.02	3
100 ppt U	Varying [U] doped into constant [Re] and [W] (20 ppb Re and 35 ppb W)	0.27	0.07	5
1 ppb U		0.25	0.10	5
10 ppb U		0.26	0.04	5
100 ppb U		0.26	0.08	5
1 ppm U		0.24	0.04	5

A process blank was put through the same procedures as the UOC samples and resulted in a total blank contribution of 195 pg Re (n = 1), less than 1% of the Re in each sample and considered negligible.

To determine if the column chromatography procedure provided reproducible data and did not introduce isotopic fractionation, two tests were performed: 1) 100 ng of NIST 989 was put through the column procedure (Fig. 3.2, Table 3.2), and 2) the sample Union Carbide was digested then the solution was split in half before any column chromatography steps. The two halves were labeled UC1 and UC2.

For test 1, the δ^{187}Re composition of the processed NIST 989 was -0.32 ± 0.04 ‰ (2SD, n =4) which agrees within uncertainty with the pure, unprocessed standard value of -0.28 ± 0.05 ‰ (2SD, n = 22; Fig. 3.2). For test 2, UC1 and UC2 had the same isotopic composition within analytical error -0.49 ± 0.07 ‰, -0.49 ± 0.10 ‰, respectively (2SD, n = 8 for both). The test 1 data indicates that the column chemistry procedure does not express isotopic fractionation, and test 2 indicates that the column chromatography procedure is reproducible.

To collect high precision Re isotope ratio data with the lowest ng of Re possible, I examined the precision of δ^{187}Re data with different Re concentrations in the running solution. To do this, an aliquot of the UOC from Somair was analyzed at 40 ng/g Re (+70 ng/g W) as well as at 20 ng/g Re (+35 ng/g W) (Fig. 3.2). Not surprisingly, I found increased precision when measuring at the higher concentration (δ^{187}Re = 0.16 ± 0.02 ‰, n = 3) compared to 20 ng/g Re (δ^{187}Re = 0.18 ± 0.07 ‰, n =3) and the accuracy agreed within uncertainties (Fig. 3.2, Table 2). The majority of UOC samples in this study did not have enough Re for multiple isotope ratio measurements at 40 ppb. A minimum of

~10 ng of Re is required for one isotope ratio measurement with the utilized sample uptake rate of 50 µl/min and 10^{-11} Ω detector. Therefore, all samples were run at 20 ppb for consistency in the data.

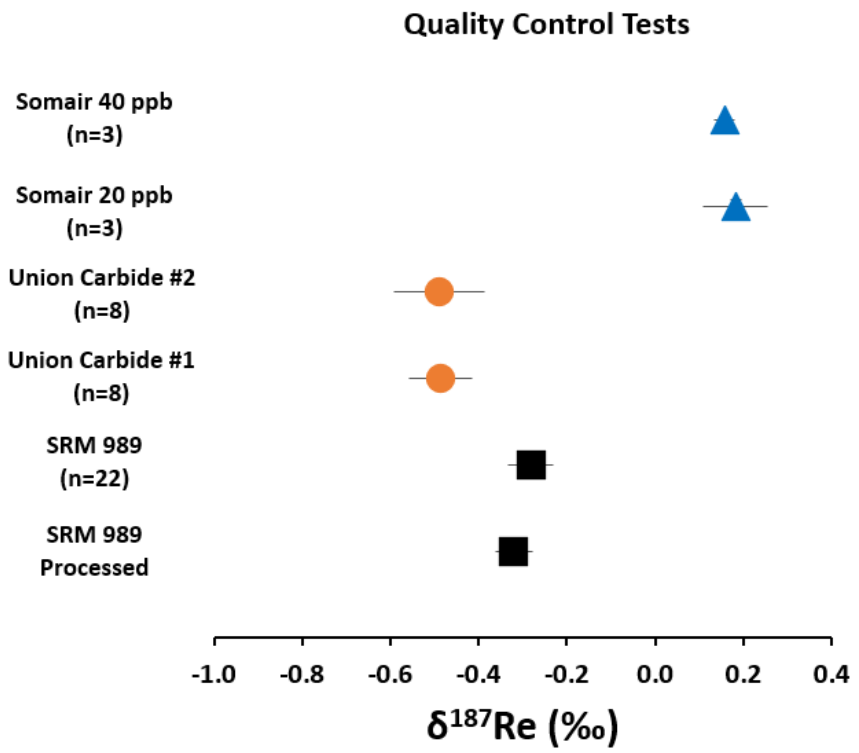

Figure 3.2 Standards and UOC Re Isotope Ratio Quality Control Tests. Quality control tests to ensure accurate isotope ratio data was collected. n for each sample indicates the number of replicate analytical measurements on the same sample. The processed standard NIST 989 was put through the column chemistry protocol and is compared to the unprocessed check standard average. Replicate isotope ratio analyses of separate Union Carbide samples were collected. Finally, the sample Somair was analyzed at 20 ng/g Re and 35 ng/g W as well as 40 ng/g Re and 70 ng/g W and resulted in a similar value and increased precision when running with increased signal intensity on the MC-ICP-MS. δ^{187}Re error bars represent the 2SD of replicate analyses, or the 2SD of replicate standard analyses, whichever is larger.

The matrix of UOC samples is >60 wt. % U. With such a high content of U in the matrix, there is potential to impact the stability of the plasma which could influence the accuracy and precision of the measured Re isotope ratios (e.g., Andrén et al., 2004). Even though all samples in the study were tested for near-blank abundances of native U prior

to Re isotopic measurement, I tested the tolerance of the plasma to high matrix abundances of U present to determine if U present in the matrix influenced the measured Re isotope ratios. I created five standards with 20 ng/g Re (+35 ng/g W) in 0.32 N HNO_3 that were each doped with varying amounts of U, ranging from 100 pg/g to 1 µg/g, increasing by an order of magnitude between steps. I found that even with 1 µg/g U (Re/U = 0.02), there was no isotopic deviation relative to the pure Re standard (Fig. 3.3, Table 3.2), indicating that even incomplete removal of U from the Re solution could still result in accurate δ^{187}Re data, up to at least 1 µg/g U.

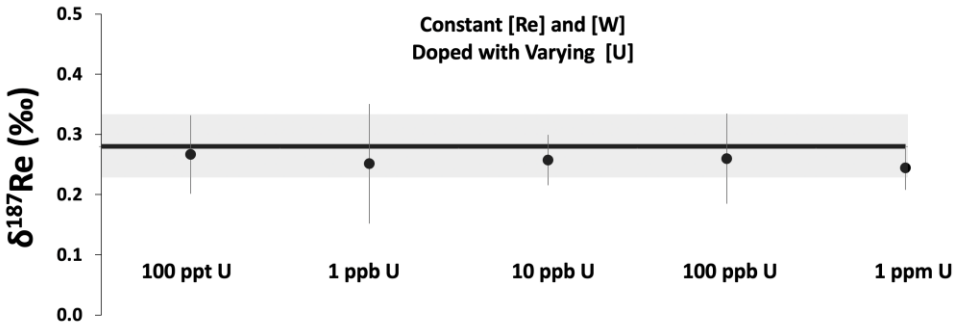

Figure 3.3 U Doping Tests. Doping tests of constant 20 ng/g NIST 3143 Re and 35 ng/g W standard with varying abundances of U. Each sample was analyzed five times and uncertainties represent the 2SD of the replicate analyses. The bracketing standard is NIST 989. The average of pure NIST 989 standard analyses is shown as the horizontal black line, and the shaded area is the 2SD (± 0.05 ‰**,** *n* = 22) of replicate standard analyses.

3.4 Results

3.4.1 Uranium Ore Concentrate Re Geochemical Data

Twelve UOC samples with known origins and depositional settings were analyzed for Re isotope compositions. The UOC samples display a δ^{187}Re range of -0.99 to 1.33 ‰ (Table 3.3, Fig. 3.4). These variations are significantly greater than the minimum

uncertainty associated with δ^{187}Re measurements of 0.05 ‰ (2SD, n = 22) determined by analyses of standards.

I analyzed eight UOC samples derived from sandstone deposits. Their δ^{187}Re ranged from -0.99 to 0.62 ‰ with an average of -0.41 ‰. The abundance of Re ranged from 37-1795 ng/g. Three UOC samples derived from unconformity deposits were analyzed and the δ^{187}Re ranged from -0.31 to 0.37 ‰. The abundance of Re ranged from 14-36 ng/g. The lone QP conglomerate deposit had a Re abundance of 19 ng/g and a δ^{187}Re of 1.24 ‰ ± 0.09 ‰ (2SD; n = 3).

Table 3.3 UOC Re Geochemical Data. δ^{187}Re, [Re], geologic information, and sample identifiers for UOC samples. NIST 3143 is used as δ=0 and W mass bias correction. n indicates the number of replicate analytical measurements. Errors for δ^{187}Re data represent the 2SD of replicate analyses, or the 2SD of replicate standard analyses, whichever is larger. IAEA = International Atomic Energy Agency.

Category	Deposit Type	Country and Identifier	Basin / Region	Re (ng/g)	δ^{187}Re (‰)	2SD	n	~Age	Age/Region Source
Low-temperature redox	Sandstone	Niger - Somair	-	1795	0.18	0.07	3	-	
	Sandstone	USA - Chevron Hill	-	81	0.57	0.05	4	-	
	Sandstone	USA - Everest Yellow	-	37	-0.47	0.05	4	-	
	Sandstone	USA - Irigary	Wyoming	1263	-0.72	0.05	4	-	IAEA database
	Sandstone	USA - Pathfinder	Wind River	86	-0.73	0.05	4	22 Ma	Dooley et al., 1974
	Sandstone	USA - Petrotomic	-	775	-0.94	0.05	4	-	
	Sandstone	USA - Shirley Basin	Wind River	532	-0.67	0.06	4	22 Ma	Dooley et al., 1974
	Sandstone	USA - Union Carbide	-	924	-0.49	0.08	16	-	
High-temperature redox	Unconformity	Australia - Rum Jungle	N. Territory	36	-0.23	0.08	4	1627-232 Ma	Von Pechmann, 1986
	Unconformity	Canada - Key Lakes	-	30	0.29	0.08	5	-	
	Unconformity	Spain - Enusa	-	14	0.13	0.05	1	-	
Non-redox	QP Conglomerate	Canada - Blind River (CUP-2 standard)	Elliot Lake	19	1.24	0.09	3	2.45-2.2 Ga	Bennett et al., 1991

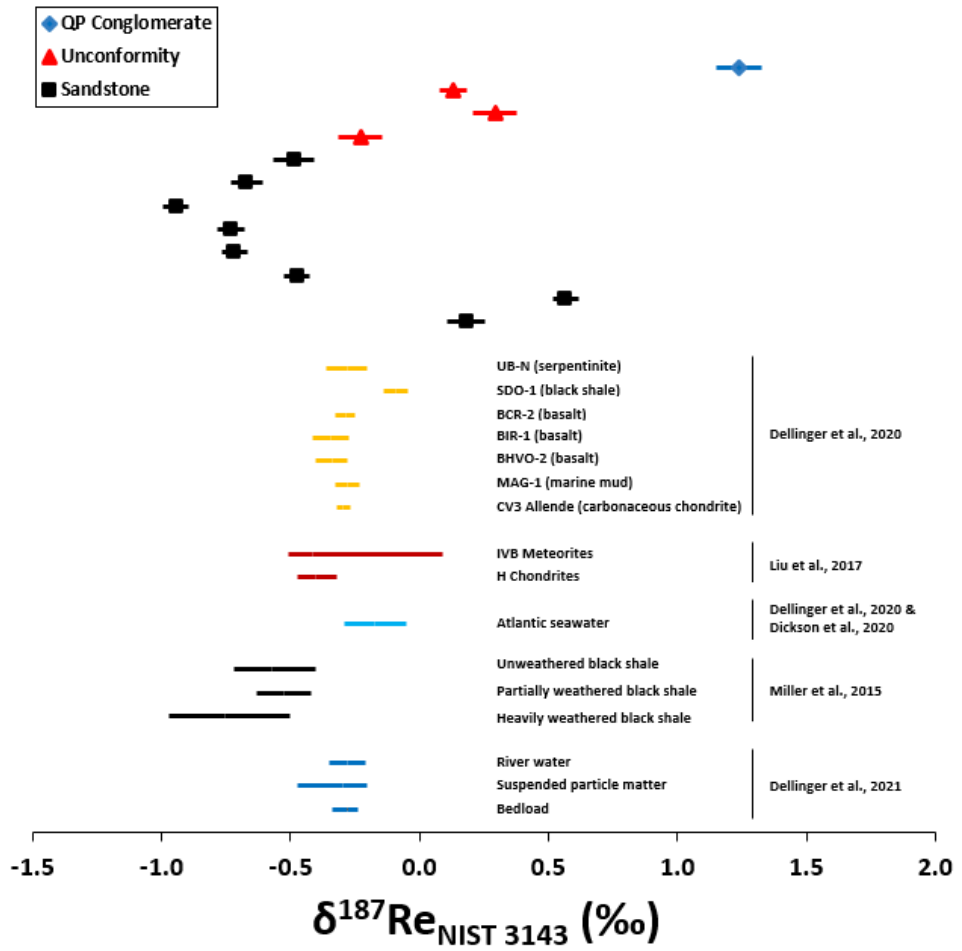

Figure 3.4 UOC Data With Published Re Isotope Ratio Data: Uranium ore concentrate δ^{187}Re data grouped by ore type: sandstone (black square), unconformity (red triangle), and quartz-pebble (QP) conglomerate (blue diamond) with published δ^{187}Re data (using NIST 3143 as the normalizing standard; Miller et al., 2015; Liu et al., 2017; Dickson et al., 2020; Dellinger et al., 2020, 2021). Error bars for UOC data represent the 2SD of replicate analyses, or the 2SD of replicate standard analyses, whichever is larger.

3.5. Discussion

The UOC samples from this study were created by milling U-rich ore material. The milling procedure consists of chemical leaching, solvent extraction, ion exchange separation techniques, and evaporation. The exact procedures that the samples underwent are unknown. Therefore, there are two possibilities to explain the δ^{187}Re values in the UOC samples: 1) The δ^{187}Re data from UOCs represent the bulk isotopic composition of

the ore material it is produced from, or 2) δ^{187}Re data of UOCs is offset due to fractionation during processing and/or contamination. These possibilities are discussed in detail below.

3.5.1 UOC Production and Geochemical Data

There is high variability in the abundance of Re in the UOC samples with a range from < 10 ng/g to 1795 ng/g (± 10% uncertainty on concentration data; Fig. 3.5). For context, in Phanerozoic black shales, the average Re abundance is ~155 ng/g (Sheen et al., 2018), and the average Solar System abundance (from CI chondrites) is ~37 ng/g (Anders and Grevesse, 1989; Lodders, 2003). While some of the Re concentration variation in UOCs could be caused by the treatment of the ore, there is also a distinct difference in the range of Re abundances between sandstone ore-derived UOCs (37-1795 ng/g), and UOCs derived from unconformity ore (<10 – 36 ng/g) or QP conglomerate ore (19 ng/g). Even though sandstone is not a major host of Re, the large range of Re concentrations is plausibly explained by incorporating organic-rich shales with the mined sandstone ore material. This is because Re (and U) in low temperature settings has an affinity to be removed from solution in association with organic matter and/or sulfides under reducing conditions (e.g., Colodner et al., 1993; Helz and Dolor, 2012; Morford et al., 2012; Helz, 2022). Thus, sandstone UOC ore material that contained organic rich shales could lead to UOCs with high Re abundances. However, there is no correlation between Re abundance and δ^{187}Re, indicated by an R2 value of 0.0877 calculated with all samples (Fig. 3.5). If black shale incorporation is indeed the reason for the very high Re abundances of some sandstone ore-derived UOCs, Re from black shales would

overwhelm the Re isotopes in those UOCs. If black shale incorporation is the cause of the high Re abundances, this would imply that the isotope compositions of black shales exhibit a wide range of fractionation that can overlap with the isotopic composition of basalts. Alternatively, the lack of correlation between Re abundance and δ^{187}Re may indicate isotopic fractionation during the processing of UOC samples and/or that contamination is affecting the isotopic ratios of the samples.

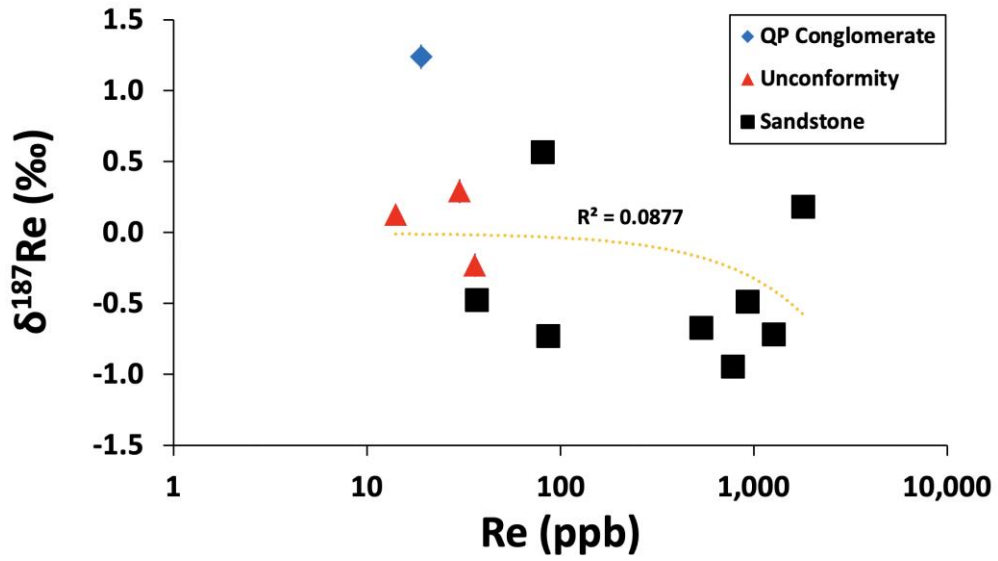

Figure 3.5 UOC Re Isotopes vs. Re Abundance. Rhenium isotope ratio data compared to Re abundance (log scale). This figure highlights the lack of correlation between Re abundance and isotopic composition for the ore types and the large range in [Re] of UOC in the samples. R^2 value calculated from all UOC data and gives a value of 0.0877 which indicates no correlation between δ^{187}Re and Re abundances. δ^{187}Re error bars represent the 2SD of replicate analyses, or the 2SD of replicate standard analyses, whichever is larger. In most cases, the symbols are larger than the error bars.

Multiple studies have examined the behavior of different elements throughout the production of UOC (e.g., Varga et al., 2017, 2013; Migeon et al., 2020). For example, U isotope data from UOCs has been inferred to represent the isotopic composition of the original ore material (e.g., Stirling et al., 2007; Bopp et al., 2009; Brennecka et al., 2010). However, paired isotopic analysis of Mo in ore material and the produced UOC has

found the UOC Mo isotope ratios can be fractionated during processing (Migeon et al., 2018,2020; Rolison et al., 2019). The milling process can lead to Mo fractionation in both positive (leaching, evaporation) and negative (solvent extraction, ion exchange, precipitation) directions with the magnitude of fractionation related to the recovery of Mo and the type of processes utilized during purification (Migeon et al., 2018, 2020). The range of fractionation in UOC extends to more negative Mo isotope values than has been found in natural systems, by ~ 1 ‰ (see Kendall et al., 2017 and references therein for a discussion of the natural range of Mo isotope values). Additionally, Rolison et al. (2019) found a + 0.75 ‰ fractionation in a UOC sample compared to the ore that it was produced from, which could be explained by adsorption of the light Mo isotope to Fe-Mn oxides during UOC production. In solution, the lighter isotopes of Mo preferentially adsorb to Fe-Mn oxides which would leave a heavy Mo isotope signature in the soluble phase. However, adsorption to Fe-Mn oxides is likely not a fractionation mechanism for Re, as Re does not significantly adsorb to Fe-Mn oxides (Yamashita et al., 2007). Therefore, this would likely not influence the isotopic composition of Re in UOCs. Future work constraining Re isotope fractionation factors by ore material and paired UOC throughout production stages will be useful to determine if there is Re isotopic fraction during processing. – and if Re isotope compositions could be useful in determining the processing methods used in purification of uranium from ore.

3.5.1.1 Possible Isotopic Fractionation Pathways During UOC Production

Fractionation of Re isotopes during UOC processing could have occurred if Re was incompletely removed from ore material, or incompletely recovered during purification procedures. Studies of Re purification via column chromatography using AG 1 X-8 (100-200 mesh) resin show that during Re recovery, the initial isotopic composition of Re that is collected is isotopically heavy, with the first 30% of Re being isotopically heavy by ~0.35 ‰ (Miller et al., 2009). This behavior is consistent with what has been reported from studies of other isotope systems on different resins (e.g., W: Irisawa and Hirata, 2006; Ca: Russell et al., 1978). If industrial purification processes behave similarly to laboratory processes, it is likely that fractionation introduced from incomplete recovery of Re would lead to heavier Re isotope ratios in the soluble phase, leaving light isotopes on the ion exchange resin.

While large amounts of isotopic fractionation are unlikely caused by UOC production, Varga et al. (2017) studied elemental abundances in UOCs and paired QP conglomerate ore material and found poor recovery of Re during the processing of the QP conglomerate ore. It is unknown if the QP conglomerate UOC in this study (CUP-2) underwent the same processing methods as the samples from Varga et al. (2017), but it is interesting that CUP-2 has the heaviest δ^{187}Re (1.24 ± 0.09 ‰ 2SD) of any sample measured so far. Incomplete transfer of Re from the ore material to the produced UOC could be the cause of the heavy isotopic compositions of CUP-2.

3.5.1.2 Possible Re Contamination During UOC Production

Rhenium contamination can occur if multiple ores are processed at the same facility, or if there is Re present in the reagents used to process the UOCs. Some UOC samples have orders of magnitude higher Re abundance than the others (Fig. 3.5) which likely arises from differences in Re abundance of the bulk ore material. If a mine processed high Re concentration ore as well as low Re concentration ore, this could lead to contamination between samples. It is important to note that UOC is a product that represents the average isotopic composition for the mined area and not distinct parts of the ore body. Milling facilities are generally within a radius of approximately 160 km to the mine(s) from which the ore is sourced (Kristo et al., 2016). Therefore, it is not unusual that all ore from a single mine is processed at a single facility, which indicates contamination from different ore materials processes at the same mill is likely uncommon. Within ore material from a single mine, there could also be Re abundance and isotopic ratio variations which could vary based on the lithology of the ore material. Sandstone UOCs have the largest variation in abundance by far (from 37 – 1795 ppb), while unconformity and QP conglomerate UOCs have low Re abundances relative to sandstone UOCs (ranging from 19-36 ppb). However, there are only three unconformity and one QP conglomerate samples in this data set, and this range will likely change as more samples are analyzed. Therefore, if a mine mills sandstone ore and other ore types, there is a possibility that traces of high Re abundance sandstone material could noticeably contaminate other samples with lower Re abundances.

Re contamination from reagents during the manufacturing process is possible. This would have been a particularly big issue for ores with low Re abundance. During

UOC processing, the reagents used vary based on ore type. Reagents that would be the most likely to have a high Re blank are those that contain - or are derived from - material that has a high abundance of Mo. This is because Mo and Re are known to concentrate together. Therefore, reagents such as phosphomolybdate, which is used to concentrate U during the milling process, may have a high Re blank. However, more work is needed to determine what the expected Re blank is in processing reagents.

Natural contamination sources that could have influenced the UOC samples are limited. This is because Re is one of the rarest elements at Earth's surface and it has an extremely low abundance in the atmosphere. It was recently noted by Ogric et al. (2023) that anthropogenic activities such as coal burning during power generation can lead to Re emissions that can be detected in stream waters (~1.5 pmol/m^2/yr), and surface soils downstream and downwind of the facilities that generated the emissions. Therefore, is it possible to have Re contamination from an atmospheric source, though this Re background, if present, is expected to be negligible due to relatively higher abundance of Re in the UOCs. Rhenium abundances in precipitation have been found to range from 0.03 – 5.90 pmol / kg (Miller et al. 2011), which indicates Re contamination from rainwater is possible, but also likely negligible. However, the large range in Re abundances of rainwater suggest that local, high abundance Re emissions may lead to high Re in rainwater. However, the residence time of Re in the atmosphere has yet to be studied so it is difficult to constrain what influence this may have on Re blanks during UOC production.

3.5.2 Natural Processes That Can Cause Isotopic Fractionation

Natural mass-dependent fractionation (MDF) of isotopes can be divided into two primary categories: biotic and abiotic. Both biotic and abiotic MDF can manifest during chemical speciation changes. However, abiotic MDF is primarily the driver of fractionation without redox changes (e.g., adsorption to Fe-Mn oxides as was discussed for Mo). Biotic MDF is possible for elements with important biologic roles (e.g., fixing of N_2 into NH_3), as well as elements without a biologic role (e.g., microbial reduction or methylation of Hg). Nitrogen fixation preferentially fixes the light isotope (Delwiche and Steyn, 1970). Similarly, microbial reduction and methylation of Hg preferentially use lighter isotopes (Kritee et al., 2007; Rodriguez-Gonzalez et al., 2009). Rhenium is a heavy element, thus the MDF range can be estimated to be similar to other heavy elements such as U and Hg which exhibit ranges of ~4 ‰ (Andersen et al., 2017 and references therein) and ~6 ‰ (Blum et al., 2014 and references therein), respectively.

Re does not have a biologic role, but some organisms in the ocean and land plants have been found to have high Re abundances which could lead to isotopic fractionation during uptake. Yang et al. (1991) found that brown algae have elevated Re abundances. The isotopic composition of Re has also been shown to be consistent through depth profile studies of Atlantic seawater (Dickson et al,, 2020; Dellinger et al., 2021), though this data is only from the Atlantic Ocean and more data is needed to confirm that the ocean has a homogenous Re isotopic composition. On land, if there is isotopic fractionation during plant uptake of Re, it would likely have an isotopic fractionation and influence the isotopic composition of the flux of Re to the oceans via rivers. Therefore, this is not a fractionation mechanism that would directly influence the UOC samples.

Abiotic MDF processes are expected to be the largest driver of isotopic fractionation of Re in the ore material. Rhenium isotope fractionation is likely to occur during reduction in solution, precipitation from solution, and during remobilization in a solid phase from postdepositional fluid interactions. These are all processes that can occur during ore formation. Sorption reactions are expected to be negligible as the oxidized form of Re perrhenate ($Re^{VII}O_4^-$) is predominantly soluble and does not exhibit significant adsorption to Fe-Mn oxides (Yamashita et al., 2007), evidenced by the consistent Re abundance and isotopic composition of seawater. Ocean and atmospheric redox variations have occurred throughout Earth history (see Lyons et al., 2014) which likely altered the Re isotopic composition of the ocean, and therefore the sediments that formed in the ocean which can be used as ore material today.

The age of the ores that the UOCs in this study were derived from vary throughout geologic time, from the Archean (~4 – 2.5 billion years ago) through the Phanerozoic (~542 million years ago to today). Sandstone ore-derived UOCs and unconformity ore-derived UOCs would be influenced by changing redox conditions as they are, at least in part, composed of sedimentary rocks. There are age constraints for some of the UOCs (Table 3.3) with ages that range from 22 million years ago at the youngest to 2.5 billion years ago as the oldest. The variations in the oxygenation of the ocean and atmosphere have influenced the release of Re into the oceans and capture of Re into sediments (see Sheen et al., 2018 for a more thorough discussion of Re mass balance through geologic time). The QP-conglomerate ore-derived UOC sample likely formed before the emergence of a consistently oxygenated atmosphere, therefore this

lone sample's ore material may have an isotopic composition that was not been altered by natural redox-related processes.

If the range of Re isotope fractionation is similar to the ranges of U and Hg, the 2.32 ‰ range found in this study will likely expand as more data is collected from natural materials and other UOCs. However, there is so little data on Re isotopes in geologic samples and a lack of studies on natural Re fractionation mechanisms that the fractionation cannot be definitively attributed to any source(s). If this range of fractionation is natural, it will have significant implications for Re-Os dating which is discussed in section 4.3.

3.5.2.1 Sandstone Ore δ^{187}Re Data

Sandstones are derived primarily from weathered continental material. Consequently, the δ^{187}Re values of sandstone-ore derived UOC would be expected to closely match granitic material and fall within a narrow range with low Re abundance. So far, the isotopic composition of granitic material is yet to been analyzed. Sandstone layers are often found interbedded with shale layers. Black shales can contain up to micrograms per gram (µg/g) levels of Re derived from seawater. The Re isotopic composition of black shales may be influenced to some extent by low-temperature redox-related fractionation during deposition. Additionally, postdepositional mobilization of Re could cause isotopic fractionation in black shales. Miller et al. (2015) investigated Re mobilization and isotopic variation in a single subaerial black shale bed that ranged from heavily weathered to well-preserved. They found a substantial loss of the heavy Re isotope during weathering (~0.3 ‰ shift), coupled with more than 90% loss of Re and

over 75% loss of total organic carbon. This suggests that as oxidative weathering progresses, the heavy isotope is preferentially released in the fluid phase. Thus, leaving behind a lighter isotopic composition in the black shale. Data from the Mackenzie River basin further supports this trend, where river water exhibits heavier δ^{187}Re values compared to both bed load and suspended sediment samples from the same area (Dellinger et al., 2021, Fig. 3.3). Therefore, the Re isotope ratios of sandstone ores that included Re from organic rich shales are likely to exhibit the highest Re abundances and largest variation in isotope ratios.

The ^{187}Re values in sandstone ore-derived UOCs have the widest range of isotopic compositions of all ore types and ranged from -0.99 to 0.62 ‰. Three UOC samples with mine location information – Irigary, Pathfinder, and Shirley Basin – were derived from Wyoming, USA. These δ^{187}Re values for Irigary, Pathfinder, and Shirley Basin are indistinguishable within uncertainty at ~0.70 ‰. It is unknown if these samples were derived from the same mine or were milled at the same location. The Re abundances of Irigary, Pathfinder, and Shirley Basin are 1263 ppb, 86 ppb, and 532 ppb, respectively. Thus, the difference in Re concentration between samples may indicate that the ore material was derived from different mines. However, the Pathfinder and Shirley Basin samples are both derived from material mined at the Wind River Basin (Dooley et al., 1974). The consistent Re isotope ratio but significantly different Re concentrations for these samples may indicate that the Re isotopic composition from ore material in this area is similar if the ore Re isotopic compositions are unaltered or have a consistent fractionation due to milling processes. Alternatively, the Re isotopic compositions may be dominated by Re contamination from a reagent used during the milling process. This

could explain the consistent Re isotope ratios despite different Re abundances that span more than a 1 ppm difference. If this is the case, then the Re abundance and paired isotope ratio data provide a signature of this processing technique that can be used to narrow down what mill a UOC was processed from for nuclear forensic investigations.

3.5.2.2 Unconformity Ore δ^{187}Re Data

Unconformity ores formed in high temperature settings associated with metamorphic processes. These deposits form from sandstone ore that was overlying basement rocks (often Archean to Paleoproterozoic aged) and experienced fluid alteration. If the fluids were oxygenated, then it is possible that Re could have been remobilized from a solid phase (e.g., Morford et al., 2005). The oxidation of Re would likely introduce a mass-dependent isotopic fractionation between the mobilized Re and Re in the ore which would alter the δ^{187}Re value of the ore material. Precipitation of Re from a fluid phase after remobilization could also lead to isotopic fractionation in this setting. It is important to note that isotopic fractionation introduced in high temperature settings is expected to be less pronounced than in low temperature settings due to decreasing differences in the mechanical properties of isotopologues as temperature increases (Urey 1947).

The δ^{187}Re values of unconformity ore ranged from -0.31 to 0.37 ‰. I found that the average δ^{187}Re value for unconformity ore fell in between the average for sandstone and QP conglomerate ore-derived UOCs. There is some overlap with sandstone-ore derived UOCs (Fig. 3.4). The Re abundance of basement rocks is unknown, however I estimate it is very low based on Re geochemical abundance in continental material.

Therefore, the Re in these UOCs is likely primarily derived from the sandstone material which may also include some organic-rich material, similar to sandstone-ore derived UOCs. However, because these deposits likely formed before the Phanerozoic, it is possible that the Re abundance in organic rich material would be lower than in Phanerozoic derived organic rich material. This would lead to UOCs with lower Re abundances on average compared to sandstone ore-derived UOCs.

3.5.2.3 QP Conglomerate δ^{187}Re Data

QP conglomerate UOCs are derived from materials that formed in the Archean prior to the emergence of a persistently oxygenated atmosphere and ocean. Thus, the ore material possibly has not been influenced by natural redox processes. The sole QP conglomerate ore-derived UOC sample exhibits a δ^{187}Re of 1.24 ± 0.09 2SD.

The formation mechanics for QP conglomerates is uncertain, with debate about if they are hydrothermal or detrital in origin (e.g., Burron et al., 2018 and references therein). If QP conglomerates have a detrital origin as Burron et al. (2018) suggest, then the uraninite and other material present in the QP conglomerates may represent eroded material from rocks and minerals. Alternatively, if the QP conglomerates have a hydrothermal origin, the heavy δ^{187}Re value may indicate that high temperature settings associated with hydrothermal settings can lead to heavy isotopic compositions.

3.5.3 Implications of Re Isotope Fractionation in UOCs

3.5.3.1 The Effect of δ^{187}Re Fractionation on Re-Os Dating

The Re-Os dating technique utilizes the known decay rate of ^{187}Re into ^{187}Os to determine the age of a sample. In the calculation, the Re isotopic composition of a sample has traditionally been assumed to be invariant and match the natural stellar abundance of the isotopes. However, fractionation in this study and others (Fig. 3.4) have shown there is variation in Re isotope ratios and thus should not be assumed to be constant. This creates an issue for Re-Os geochronology and means that measuring the Re isotopic composition of samples may become necessary for accurate geochronologic ages. If a sample has an isotopic composition with a lower ^{187}Re/^{185}Re than the traditional value and is left uncorrected, it will lead to a calculated age that is younger than the true value, and vice versa for a sample with higher ^{187}Re/^{185}Re.

Traditionally, the Re isotope ratio value of ^{185}Re/^{187}Re = 0.59740 (Gramlich et al., 1973) has been utilized for Re-Os dating, which uses equation (3.2) to calculate the age of a sample:

$$\left(\frac{187_{Os}}{188_{Os}}\right) = \left(\frac{187_{Os}}{188_{Os}}\right)_{initial} + \left(\frac{187_{Re}}{188_{Os}}\right) * \left(e^{\lambda t} - 1\right) \qquad (3.2)$$

In this equation, *t* is the age, and λ is the decay constant of ^{187}Re (= 1.666×10^{-11} a^{-1}; Smoliar et al., 1996; Selby et al., 2007). Setting up a traditional isochron places ^{187}Os/^{188}Os is on the y-axis, and ^{187}Re/^{188}Os on the x-axis. The y-intercept of the isochron line represents the initial Os isotope composition at the time of deposition, assuming the

Re-Os system has remained closed since sample formation, and ($e^{\lambda t}$- 1) is the slope of the isochron which is proportional to the age of the sample.

For this equation, isotope dilution is used to calculate the Re abundance (used for the numerator of $^{187}Re/^{188}Os$) because it provides the most accurate and precise Re abundance measurements. To do this, a spike containing a known $^{185}Re/^{187}Re$ ratio is added to a sample before digestion and can correct for Re loss during sample processing. In the Re abundance calculation, the natural ratio of ^{185}Re to ^{187}Re is assumed to be invariant.

I calculated the influence of 3 ‰ fractionation on a calculated Re-Os age and associated uncertainty using Isoplot. If a sample had a 3 ‰ different isotope ratio from the traditionally assumed $^{185}Re/^{187}Re$ value, the calculated Re abundance would be incorrect by ~1.1 %. I aggregated Re abundance uncertainty data from multiple Re-Os geochronology studies with different sample types and Re abundance ranges (e.g., Kendall et al., 2006; Markey et al., 2007; Rooney et al., 2014) and found that the Re abundance error generally ranges from 0.15–- 0.40 %, which does not consider natural fractionation of Re. Therefore, isotopic variations would have errors outside the typical range which could lead to meaningfully different calculated ages and uncertainties. The full impact of Re isotopic fractionation on Re-Os dating depends on the age of the sample and extent of fractionation, however, given the large Re isotopic variability measured in nature already, future Re-Os dating should include measurement of the $^{185}Re/^{187}Re$ from the sample of interest for the most accurate data possible.

3.5.3.2 Rhenium as A Nuclear Forensics Tool

The wide range Re abundance and isotope ratios within the UOC samples indicate the usefulness of Re as a nuclear forensics tool. Many elements have previously been studied in UOCs for nuclear forensic purposes (e.g., U; Brennecka et al., 2010; Varga et al., 2017; Mo; Rolison et al., 2019; Sm; Shollenberger et al., 2021; Nd; Devlin McLoughlin et al., 2023). These studies found that isotope ratios can be diagnostic of where a sample was processed, thus can be used to assess the provenance of a sample. Regardless of if the source of an isotopic value found in a UOC is derived fully from the ore material or is altered during processing to some degree, the isotopic value of a UOC represents a characteristic of that UOC and is thus a potential signature of the material.

I found there are distinguishable differences and some overlap in the δ^{187}Re values of samples within an ore type. This information can aid in determining the source of a UOC, even when there is little additional information about a sample. For example, with the UOCs in this study, δ^{187}Re values between -0.99 to -0.15 ‰ are distinct to sandstone ore, values between -0.16 to 0.62 ‰ can represent sandstone or unconformity ore material, and values above 1.15 ‰ are distinct to QP conglomerate ore. I note that these generalizations are based on a small number of samples, and as more δ^{187}Re data is collected, these interpretations will likely evolve.

However, Re isotope ratios alone cannot definitively determine the provenance of UOC samples. This is highlighted by eight of the twelve samples in this study have δ^{187}Re values that are indistinguishable within uncertainty. Taken at face value, Re abundance and isotope ratio data can be paired to provide a unique geochemical signature for each mine (Fig. 3.5). However, using elemental abundances alone as a forensics

signature can be dubious due to their ease in being overprinted. A powerful approach to increase the certainty in the provenance assessment of a sample is to pair data from multiple isotopic systems.

Pairing δ^{187}Re data with other isotope ratio data can help identify the provenance of a sample that a single isotope system cannot distinguish by itself. Nine out of the twelve UOC samples in this study were analyzed for U isotopes by Brennecka et al. (2010), and five out of twelve UOC samples were analyzed for Nd isotopes by Krajkó et al. (2014) and Devlin McLoughlin et al. (2023). Plotting δ^{187}Re vs U isotope ratios ($^{235}U/^{234}U$ and $\delta^{238}U$; Fig. 3.6) provides a unique value for each sample (i.e., the position of each sample does not overlap) providing unique combinations in the plots. Plotting δ^{187}Re vs. εNd also provided unique values for each sample. These data indicate that each UOC has a unique geochemical signature that can be used to identify the UOCs.

Additional isotope ratio data from other elements (e.g., Mo, Sm, Sr, Pb) can also be compared to Re data to further provide unique geochemical signatures for UOC samples to provide higher confidence in the assessment of a samples provenance.

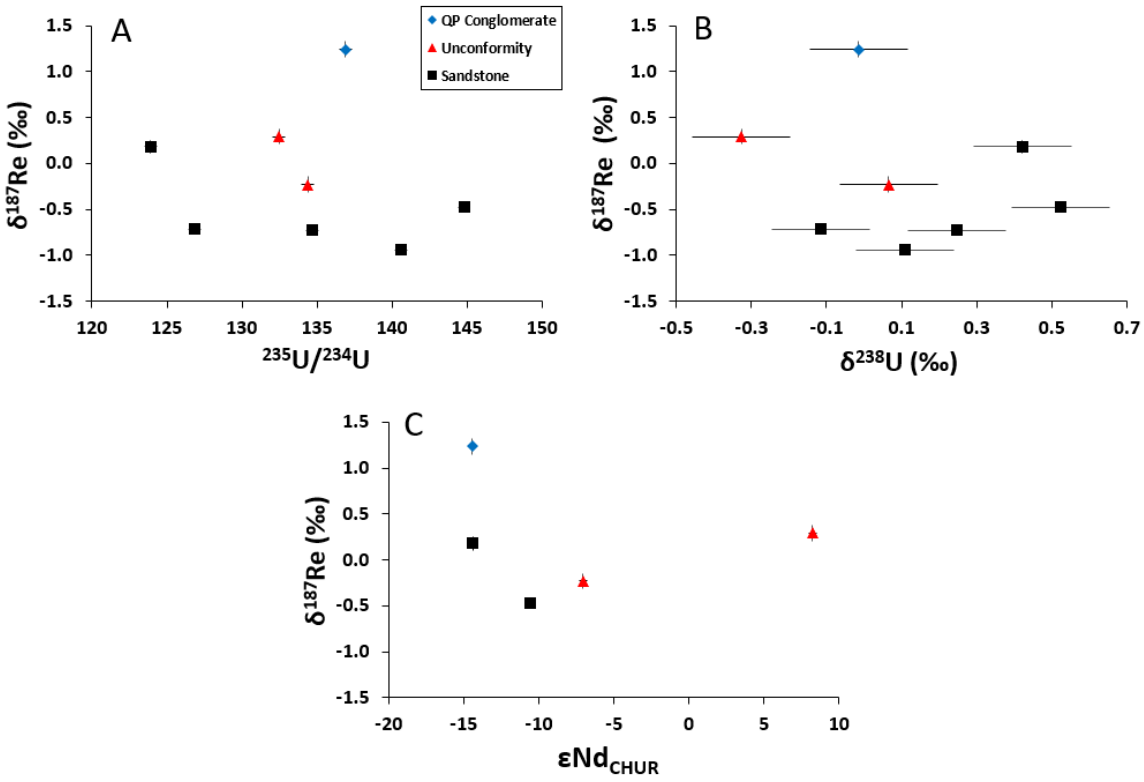

Figure 3.6 UOC Re Isotopes Compared to U and Nd Isotopes: δ^{187}Re data compared to U isotope (panels A and B) sand Nd isotopes (panel C). These plots highlight the unique combinations of Re isotope ratios vs. U and Nd isotope ratios, providing a unique geochemical signature for each sample that can be helpful in identification of the location a UOC sample was processed from. Not all UOC samples in this study had comparable U isotope and Nd isotope data. The εNd values represent parts per 10,000 deviations of a sample ^{143}Nd/^{144}Nd relative to the Chondritic Uniform Reservoir (CHUR). U isotope data from: Brennecka et al. (2010). Nd isotope data from: Krajkó et al. (2014) and Devlin McLoughlin et al. (2023). δ^{187}Re error bars represent the 2SD of replicate analyses, or the 2SD of replicate standard analyses, whichever is larger. In most cases, the symbols are larger than the error bars. U and Nd isotope error bars represent the error on standards from the papers they were collected from.

3.6 Conclusions

I collected the first δ^{187}Re data from UOCs utilizing a novel ion exchange chromatography protocol based on DGA resin to quantitatively separate Re from matrix elements. Ore types included in the study are sandstone, unconformity, and QP

conglomerate which span a range of depositional ages (from the Archean to the Phanerozoic Eons) and geologic settings. I found that UOC δ^{187}Re values derived from these ore types had a significant range in Re isotopic compositions from -0.99 to +1.33 ‰ for a total range of 2.32 ‰. This has greatly expanded the previously reported range of 0.93 ‰ (-0.97 to -0.04 ‰) found in the peer-reviewed literature.

Our working hypothesis is that the milling of ore material is primarily responsible for the large variations seen in Re isotope ratios. I note that other explanations are possible (e.g., natural processes), and there has not been a comparison of the Re isotope ratios from ore material and the paired UOC to confirm if there is fractionation introduced during processing. If there is fractionation introduced during processing, there are likely differences in fractionation between ore types due to differences in the processing of the ore material. The most likely causes of fractionation during processing for Re is incomplete recovery during ion exchange processes, solvent exchange processes, and precipitation. Contamination of Re is a less likely cause of fractionation during sample processing as Re abundances are generally very low in most materials.

I found that the isotopic composition of Re varies significantly between and within ore types and postulate that some of the variability in δ^{187}Re of sandstone ore-derived UOCs represents isotopic variability driven by redox-related deposition. Unconformity ore-derived UOCs represent ore derived from a high temperature setting and have isotopic compositions that may indicate high temperature settings lead to heavy isotopic compositions. QP conglomerate ore-derived UOCs formed in the Archean prior to the GOE and exhibit the heaviest δ^{187}Re value measured to date. The formation mechanism of QP conglomerates is debated, making it difficult to postulate what

potential natural mechanisms could have led to the very heavy isotopic composition. Future work targeting ore material with paired UOC samples will help constrain the sources of δ^{187}Re variability in UOCs.

δ^{187}Re data is a promising new tool to aid in provenance assessments of UOC found outside regulatory control due to the wide range of Re isotope ratios found so far. Rhenium isotope ratio data, when paired with other isotopic compositions of different elements (U, Nd), produces unique signatures for UOCs from different mining and milling locations. Paired comparison of Re isotope ratio data with other elemental systems (e.g., U, ND) can help determine the provenance of a intercepted UOC sample if there is a database of known geochemical signatures to compare to. Currently, large sample sizes (> 2g) are required for low abundance Re samples, however, future work optimizing running conditions (e.g., changing to more sensitive detectors, modifying sample introduction techniques) can lead to lower required sample sizes.

3.7 Acknowledgements

Thanks are owed to R. Lindvall, V. Genetti, and D. Hoffman for their assistance in the laboratory at LLNL during this study. This work was performed under the auspices of the U.S. Department of Energy by Lawrence Livermore National Laboratory under contract DE-AC52-07NA27344 with release number LLNL-JRNL-849954.

3.8 References

Anbar, A.D., Knab, K.A., Barling, J. (2001) Precise Determination of Mass-Dependent Variations in the Isotopic Composition of Molybdenum Using MC-ICPMS. Analytical Chemistry, 73, 1425–1431.

Anders, E. and Grevesse, N. (1989) Abundance of the elements: Meteoritic and solar. Geochimica et Cosmochimica Acta, 53, 197–214.

Andersen, M.B., Stirling, C.H., Weyer, S. (2017) Uranium Isotope Fractionation. Reviews in Mineralogy and Geochemistry, 82, 799–850.

Andrén, H., Rodushkin, I., Stenberg, A., Malinvsky, D., Baxter, D.C. (2004) Sources of mass bias and isotope ratio variation in multi-collector ICP-MS: optimization of instrumental parameters based on experimental observations. Journal of Analytical Atomic Spectrometry, 19, 1217–1224.

Bopp, C.J., Lundstrom, C.C., Johnson, T.M., Glessner, J.J.G. (2009) Variations in $^{238}U/^{235}U$ in uranium ore deposits: isotopic signatures of the U reduction process? Geology, 37, 611–614.

Barling, J. and Anbar, A.D. (2004) Molybdenum isotope fractionation during adsorption by manganese oxides. Earth and Planetary Science Letters, 217(3–4), 315–329.

Bennett, G., Dressler, B.O., Roberston, J.A. (1991) The Huronian supergroup and associated intrusive rocks, in: P.C. Thurston, H.R. Williams, R.H. Sutcliffe, G.M. Stott (Eds.), Geology of Ontario, Ontario Geologic Survey, 4, 549–591.

Blum, J.D., Sherman, L.S., Johnson, M.W. (2014) Mercury Isotopes in Earth and Environmental Sciences. Annual Review of Earth and Planetary Sciences, 42, 249–269.

Brennecka, G.A., Borg, L.E., Hutcheon, I.D., Sharp, M.A., Anbar, A.D. (2010) Natural variations in uranium isotope ratios of uranium ore concentrates: Understanding the $^{238}U/^{235}U$ fractionation mechanism. Earth and Planetary Science Letters, 291, 228–233.

Brennecka, G.A., Wasylenki, L.E., Bargar, J.R., Weyer, S., Anbar, A.D. (2011) Uranium Isotope Fractionation during Adsorption to Mn-Oxyhydroxides. Environmental Science and Technology, 45, 1370–1375.

Burron, I., Costa, D., Sharpe, R., Fayek, M., Gauert, C., Hofmann, A. (2018) 3.2 Ga detrital uraninite in the Witwatersrand Basin, South Africa: Evidence of a reducing Archean atmosphere. Geology, 46, 295–298.

Colodner, D., Edmond, J., Boyle, E. (1995) Rhenium in the Black Sea: comparison with molybdenum and uranium. Earth and Planetary Science Letters, 131, 1–15.

Colodner, D., Sachs, J., Ravizza, G., Turekian, K., Edmond, J., Boyle, E. (1993) The geochemical cycle of rhenium: a reconnaissance. Earth and Planetary Science letters, 117, 205–221.

Dellinger, M., Hilton, R.G., Nowell, G.M. (2020) Measurements of rhenium isotopic composition in low-abundance samples. Journal of Analytical Atomic Spectrometry, 35, 377–387.

Dellinger, M., Hilton, R.G., Nowell, G.M. (2021) Fractionation of rhenium isotopes in the Mackenzie River basin during oxidative weathering. Earth and Planetary Science Letters, 573, 117131.

Delwiche, C.C. and Steyn, P.L. (1970) Nitrogen Isotope Fractionation in Soils and Microbial Reactions. Environmental Science and Technology, 11, 929–935.

Denton, J.S., Bostick, D.A., Boulyha, S.F., Cunningham, J.A., Dimayuga, I., Hexel, C.R., Hiess, J., Jovanovic, S.V., Kaye, P, et al. (2022) International interlaboratory compilation of trace element concentrations in the CUP-2 uranium ore concentrate standard. Journal of Radioanalytical and Nuclear Chemistry, 332, 2817–2832.

Devlin McLoughlin, V.E.D., Shollenberger, Q.R., Brennecka, G.A. (2023) Determining provenance of uranium ore concentrates using $^{143}Nd/^{144}Nd$. Talanta, 253, 124088.

Dickson, A.J., Hsieh, Y., Bryan, A. (2020) The rhenium isotope composition of Atlantic Ocean seawater. Geochimica et Cosmochimica Acta, 287, 221–228.

Dooley, J.R., Harshman, E.N., Rosholt, J.N. (1974) Uranium-Lead ages of the uranium deposits of gas hills and Shirley basin, Wyoming, Economic Geology, 69, 527–531.

Gramlich, J.W., Murphy, T.J., Garner, E.L., Shields, W.R. (1973) Absolute isotopic abundance ratio and atomic weight of a reference sample of rhenium. Journal of Research of the National Bureau of Standards, 77A, 691–698.

Helz, G. R. (2022) The Re/Mo redox proxy reconsidered. Geochimica et Cosmochimica Acta, 317, 507–522.

Helz, G.R. and Dolor, M.K. (2012) What regulates rhenium deposition in euxinic basins? Chemical Geology, 305, 131–141.

IAEA-TEC-DOC-328 (1985) Geological Environments of Sandstone-type Uranium Deposits. Technical document issued by the International Atomic Energy Agency, Vienna.

Irisawa, K. and Hirata, T. (2006) Tungsten isotopic analysis on six geochemical reference materials using multiple collector-ICP-mass spectrometry coupled with a rhenium-external correction technique. Journal of Analytical Atomic Spectrometry, 21, 1387–1395.

Kendall, B., Creaser, R.A., Selby, D. (2006) Re-Os geochronology of postglacial black shales in Australia: Constraints on the timing of "Sturtian" glaciation. Geology, 34, 729–732.

Kendall, B., Dahl, T.W., Anbar, A.D. (2017) The stable isotope geochemistry of molybdenum. Reviews in Mineralogy and Geochemistry, 82, 683–732.

Krajkó, J., Varga, Z., Yalcintas, E., Wallenius, M., Mayer, K. (2014) Application of neodymium isotope ratio measurements for the origin assessment of uranium ore concentrates. Talanta, 129, 499–504.

Kristo, M.J., Gaffney, A.M., Marks, N.E., Knight, K., Cassata, W.S., Hutcheon, I.D. (2016) Nuclear forensic science: analysis of nuclear material out of regulatory control. Annual Review of Earth and Planetary Science, 44, 555–579.

Liu, R., Hu, L., Humayun, M. (2017) Natural variations in the rhenium isotopic composition of meteorites. Meteoritics and Planetary Science, 52, 479–492.

Lodders, K. (2003) Solar system abundances and condensation temperatures of the elements. The Astrophysical Journal, 591, 1220–1247.

Lyons, T.W., Reinhard, C.T., Planavsky, N.J. (2014) The rise of oxygen in Earth's early ocean and atmosphere. Nature, 506, 307–315.

Markey, R., Stein, H.J., Hannah, J.L., Zimmerman, A., Selby, D., Creaser, R.A. (2007) Standardizing Re–Os geochronology: A new molybdenite Reference Material (Henderson, USA) and the stoichiometry of Os salts. Chemical Geology, 244, 74–87.

Migeon, V., Fiteoussi, C., Pili, E., Bourdon, B. (2020) Molybdenum isotope fractionation in uranium oxides and during key processes of the nuclear fuel cycle: Towards a new nuclear forensic tool. Geochimica et Cosmochimica Acta, 279, 238–257.

Miller, C.A., Peucker-Ehrenbrink, B., Ball, L. (2009) Precise determination of rhenium isotope composition by multi-collector inductively-coupled plasma mass spectrometry. Journal of Analytical Atomic Spectrometry, 24, 1069–1078.

Miller, C.A., Peucker-Ehrenbrink, B., Schauble, E.A. (2015) Theoretical modeling of rhenium isotope fractionation, natural variations across a black shale weathering profile, and potential as a paleoredox proxy. Earth and Planetary Science letters, 430, 339–348.

Morford, J.L., Emerson, S.R., Breckel, E.J., Kim, S.H. (2005) Diagenesis of oxyanions (V, U, Re, and Mo) in pore waters and sediments from a continental margin. Geochimica et Cosmochimica Acta, 69, 5021–5032.

Morford, J.L., Martin, W.R., Carney, C.M. (2012) Rhenium geochemical cycling: Insights from continental margins. Chemical Geology, 325, 73–86.

Noddack, W., Tacke, I., Berg, O. (1925) Zwei neue Elemente der Mangangruppe. Sitzung der physikalisch-mathematischen Klasse, 11, 400–409.

Novo, L.A.B., Mahler, C.F., González, L. (2015) Plants to harvest rhenium: scientific and economic viability. Environmental Chemistry Letters, 13, 439–445.

Ogrič, M., Dellinger, M., Grant, K.E., Galy, V., Gu, X., Brantley, S.L., Hilton, R.G. (2023) Low rates of rock organic carbon oxidation and anthropogenic cycling of rhenium in a slowly denuding landscape. Earth Surface Processes and Landforms, 48, 1202–1218.

Peel, K., Weiss, D., Chapman, J., Arnold, T., Coles, B. (2008) A simple combined sample–standard bracketing and inter-element correction procedure for accurate mass bias correction and precise Zn and Cu isotope ratio measurements. Journal of Analytical Spectrometry, 23, 103–110.

Pourmand, A. and Dauphas, N. (2010) Distribution coefficients of 60 elements on TODGA resin: Application to Ca, Lu, Hf, U, and Th isotope geochemistry. Talanta, 81, 741–753.

Reading, D.G. (2016) Nuclear forensics: determining the origin of uranium ores and uranium ore concentrates via radiological, elemental and isotopic signatures. Doctoral Thesis, University of Southampton, Ocean and Earth Science, 1–247.

Rodríguez-González, P., Epov, V.N., Bridou, R., Tessier, E., Guyoneaud R., Monperrus., Amouroux, D. (2009) Species-Specific Stable Isotope Fractionation of Mercury during Hg(II) Methylation by an Anaerobic Bacteria (Desulfobulbus propionicus) under Dark Conditions. Environmental Science and Technology, 43, 9183–9188.

Rolison, J.M., Druce, M., Shollenberger, Q.R., Kayzar-Boggs, T.M., Lindvall, R.E., Wimpenny, J. (2019) Molybdenum isotope composition of uranium ore concentrates by double spike MC-ICP–MS. Applied Geochemistry, 103, 97–105.

Rolison, J.M., Stirling, C.H., Middag, R., Rijkenberg, M.J.A. (2017) Uranium stable isotope fractionation in the Black Sea: Modern calibration of the $^{238}U/^{235}U$ paleo-redox proxy. Geochimica et Cosmochimica Acta, 203, 69–88.

Rooney, A.D., Macdonald, F.A., Strauss, J.V., Dudas, F.Ö., Hallmann, C., Selby, D. (2014) Re-Os geochronology and coupled Os-Sr isotope constraints on the Sturtian snowball Earth. Proceedings of the National Academy of Sciences, 111, 51−56.

Rudnick, R.L. and Gao, S. (2003) Composition of the Continental Crust. Treatise on Geochemistry, 3, 1−64.

Russell, W.A., Papanastassiou, D.A., Tombrello, T.A. (1978) Ca isotope fractionation on the Earth and other solar system materials. Geochimica et Cosmochimica Acta, 42, 1075–1090.

Selby, D., Creaser, R.A., Stein, H.J., Markey, R.J., Hannah, J.L. (2007) Assessment of the ^{187}Re decay constant by cross calibration of Re–Os molybdenite and U–Pb zircon chronometers in magmatic ore systems. Geochimica et Cosmochimica Acta, 71, 1999–2013.

Sheen, A.I., Kendall, B., Reinhard, C.T., Creaser, R.A., Lyons, T.W., Bekker, A., Poulton, S.W., Anbar, A.D. (2018) A model for the oceanic mass balance of rhenium and implications for the extent of Proterozoic ocean anoxia. Geochimica et Cosmochimica Acta, 227, 75–95.

Shollenberger, Q.R., Borg, L.E., Ramon, E.C., Sharp, M.A., Brennecka, G.A. (2021) Samarium isotope compositions of uranium ore concentrates: A novel nuclear forensic signature. Talanta, 221, 121431.

Smoliar, M.I., Walker, R.J., Morgan, J.W. (1996) Re-Os Ages of Group IIA, IIIA, IVA, and IVB Iron Meteorites. Science, 271, 1099–1102.

Stirling, C.H., Anderson, M.B., Potter, E.-K., Halliday, A. (2007) Low-temperature isotopic fractionation of uranium. Earth and Planetary Science Letters, 264, 208–225.

Teng, F-Z., Dauphas, N., Watking, J.M. (2017) Non-Traditional Stable Isotopes: Retrospective and Prospective. Reviews in Mineralogy & Geochemistry book, 82, 1–26.

Tzvetkova, C., Novo, L. A. B., Atanasova-Vladimirova, S., Vassiliv, T. (2021) On the uptake of rhenium by plants: Accumulation and recovery from plant tissue. Journal of Cleaner Production, 328, 129534.

Urey, H.C. (1947) The Thermodynamic Properties of Isotopic Substances, Liverside lecture, delivered before the Chemical Society in the Royal Institution on December 18th, 1946. Journal of the Chemical Society (Resumed), 562–581.

U.S. Geological Survey (USGS) (2021) Mineral commodity summaries 2021: U.S. Geological Survey, 200 p., doi.org/10.3133/mcs2021.

Varga, Z., Krajkó, J., Peńkin, M., Novák, M., Eke, Z., Wallenius, M., Mayer, K. (2017) Identification of uranium signatures relevant for nuclear safeguards and forensics. Journal of Radioanalytical and Nuclear Chemistry, 312, 639–654.

Varga, Z., Nicholl, A., Wallenius, M., Mayer, K., Mock, T. (2023) Propagation and variation of material characteristics during the uranium ore concentrate production at Dolní Rožinka, Czech Republic. Journal of Radioanalytical and Nuclear Chemistry, 332, 2863–2873.

Varga, Z., Wallenius, M., Mayer, K., Keegan, E., Millet, S. (2009) Application of Lead and Strontium Isotope Ratio Measurements for the Origin Assessment of Uranium Ore Concentrates. Analytical Chemistry, 81, 8327-8334.

Von Pechmann, E. (1986) Mineralogy, age dating, and genesis of the kylie and spring creek uranium prospects, waterhouse complex, Mineral Paragenesis, Theophrastus Publications S.A., Athens, 303–343.

Yamashita, Y., Takahashi, Y., Haba, H., Enomoto, S., Shimizu, H. (2007) Comparison of reductive accumulation of Re and Os in seawater-sediment systems. Geochimica et Cosmochimica Acta, 71, 3458-3475.

CHAPTER 4

MERCURY ISOTOPE FRACTIONATION DURING CHEMICAL WEATHERING OF BLACK SHALES: LESSONS FROM CLAY CITY

4.1 Abstract

The investigation of mercury (Hg) abundance and stable isotope ratios in sedimentary rocks has emerged as a powerful tool to investigate paleoenvironmental changes and track the cycling and mobility of Hg in the modern environment. In particular, black shales—which typically have elevated Hg abundances—are commonly targeted for Hg isotope analyses to provide insights into ancient redox conditions, volcanism, and other sources of Hg to the ocean. However, recent work has found that up to ~90% of authigenic Hg is lost during chemical weathering of black shales, with greater loss associated with greater degrees of weathering. Yet, the influence of chemical weathering on Hg isotope fractionation remains unclear.

In this study, I investigate the consequences of chemical weathering on the preservation and alteration of Hg isotope signatures in the well-characterized New Albany Shale (USA). I measured the abundances of Hg and other elements, and Hg isotope compositions, in samples from an outcrop of this shale that has been the subject of extensive prior geochemical study in a forested location in Clay City, KY. The samples are from a single horizontal bed that varies from heavily weathered to well-preserved, allowing examination of Hg abundance and isotope variations as weathering progressed.

Significant mass-dependent fractionation (MDF) and mass-independent fractionation (MIF) of Hg isotopes are observed that correlates positively with the degree of weathering. No variations in even-MIF were observed. These data indicate that postdepositional processes influenced the Hg isotope compositions. MDF (δ^{202}Hg) variations span -1.09 ‰ (± 0.08‰ 2SD), odd-isotope MIF (Δ^{199}Hg and Δ^{201}Hg) spans 0.20 ‰ (±0.05‰ 2SD) and 0.21 (±0.04‰ 2SD), respectively. The most heavily weathered samples exhibit lighter δ^{202}Hg and Δ^{199}Hg values, while less-weathered samples display heavier δ^{202}Hg values and slight to no Δ^{199}Hg variations. I propose that these Hg isotope variations result from combinations of loss of authigenic Hg during oxidative weathering, gain of soil derived Hg in weathering fluids by adsorption to secondary iron and manganese oxides, and gain of Hg from overlying beds by binding to organic matter.

These findings highlight the importance of considering weathering effects when using Hg isotope for paleoenvironmental reconstructions, as these processes can modify primary Hg isotope compositions, potentially obscuring signatures and leading to erroneous conclusions.

4.2. Introduction

Mercury (Hg) isotope studies have proven useful in providing information on a range of Earth processes, paleoenvironmental studies, and tracing the cycling of Hg in the modern environment. In particular, the study of Hg isotopes in sedimentary rocks has become a valuable tool for investigating photic zone euxinia (a condition where there is abundant H_2S and no O_2 in the photic zone of a body of water) and volcanism (Thibodeau

et al., 2016; Sial et al., 2016; Percival et al., 2017; Scaife et al., 2017; Zheng et al., 2018; Sun et al., 2023; Wu et al., 2023). These processes are detected by measuring Hg abundances and/or isotope ratios in sedimentary rocks. Odd-MIF, which is primarily caused by photochemical reactions, is one of the key signatures in Hg isotope studies. Mercury also exhibits mass-dependent fractionation (MDF), which can be caused by a variety of factors, including volatilization and condensation, diffusive transport, and abiotic reduction and oxidation (Blum et al., 2014). As a result, studying Hg MDF and MIF in sedimentary rocks provides valuable information about the geological processes that occurred throughout Earth history. Organic carbon-rich shales (aka black shales) are a particularly useful rock for studying Hg isotope variations. Authigenic Hg abundances in black shales are often significantly enriched relative to upper continental crust ([Hg] ~30 ppb; Rudnick and Gao, 2003) due to the affinity for soluble Hg to bind to organic matter and/or sulfide phases under reducing conditions (Selin, 2009; Mason et al., 2012). Thus, black shales are a common sedimentary rock targeted for Hg isotope studies of paleoredox conditions and past volcanism.

Recent work has examined Hg concentrations of black shales that have experienced chemical weathering (e.g., Charbonnier et al., 2020; Park et al., 2022). These studies found up to ~90% of authigenic Hg can be released during weathering, with higher loss of Hg related to higher degrees of weathering. These studies also found that Hg is released before TOC loss occurs during incipient weathering which can lead to various stages of altered Hg/TOC values. This is important because Hg/TOC values are often used to determine if sediment Hg enrichments are authigenic or simply created by an increase in the burial of organic carbon. Additionally, Richardson et al. (2018)

examined Hg sequestration in soil and weathered bedrock (from ~0-8 m). They found that Hg surface samples (~0-0.3 m) generally had lower Hg concentrations than depths from ~1.5-8 m. They interpreted the higher abundance of Hg in the lower sections as being derived from atmospheric deposition. The gain of atmospheric Hg to an outcrop could alter the MDF and MIF values of a sample, potentially leading to erroneous assumptions about past Earth processes if analyzed for a paleoenvironmental study.

Despite the usefulness of black shales for Hg isotope studies, the effect of chemical weathering on the isotopic signatures in black shales has not been studied. Mercury has complex biogeochemical cycling involving multiple forms and transformations. Understanding its behavior in the environment is crucial for assessing its transport and mobility, as well as the impact of Hg mobilization and gain on isotopic signatures in sediments. This research is also important for understanding the transport and mobility of Hg which is crucial for assessing human exposure pathways and developing strategies to mitigate Hg contamination.

In this paper, I examine the well-studied Clay City black shale outcrop that transitions from heavily weathered into well-preserved due to oxidative chemical weathering (e.g., Petsch et al., 2000, 2001a,b; Jaffe et al., 2002; Tuttle and Breit, 2009; Miller et al., 2015). The goal is to examine the influence of chemical weathering on Hg isotopic signatures in black shales to assess the influence of weathering. This work helps to advance our understanding of Hg isotopic changes during weathering, as well as elucidate Hg mobility and retention in black shales. By providing new insights into the processes that drive Hg isotope fractionation, this study helps improve the fidelity of geochemical applications of Hg isotopes.

4.3. Background

4.3.1. Sample Geologic Background

The New Albany Shale was deposited in the Mid to late Devonian in a highly productive and anoxic at depth epeiric sea on the eastern side of the North American craton. This formation contains abundant aluminum, iron, clay, and detrital quartz (Petsch et al., 2000). The major source of organic matter (OM) is derived from marine phytoplankton (kerogen type II), and to a lesser extent terrestrial plants and bacteria (Eglinton, 1994). Pyrite and limited OM sulfurization are present indicating early diagenetic alteration (Petsch et al., 2000).

The studied outcrop is in modern day Clay City, KY, USA (37°5’'10.”"N 83°56’46.0”W). The Huron Member on the New Albany Shale (Hayes, 1993) is the only unit exposed on the outcrop. Road construction in 1960 exposed an outcrop with a heavily weathered rind surrounding a well-preserved interior (Fig. 4.1) of the hill (Tuttle et al., 2009). The location that currently experiences ~117 cm of precipitation per year. The strata are horizontal which allows stratigraphic control while sampling across the weathering profile. The outcrop hill is forested and hosts significant plant life (Fig. 4.1).

4.3.2. Previous Publications Utilizing This Outcrop

This outcrop was sampled twice by Dr. Steven Petsch and collaborators to examine changes in the heavily weathered into well-preserved sections. The first trip was in circa 1996 and the second trip was in circa 2002. The beds that were targeted during the sampling trips were not the same. Thus, it is important to consider the different beds which contain different geochemical signatures when thinking about comparing data

from publications utilizing Clay City samples. Some publications utilizing samples from the first sampling trip include Petsch et al. (2000), Petsch et al. (2001a,b), and some publications from the second sampling trip include Jaffe et al. (2002) and Miller et al. (2015). The samples in this study are from the first sampling trip.

For both trips, sampling took place from a single bed that transitioned from heavily oxidatively weathered to well preserved which was easily accessible along a road cut (Fig. 4.1). Prior to sampling, 5-10 cm of detritus/thin coating from recent weathering of the exposed surfaces were removed. Particular attention was paid to maintaining vertical positioning during sampling of the bed to minimize any bed-to-bed heterogeneity. For a more comprehensive description of sampling procedures, refer to Petsch et al. (2000).

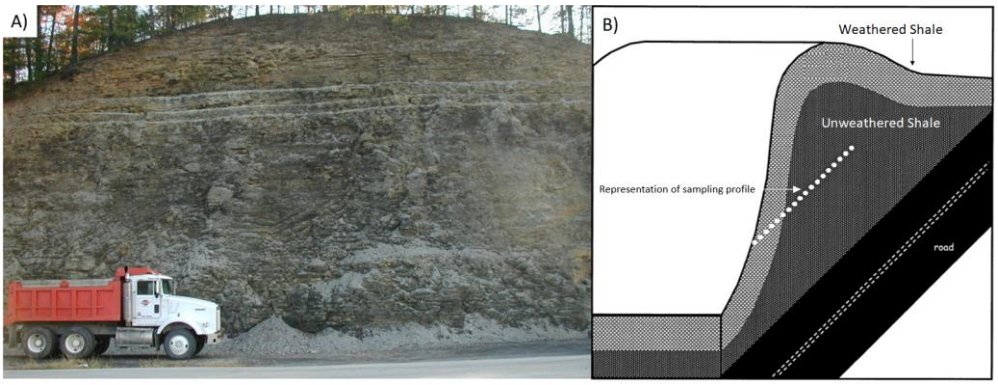

Figure 4.1 Clay City Outcrop Photo and Cartoon. A) Clay City, KY, USA outcrop where samples were collected. The truck and trees on top of the hill provide a sense of scale. B) Cartoon illustration from Petsch et al. (2000) highlighting the weathering pattern of the outcrop, with a heavily weathered few meters around the surface surrounding a well-preserved interior. A) photo credit: E.W. Bolton. B) Modified from Petsch et al. (2000).

4.4. Methods

4.4.1. Sample Preparation

4.4.1.1 Digesting Samples and Creating Reagents

Mercury was extracted from powdered sediment samples using the acid digestion protocol from Zheng et al. (2018). Briefly, samples were weighed and placed into 20 ml Teflon beakers with an acid mixture containing 6 ml concentrated HNO_3, 3 ml concentrated HCl, and 0.5 ml BrCl. The HNO_3 and HCl were all trace metal grade. BrCl was made using KBr and $KbrO_3$ powders that were heated at 300°C for 8 hours to volatilize any Hg present before use. ~1 gram of KBr powder was mixed with 100 ml concentrated HCl (trace metal grade) in a glass bottle (that was previously cleaned with 1% BrCl to reduce the Hg blank of the bottle). The powder and acids were allowed to mix in a fume hood for 1 hour on a stirring plate. Then, ~1.5 g of $KbrO_3$ was added and stirred until fully dissolved, completing the preparation of BrCl.

The samples were heated while tightly capped at ~100°C for 48 hours. Previous work established that this procedure quantitatively extracts Hg (Zheng et al., 2018), which was verified with a sample of SDO-1 black shale standard in each batch of samples. The digested samples were allowed to cool to room temperature, transferred to 50 ml trace metal clean centrifuge tubes, and centrifuged in a Beckman Coulter Allegra X14 at 4000 RPM for 5 minutes. The supernatant was then decanted into fresh 20 ml Teflon beakers. Mercury concentrations were measured in an aliquot of the decanted solutions using a Thermo Scientific iCAP-Q quadrupole inductively coupled plasma mass spectrometer. The aliquoted solutions were introduced into the ICP-MS via online $SnCl_2$

reduction using a liquid-vapor separator which delivers Hg to the ICP-MS as Hg(0) vapor (Yin et al., 2016).

4.4.1.2. Purifying Hg With Column Chromatography

The decanted solutions were purified using an anion-exchange chromatographic protocol to isolate Hg from organics and matrix that may interfere with isotopic measurements (Chen et al., 2010; Huang et al., 2015; Chen et al., 2016; Zheng et al., 2018). Before chromatography, the decanted solutions were partially dried down (stopped at ~2 ml of solution). The samples were carefully monitored to not allow a full dry down which would result in a loss of Hg via volatilization. The partially dried down samples were then diluted using 10 ml 1 M HCl for each sample. These solutions were then loaded onto columns containing 1 ml AG 1-X4 (200-400 mesh, Bio-Rad) resin. Matrix elements were removed with 19 ml of 1 M HCl, in increments of 3 ml, 3 ml, 3 ml, 5 ml, 5 ml. Mercury was then eluted with 12 ml of 0.5 M HNO_3 + 0.05% L-cysteine, in increments of 2 ml following the methodology from Zheng et al. (2018).

The Hg recovery after the chromatographic procedure was calculated by comparing the amount of Hg in the eluted solution with the measured abundance before the chromatographic procedure. The yield for all samples was 100 ± 12% (2SD), which is typical for this methodology (e.g., Zheng et al., 2018). The eluted solutions containing Hg (~ 12 ml) were digested with ~10% by volume BrCl (~1.2 ml).

4.4.2. Isotope Ratio Analyses

4.4.2.1. Sample Preparation and Run Parameters

The procedure used for Hg isotopic analysis is described in Zheng et al. (2018). Briefly, Hg isotope ratios were measured on a Thermo Scientific Neptune multi collector – inductively coupled plasma – mass spectrometer (MC-ICP-MS) at Arizona State University. Samples eluted from the chromatographic procedure were diluted to 2 ng Hg / ml using a matrix solution containing 0.5% BrCl, 0.5% concentrated HCl, and 0.1% $NH_2OH{\cdot}HCl$. The 2 ng Hg / ml solutions were introduced to the instrument via online $SnCl_2$ reduction and Hg(0) vapor separation using a liquid-vapor separator (Yin et al., 2016). Instrumental mass bias was corrected using standard-sample-standard bracketing with NIST 3133, and simultaneous internal introduction of the NIST thallium (Tl) standard SRM 997. The Tl solution was introduced via an ESI Apex Q desolvating nebulizer. The bracketing standard was matched to samples in both matrix and Hg concentration (typically less than 10% difference).

I simultaneously measured ^{198}Hg, ^{199}Hg, ^{200}Hg, ^{201}Hg, ^{202}Hg, ^{203}Tl, ^{205}Tl, and ^{207}Pb. ^{204}Hg was not measured due to detector position limitations. On-peak zero corrections were applied to all masses.

4.4.2.2 Isotope Ratio Data Nomenclature

The isotopic compositions of Hg are calculated using delta (δ) notation, defined by equation (4.1).

$$\delta^{x}Hg(‰) = [(\delta^{x}Hg/\delta^{198}Hg)_{sample}/(\delta^{x}Hg/\delta^{198}Hg)_{standard} -1] \times 1000 \qquad (4.1)$$

where x is the mass of an isotope listed above. In the text, δ^{202}Hg is used to report mass-dependent fractionation because ^{202}Hg has the largest mass difference from the denominator isotope ^{198}Hg.

Mass-independent fractionation (Δ^{x}Hg) is the difference between measured δ^{x}Hg and theoretical values based on kinetic mass-dependent fractionation law (Blum and Bergquist, 2007; Bergquist and Blum, 2009). MIF is defined by equation (4.2):

$$\Delta^{x}Hg = \delta^{x}Hg - \beta \times \delta^{202}\text{Hg} \qquad (4.2)$$

where x is the mass number of an isotope of Hg (^{199}Hg, ^{200}Hg, or ^{201}Hg) and β is a scaling constant to estimate the theoretical kinetic MDF which is 0.2520, 0.5024, and 0.7520 for ^{199}Hg, ^{200}Hg, and ^{201}Hg, respectively.

4.4.3. Major and Trace Element Abundances

For major and trace element analyses, powdered samples were weighed in ceramic crucibles and ashed in a furnace at 450°C overnight to oxidize organic material. Ashed samples were transferred into 20 ml Teflon beakers and 4 ml concentrated HNO_3 and 1 ml concentrated HF (all trace metal grade) were added. The samples were then heated while tightly capped at ~100°C for 24 hours. The samples were allowed to cool to room temperature then 2 ml of HCl (trace metal grade) was added to each sample. Then they were heated again while tightly capped at ~100°C for 24 hours. The samples were then dried down fully. Then, 6 ml concentrated HCl and 2 ml concentrated HNO_3 were added to each sample. The samples were heated while tightly capped at ~100°C for 48 hours, completing the digestion. Major and trace element abundances were measured

from an aliquot of the solution with a Thermo Scientific iCAP-Q at Arizona State University.

All elements were measured in the same analytical session using multi-element calibration standards. An internal standard containing Sc, Ge, Y, In, and Bi was introduced to the instrument in parallel with all samples and standards to correct for signal drift. A check standard containing all the elements in the calibration standard was analyzed after every five samples to assess accuracy and precision throughout the analytical session. The relative standard deviation of each analyte in the check standard was typically less than 2%. The signal intensity of each analyte was at least four times that of the blank. The reproducibility for the concentration of each element was always better than 3% and typically ~ 1%. To monitor the yields and the accuracy of abundance measurements, I included the standard USGS SDO-1 and a procedural blank in each set of samples.

Elemental abundances for sodium (Na), potassium (K), aluminum (Al), and calcium (Ca) were converted to oxide values and used to calculate chemical index of alteration (CIA) values using the following equation (4.3):

$$CIA = \left(\frac{Al_2O_3}{Al_2O_3 + Na_2O + CaO + K_2O}\right) * 100 \qquad (4.3)$$

Using the certified values for Na, K, Al, and Ca for SDO-1 yields a CIA value of 72.0 (Kane et al., 1990). The CIA value for SDO-1 using data from this study is 72.3, a difference of less than 0.5%. CIA is used as a proxy for calculating chemical weathering intensity by examining the ratio of mobile elements (Na, K, Ca) to immobile Al (Nesbitt and Young, 1982; Li et al., 2023).

Elemental abundances were also used to create Tau (τ) values, a proxy for loss and gain of elements during weathering. Tau values are calculated using equation (4.4):

$$\tau_{Ti,i} = 100 * \left[\frac{\left(\frac{C_i}{C_{Ti}}\right)_{sample}}{\left(\frac{C_i}{C_{Ti}}\right)_{original}} - 1 \right] \quad (4.4)$$

Where C_i is the concentration of an element of interest compared to the concentration of Ti (C_{Ti}) in the same sample. For this study, zone 3 (defined in section 4.1) elemental abundances are used as the 'original' value that each sample is compared to. To interpret τ values, $\tau > 0$ indicates gain during weathering, $\tau < 0$ indicates loss during weathering, and $\tau = 0$ indicates no gain or loss of the element of interest.

4.4.4. Precision and Accuracy of Hg Abundance and Isotope Ratio Data

To monitor the precision and accuracy of Hg isotopic measurements and the blank Hg concentration, in each set of samples I included the standard reference sample USGS SDO-1 (Devonian Ohio Shale) which has a matrix similar to the samples in this study, as well as a procedural blank. The measured average of two individual SDO-1 digestions of 186 ± 10 ppb (2SD) is consistent with the certificate value of 190 ± 80 ppb (1SD) (Kane et al., 1990), as well as the published value of 213 ± 30 ppb (2SD) (Zheng et al., 2018). The Hg abundance of procedural blanks was always less than 2% of the concentration of Hg in samples.

The in-house Hg standard J.T. Baker (JTB; Baker instar-analyzed plasma standard) was measured at least two times before each analytical session and interspersed throughout analytical sessions. In total, JTB was analyzed 24 times. The average of the

measured isotopic compositions of JTB (δ^{202}Hg = -0.63 ± 0.08‰, Δ^{200}Hg = 0.02 ± 0.04‰, Δ^{201}Hg = -0.01 ± 0.04‰, 2SD, n = 24) are consistent with published values (Zheng et al., 2015, 2016, 2018; Thibodeau et al., 2016). Uncertainties for Clay City samples are reported as the 2SD of all measurements of the JTB standard or the 2 standard error of sample replicates, whichever uncertainty was largest.

To ensure data reproducibility, every sample was digested twice (except for two samples: 0 m and 0.91 m that were limited by the amount of material available) following the same procedures outlined above. Both sets of samples included a USGS SDO-1 standard and a procedural blank. The two separate SDO-1 samples were analyzed on the MC-ICP-MS twice each for a total of four analyses (Table 4.1). The average of the combined SDO-1 analyses agrees with previously published values. Because the results of the separately processed SDO-1 samples are consistent, the results of the individually processed Clay City samples were combined to create an average.

Table 4.1 Mercury Isotopic Compositions of Reference Materials and Standards. *n* is the number of analyses per sample. In this study, the 2 standard deviation (2SD) for the USGS black shale standard SDO-1 data represents the 2SD of four total analyses from two separately digested and processed SDO-1 samples. In this study, the 2SD of the Hg standard JTBaker (JTB) represents the 2SD of replicate analyses of the standard throughout the analytical session. For Zheng et al. (2018) data, the 2SD data represents error on replicate analyses.

	n	δ^{202}Hg (‰)	2sd	δ^{201}Hg (‰)	2sd	δ^{200}Hg (‰)	2sd	δ^{199}Hg (‰)	2sd	Δ^{201}Hg (‰)	2sd	Δ^{200}Hg (‰)	2sd	Δ^{199}Hg (‰)	2sd
SDO-1 (this study)	4	-0.34	0.03	-0.29	0.07	-0.18	0.06	-0.13	0.09	-0.04	0.06	-0.01	0.05	-0.05	0.08
SDO-1 (Zheng et al., 2018)	3	-0.38	0.02	-0.36	0.02	-0.18	0.01	-0.16	0.03	-0.08	0.01	0.01	0.02	-0.04	0.03
JTBaker (this study)	22	-0.63	0.08	-0.49	0.09	-0.30	0.07	-0.12	0.07	-0.01	0.04	0.02	0.04	0.04	0.05
JTBaker (Zheng et al., 2018)	34	-0.66	0.07	-0.52	0.06	-0.32	0.06	-0.14	0.06	-0.02	0.04	0.02	0.04	0.03	0.05

4.5. Results

4.5.1. Clay City Samples

Thirteen sediment samples spanning ~14 meters along a single bed of the Clay City outcrop were analyzed for mercury, other trace element, major element abundances, and mercury isotope ratios. Total organic carbon (TOC) data is from Petsch et al. (2000). The weathering profile transitions from low TOC (wt.%) values beginning at 0 m, then gradually to higher values as sampling along the bed progressed (Fig. 4.2, Table 4.3). Mercury abundances throughout the profile range from 65 – 102 ppb ± 10%, with an average of 76 ppb. The lack of significant variation in Hg abundances throughout the profile paired with significant variations in TOC create Hg (ppb)/TOC (wt. %) values that vary significantly throughout the sample set.

For ease of discussion, the samples are subdivided into three zones based on the degree of weathering inferred from TOC abundances and chemical index of alteration (CIA) values. Chemical index of alteration values are calculated from measured trace metal abundance data (Table 4.2)

Table 4.2 Major and Trace Element Abundances in Clay City Samples. Sodium (wt. %), Al (wt. %), K (wt. %), Ca (ppm), Ti (wt. %), Mn (ppm), and Fe (wt. %) abundance data.

Meters	Na (wt. %)	Al (wt. %)	K (wt. %)	Ca (ppm)	Ti (wt. %)	Mn (ppm)	Fe (wt. %)
0.0	0.11	6.9	2.6	720	0.51	47	4.2
0.6	0.10	7.2	2.7	655	0.47	52	4.6
0.9	0.09	7.4	2.8	682	0.45	63	5.4
1.2	0.09	8.0	2.9	671	0.45	64	5.8
1.5	0.09	7.0	2.9	683	0.49	36	2.7
1.8	0.10	6.7	2.9	690	0.49	33	3.5
2.1	0.10	6.7	2.9	732	0.50	32	1.6
2.4	0.10	6.5	3.0	748	0.47	33	4.1
2.7	0.10	6.4	2.8	706	0.47	32	2.6
3.0	0.11	6.5	3.0	820	0.47	33	4.0
3.7	0.11	5.8	2.7	834	0.43	29	4.7
6.4	0.19	6.1	2.7	732	0.45	30	1.6
13.7	0.26	6.0	2.7	777	0.42	31	1.7

Zone 1 represents samples that have experienced the highest level of chemical weathering indicated by the lowest TOC abundances, low pyrite S abundances, and the highest CIA values (Fig. 4.2). Zone 1 has the lightest MDF (δ^{202}Hg = -1.59 to -1.15 ± 0.08 ‰) and odd-MIF values (Table 4.3). Δ^{199}Hg and Δ^{201}Hg = -0.11 to -0.02 ± 0.05 ‰ (2SD) and -0.24 to -0.22 ± 0.04 ‰ (2SD), respectively).

Zone 2 represents samples transitioning from heavily weathered into well preserved, identified by consistently low pyrite S abundances, low TOC values that gradually increase as sampling progressed along the bed, as well as gradually decreasing CIA values. Zone 2 has the heaviest MDF values (δ^{202}Hg = -0.93 to -0.66 ± 0.08 ‰ (2SD)), and the MIF values are consistent with zone 3 within uncertainty.

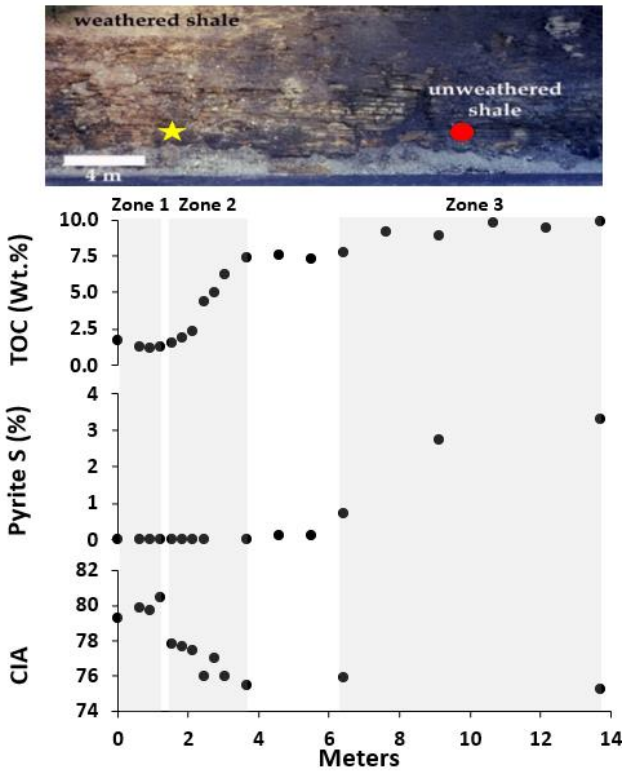

Figure 4.2 Geochemical Data Indicating the Degree of Weathering. Total organic carbon (TOC, wt. %), Pyrite S (%), chemical index of alteration (CIA) data used to define the three weathering zones. Pyrite S (%) and TOC (wt. %) data are from Petsch et al. (2000), while CIA data are from this study. An estimate of the sampling locations beginning (yellow star) and end (red circle) is indicated in the photo. Photo credit: E.W. Bolton.

Zone 3 represents the most well-preserved chemical signature of the bed that is also farthest into the well-preserved interior of the hill. Zone 3 is made up of two samples at 6.4 m and 13.7 m. The samples are spaced apart by 7.3 m but still maintain consistent Hg geochemical signatures. The δ^{202}Hg, Δ^{199}Hg, and Δ^{201}Hg values all agree within error (Table 4.3, Fig. 4.3). However, the Pyrite S and TOC values are lower in the sample at 6.4 m by ~80% and 20%, respectively. Notably, the CIA values show similar retention of soluble elements indicating a low degree of loss of soluble elements in both samples. The δ^{202}Hg value of the next closest sample at the end of zone 2 (at 3.7 m) has a different

δ^{202}Hg value outside error that indicates the zones are geochemically distinct. Thus, zone 3 hosts the most well-preserved samples and is inferred to represent the pre-weathered Hg isotopic composition of the bed. Zone 3 is used throughout the paper as a point of comparison for the isotopic fractionation observed in zones 1 and 2.

Δ^{199}Hg is typically used in Hg isotope studies to represent odd-mass MIF in both Δ^{199}Hg and Δ^{201}Hg (e.g., Blum et al., 2014). I found that Δ^{201}Hg had slightly more negative and positive variations than Δ^{199}Hg. To facilitate comparisons with previous studies, Δ^{199}Hg is used to represent odd-MIF, but Δ^{201}Hg is also reported when useful. The even-MIF values (Δ^{200}Hg) are indistinguishable from zone 3 for all samples (Table 4.3) and therefore I do not discuss even-MIF, and "MIF" hereafter refers only to odd-MIF.

	Meters	Hg (ppb)	Hg ppb (2sd)	TOC (wt.%)	Hg (ppb) / TOC (wt.%)	S pyrite (%)	Fe (wt.%) / Ti (wt.%)	Mn (ppm) / Ti (wt.%)	Chemical Index of Alteration (CIA)	δ^{202}Hg (‰)	δ^{202} (2sd)	δ^{201}Hg (‰)	δ^{201} (2sd)	δ^{200}Hg (‰)	δ^{200} (2sd)	δ^{199}Hg (‰)	δ^{199} (2sd)	Δ^{201}Hg (‰)	Δ^{201} (2sd)	Δ^{200}Hg (‰)	Δ^{200} (2sd)	Δ^{199}Hg (‰)	Δ^{199} (2sd)
Zone 1	0.0	65	1	1.5	44	0.000	8.2	91.3	79.3	-1.59	0.08	-1.42	0.09	-0.80	0.07	-0.51	0.07	-0.22	0.04	0.00	0.04	-0.11	0.05
	0.6	102	2	1.1	93	0.002	9.8	109.6	79.8	-1.33	0.08	-1.22	0.09	-0.63	0.07	-0.35	0.07	-0.22	0.04	0.04	0.04	-0.02	0.05
	0.9	69	2	1.0	69	0.004	12.0	138.3	79.7	-1.15	0.08	-1.09	0.09	-0.52	0.07	-0.36	0.07	-0.23	0.04	0.05	0.04	-0.07	0.05
	1.2	73	2	1.2	61	0.006	12.8	140.5	80.4	-1.21	0.08	-1.15	0.09	-0.56	0.07	-0.41	0.07	-0.24	0.04	0.05	0.04	-0.11	0.05
Zone 2	1.5	74	2	1.4	52	0.008	5.4	73.1	77.8	-0.83	0.08	-0.78	0.09	-0.41	0.07	-0.28	0.07	-0.15	0.04	0.00	0.04	-0.07	0.05
	1.8	72	2	1.8	40	0.010	7.2	67.8	77.6	-0.66	0.08	-0.63	0.09	-0.30	0.07	-0.23	0.07	-0.13	0.04	0.03	0.04	-0.06	0.05
	2.1	80	1	2.2	36	0.012	3.1	64.8	77.4	-0.81	0.08	-0.77	0.09	-0.42	0.07	-0.27	0.07	-0.15	0.04	-0.02	0.04	-0.07	0.05
	2.4	68	0	4.3	16	0.015	8.6	68.9	76.0	-0.82	0.08	-0.73	0.09	-0.39	0.07	-0.21	0.07	-0.11	0.04	0.03	0.04	-0.01	0.05
	2.7	80	1	4.9	16	-	5.5	68.9	77.0	-0.71	0.08	-0.65	0.09	-0.29	0.07	-0.19	0.07	-0.11	0.04	0.07	0.04	-0.01	0.05
	3.0	69	0	6.1	11	-	8.6	70.5	75.9	-0.78	0.08	-0.70	0.09	-0.36	0.07	-0.23	0.07	-0.11	0.04	0.04	0.04	-0.03	0.05
	3.7	82	1	7.2	11	0.026	10.9	67.2	75.4	-0.93	0.08	-0.82	0.09	-0.43	0.07	-0.27	0.07	-0.12	0.04	0.03	0.04	-0.04	0.05
Zone 3	6.4	68	1	7.6	9	0.725	3.5	67.2	75.9	-1.14	0.08	-1.00	0.09	-0.57	0.07	-0.30	0.07	-0.14	0.04	0.00	0.04	-0.02	0.05
	13.7	79	1	9.7	8	3.310	4.0	74.1	75.2	-1.19	0.08	-1.07	0.09	-0.58	0.07	-0.33	0.07	-0.17	0.04	0.02	0.04	-0.03	0.05

Table 4.3 Hg Geochemical Data From Clay City. Mercury (Hg) abundance, total organic carbon (TOC), S pyrite (wt. %), mass-dependent fractionation (MDF, δ), mass-independent fractionation (MIF, Δ), metals normalized to Ti, and chemical index of alteration (CIA). All data is from this study except TOC and S Pyrite which is from Petsch et al. (2000). Uncertainties for isotope ratio data are reported as the 2SD of all measurements of the JTB standard or the 2 standard error of sample replicates, whichever uncertainty was largest.

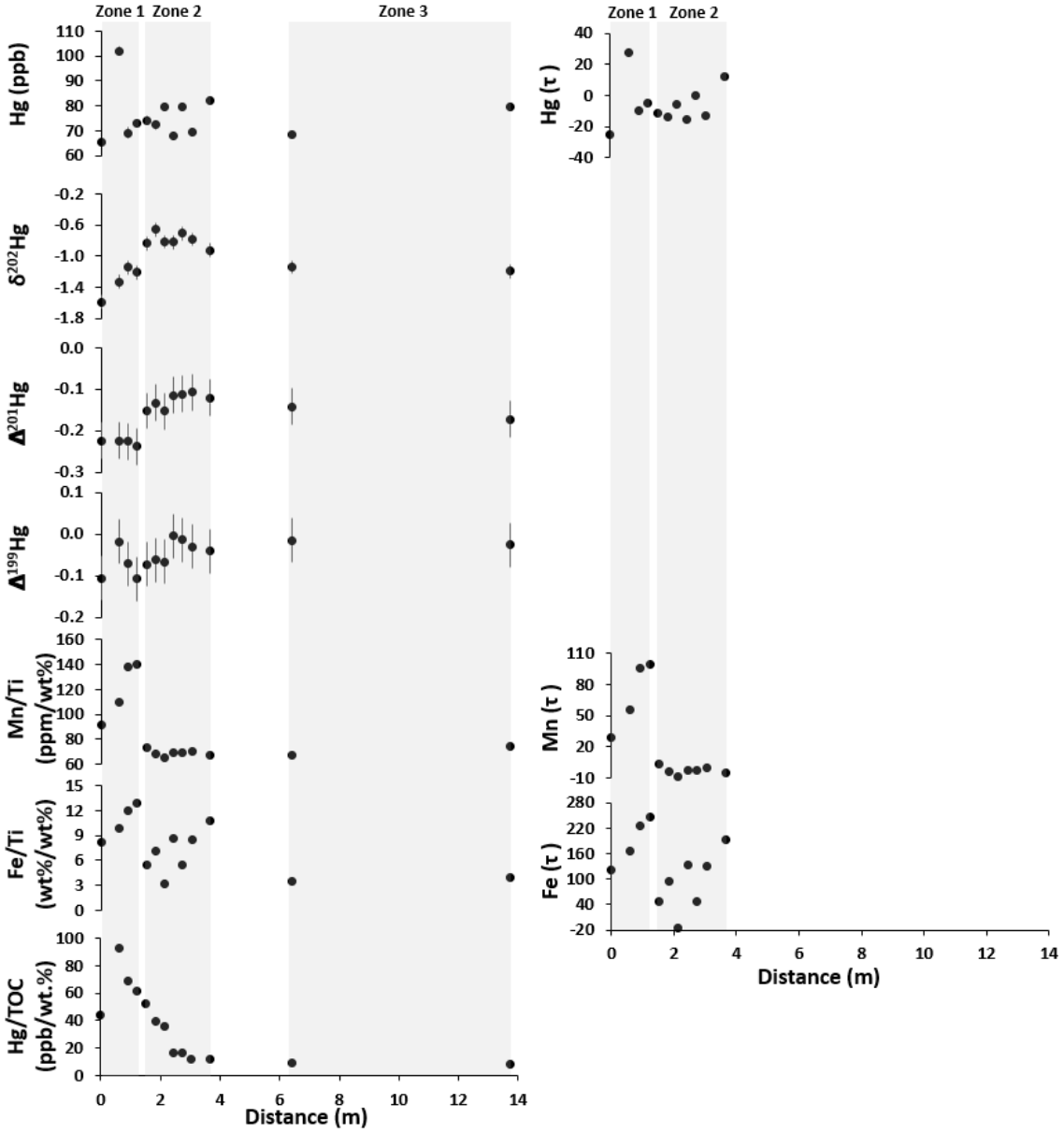

Figure 4.3 Geochemical Data from Clay City. Mercury abundance, δ^{202}Hg (‰), Δ^{201}Hg (‰), Δ^{199}Hg (‰), Mn (ppm)/Ti (wt.%), Fe (wt.%)/Ti (wt. %), Hg (ppb)/TOC (wt. %), and τ values for Hg, Fe, and Mn. Uncertainties for isotope ratio data are reported as the 2SD of all measurements of the JTB standard or the 2 standard error of sample replicates, whichever uncertainty was largest.

4.6 Discussion

The goal of this study is to characterize the influence of oxidative weathering on Hg geochemical signatures and mobility in black shales. The black shale samples in this study were collected from a forested location. The impact of oxidative weathering on the outcrop is evident both visually (Fig. 4.1) and geochemically. The heavily weathered end of the bed (zone 1) exhibits significant loss of organic carbon and pyrite S indicating substantial oxidation, and the highest CIA values indicating the greatest loss of soluble elements (Fig. 4.2). Previous studies examining Hg abundances in oxidatively weathered black shales found up to ~90% of authigenic Hg can be lost during weathering, with greater Hg loss related to greater degrees of weathering (Charbonnier et al., 2020; Park et al., 2022). Surprisingly, the abundance of Hg is broadly constant across the entire bed, including the heavily oxidatively weathered Zone 1 where Fe-oxides have been found, and Hg/TOC is elevated in Zone 1. It is unlikely that Hg was not lost during oxidative weathering in Zone 1, as elaborated below (section 5.1). Accordingly, I am driven to speculate that in addition to Hg loss, the outcrop experienced Hg gain, possibly by adsorption to Fe- and Mn- oxides which is a known mechanism for Hg (Lockwood and Chen, 1973; Jiskra et al., 2012). Input of secondary fluids to the outcrop at Clay City may come from above, where heavy vegetation across the hilltop in which the outcrop is found has accelerated weathering (Fig 1).

Hg MDF (δ^{202}Hg) and MIF (Δ^{199}Hg and Δ^{201}Hg) can provide insight into the processes and sources that affect Hg budgets. Therefore, in the discussion below I consider MDF and MIF alongside Hg concentrations in each zone, with the aim of understanding what controlled the distribution of Hg. I end by considering implications

for paleoredox preservation, which motivated this study. Throughout the discussion Zone 3 – which shows little evidence of alteration – is utilized as a reference to compare the weathering in zones 1 and 2.

4.6.1 Zone 1 – Loss of Authigenic Hg and Gain of Soil-Derived Hg

Zone 1 has the lightest δ^{202}Hg values paired with the lightest Δ^{199}Hg and Δ^{201}Hg values in the sample set (Fig. 4.3). As explained below, I propose that the isotope data observed in the heavily weathered Zone 1 are best explained by the loss of Hg during oxidative weathering of organic matter, combined with the gain of soil-derived Hg delivered by weathering fluids. The weathering fluids likely entered the outcrop through fractures created by root development and exogenous Hg from soil adsorbed to secondary Fe-Mn oxides in Zone 1.

The loss of Hg is likely because the host of Hg during formation of organic-rich sediments in the ocean is primarily organic matter and/or sulfides (Selin, 2009), and associations with organic matter and pyrite S persist when these sediments are lithified to form black shales. Furthermore, other studies of black shale weathering have found significant loss of Hg during oxidative weathering (Charbonnier et al., 2020; Park et al., 2022). I therefore assume that significant Hg was lost along with loses of TOC and S pyrite. Furthermore, there are shifts in the isotope ratios of Hg that are most parsimoniously explained by loss and subsequent gain of Hg.

The gain of Hg in this zone is supported by high Hg/TOC values despite loss of TOC and pyrite S (relative to zone 3); the loss of these elements themselves indicate considerable oxidative weathering and unsubstantial loss of Hg. As loss of Hg is

associated with oxidative weathering (Charbonnier et al., 2020; Park et al., 2022), finding substantial Hg still present in the outcrop suggests that extensive Hg gain. I infer that secondary Hg is found in the samples and was derived from overlying soil and entered the bed in rainwater through fractures created by plant roots in this forested hill. Mercury is likely derived from soil based on MIF values (discussed in detail in the following section), which is reasonable as soil is the largest repository of Hg in terrestrial ecosystems (Selin, 2009). Soil becomes enriched in Hg through direct atmospheric deposition of Hg(0), and plant foliage incorporating Hg(0) which is transferred to soil upon decomposition (Ericksen et al., 2003).

I propose that soil-derived Hg was gained in Zone 1 by adsorption to Fe and Mn oxides, consistent with elevated Fe/Ti and Mn/Ti abundances (Fig. 4.3). This is supported by previous studies that have shown Hg in fluids can adsorb to Fe-Mn oxides (Lockwood and Chen, 1973; Jiskra et al., 2012). Weathering effects should be most pronounced in Zone 1 because it hosts the most chemically weathered samples that are closest to the surface of the hill, where the influence of fluids should have been strongest and where Fe-oxides are known to occur (Tuttle et al., 2009).

4.6.1.1 MIF and MDF Indicate Gain of Soil-Derived Hg

The most striking isotopic feature in zone 1 is MDF and MIF (Δ^{199}Hg and Δ^{201}Hg) shifts that are not well correlated with changes in Hg concentrations or Hg/TOC (Fig. 4.3). Atmospheric Hg in the Midwestern United States has negative Δ^{199}Hg values down to ~ -0.35 ‰ (Demers et al., 2015) which is lighter than zone 3 with Δ^{199}Hg = ~0.02 ± 0.05 ‰. As Hg in soil is primarily derived from the atmosphere, the shift to light

MIF values is consistent with Hg derived from soil. Supporting this observation, the Δ^{201}Hg values also show a decrease in MIF, which is expected as MIF is caused by similar processes. The Δ^{201}Hg variations are more pronounced than Δ^{199}Hg variations, therefore I will use Δ^{201}Hg throughout the discussion of MIF in this zone.

The light δ^{202}Hg values found in this zone are also consistent with a soil source for the exogenous Hg. Soil and plant matter are characterized by light MDF values ranging from ~ -4 to -1 ‰ (Tsui, et al., 2012; Demers et al., 2013; Jiskra et al., 2015; Yu et al., 2016; Zheng et al., 2016; Obrist et al., 2017; Woerndle et al., 2018; Olson et al., 2019; Liu et al., 2019; Zhou et al., 2021). These values are lighter on average than the starting δ^{202}Hg value of ~1.16 ± 0.08 ‰ based on the zone 3 data, thus a shift to light MDF values is expected for a soil source of Hg.

In zone 1, Fe-oxides (FeO(OH)) were detected by Tuttle et al. (2009). Additionaly, Fe/Ti and Mn/Ti values are elevated in this section, indicating retention of these elements during oxidative weathering (Fig. 4.3). Therefore, the exogenous Hg in weathering fluids is likely adsorbed to secondary Fe-Mn oxides which formed during oxidative weathering. Light Hg isotopes are preferentially adsorbed to Fe-oxides (Jiskra et al., 2012), which suggests that light isotopes of the already-light MDF soil-derived Hg would adsorb to secondary Fe-Mn oxides in the samples. Thus, a shift to light δ^{202}Hg is expected for Hg derived from soil adsorbing to secondary Fe-Mn oxides in the samples.

All processes discussed thus far have induced light MDF values in the samples. However, I infer that light isotopes of authigenic Hg are preferentially removed from the rock during oxidative weathering as TOC is broken down, leading to positive MDF in the rock. I note this is inferred because there have been no experimental studies of isotopic

fractionation during the loss of Hg due to oxidative weathering of organic matter. Additionally, in zone 1 no positive MDF fractionation is apparent where I suggest significant loss of authigenic Hg as occurred. I suggest this is due to the positive MDF during mobilization of authigenic Hg being overprinted by gain of soil derived Hg with more negative MDF values (δ^{202}Hg ranging from ~ -4 to -1 ‰), and preferential incorporation of light isotopes onto Fe-Mn oxides of the soil derived Hg.

In summary, the isotope data in zone 1 show evidence for the addition of Hg from overlying soil and mobilization of Hg within the profile based on the light Δ^{199}Hg, Δ^{201}Hg, and δ^{202}Hg values.

4.6.1.2 Possibility of Direct Deposition of Hg(0) to the Sediments

An alternative, or potentially additional, possibility to explain the gain of Hg with negative MIF is direct atmospheric deposition of Hg into the samples. Physical weathering by roots could have promoted the incorporation of atmospheric Hg(0) by providing freshly exposed mineral and organic surfaces which lead to enhanced atmospheric deposition into the samples. However, this process is already accounted for as a source of Hg to soil. I cannot directly rule out direct atmospheric deposition to the samples, but it is difficult to disentangle from the delivery of Hg from soil as the isotopic compositions are expected to be similar. Additionally, in the current forested Clay City, KY there are many sinks for Hg(0) which reduces the significance of this process for the samples.

4.6.2 Zone 2 – Evidence for Mobilization of Hg in the Outcrop

Zone 2 hosts samples transitioning from heavily weathered into slightly weathered, indicated by near complete depletion of pyrite S throughout and low TOC values that gradually increase moving from the heavily weathered section towards the well-preserved interior. This zone has consistently heavy δ^{202}Hg values relative to zone 3 with slightly negative variations in Δ^{199}Hg and Δ^{201}Hg MIF in the three samples from 1.5 – 2.1 m where zone 2 begins and TOC values are similar to zone 1 (Fig. 4.3). As the Δ^{201}Hg values are more pronounced, I will use these values to discuss MIF in this section. The slightly negative MIF from 1.5 – 2.1 m relative to zone 3 indicates contribution of soil-derived or atmospheric deposition of Hg to a lesser degree than zone 1, and I infer the heavy δ^{202}Hg indicates loss of authigenic Hg during weathering. From 2.4 m to the end of zone 2, there is still a shift to heavy MDF values relative to zone 3, but no variation in MIF. Therefore, I propose that these positive MDF data are best explained by loss of Hg during weathering of organic matter throughout zone 2, and the negative MIF from 1.5 – 2.1 m indicates gain of soil derived Hg to a lesser degree than zone 1.

As discussed in the previous section, weathering of organic matter is inferred to preferentially mobilize light isotopes from authigenic Hg, leaving heavy isotope compositions in the rock and explaining the heavy MDF values in zone 2. Evidence for oxidative weathering interactions in this zone can be seen in the >99 % loss of pyrite S throughout the entire zone and gradually increasing TOC values when moving from the beginning of zone 2 towards zone 3. The CIA values indicate loss of soluble elements from 1.5 – 2.1 m, and less substantial loss from 2.4 m to the end of zone 2. Thus, fluid interaction occurred in this zone, with more loss of soluble elements from 1.5 – 2.1 m,

and minimal loss of soluble elements from 2.4 m to the end of zone 2. These data substantiate the idea that oxidative weathering (via fluid intrusions) played a significant role in the geochemistry of Zone 2. Therefore, it is possible authigenic Hg was mobilized during weathering, and Hg could have been gained from fluids.

Mercury loss via oxidative weathering may not be the only Hg transformation in Zone 2; Hg abundances in zone 2 are more variable than within the other zones, which may support the idea that Hg was gained. There is no evidence for formation of secondary Mn oxides in zone 2, as Mn (τ) and Mn/Ti values are constantly low and flat (Fig. 4.3), which indicates that Hg gain by adsorption to Mn-oxides is unlikely. However, Fe (τ) and Fe/Ti values are elevated and variable in this zone. Therefore, Hg in solution may have adsorbed to Fe-oxides (if present) or bound to organic matter ligands. The shifts to light MIF values from 1.5 – 2.1 m in this zone indicate gain of Hg may have been derived from soil. However, if there was gain of Hg from 2.4m to the end of zone 2, it would likely not be derived from soil as there is no MIF variation, which would be indicative of atmospheric/soil Hg.

4.6.2.1 Alternative/Additional Explanations for positive MDF

4.6.2.1.1 Gain of Hg from Elsewhere in the Outcrop

An alternative mechanism for gain of heavy MDF values in zone 2 is the gain of Hg from upper sections of the outcrop that have heavy MDF values. This outcrop hosts multiple black shale beds, thus it is possible Hg from another bed was mobilized and transported to zone 2 where it was bound to organic matter, or potentially adsorbed to a

secondary Fe-oxide. This possibility is difficult to support with data as there is no information about the Hg isotopic composition of the overlying sediments.

4.6.2.1.2 Microbial Demethylation/Reduction of Hg

Another alternative mechanism that could lead to positive MDF is microbial demethylation/reduction of Hg. Laboratory experiments of have shown microbial demethylation/reduction reduces methylmercury and Hg(II), respectively, creating gaseous Hg. These processes preferentially target light isotopes, which would leave a heavy isotopic signature in the rock and does not induce MIF (Kritee et al., 2007, 2009). These processes are assumed to occur after deposition of the outcrop and be related to weathering. Aerobic heterotrophs in the outcrop have been shown to utilize the ancient organic carbon as an energy source (Petsch et al., 2001a). However, it is unknown whether organisms in Clay City possess the capability to metabolize Hg.

4.6.3 Implications for Paleoenvironmental Studies

The data from this study reveals significant shifts in the isotopic composition of Hg and minimal Hg abundance variations during weathering of black shales. I observed a range of δ^{202}Hg values spanning 1.09 ‰ (±0.08‰ 2SD), Δ^{199}Hg values spanning 0.20 ‰ (±0.05‰ 2SD), , and Δ^{201}Hg values spanning 0.21 ‰ (±0.04‰ 2SD).

Paleoenvironmental studies have utilized Hg isotope ratios and/or Hg abundances in ancient sedimentary rocks to investigate volcanism (e.g., Sanei et al., 2012; Sial et al., 2013; Grasby et al., 2013; Thibodeau et al., 2016; Charbonnier & Follmi, 2017; Percival et al., 2017; Scaife et al., 2017), sources of Hg to the ocean (e.g., Yuan et al., 2023), and

paleoredox conditions (Zheng et al., 2018, 2023; Sun et al., 2023; Wu et al., 2023). The implications for each study type is discussed below.

For studies of ancient volcanism utilizing black shales, Hg abundances normalized to TOC and/or total S have become universally used to signify enrichments of Hg that are not due to an increase of organic matter and/or S burial (Charbonnier & Follmi, 2017; Percival et al., 2017; Scaife et al., 2017; Charbonnier et al., 2020; Park et al., 2022). I found that heavily weathered samples retained significant abundances of Hg even after substantial loss of TOC, resulting in high Hg/TOC ratios. Without considering the effects of weathering, high Hg/TOC ratios would incorrectly indicate a large flux of Hg to the ocean at the time of deposition. Notably, the findings agree with the observations from the black shale weathering studies of Charbonnier et al. (2020) and Park et al. (2022) which showed variations of Hg/TOC ratios during weathering. However, while these studies reported significant Hg loss in heavily weathered samples, our findings indicate that Hg was lost and gained. As noted previously, I suggest the gain of Hg is due to secondary enrichments of Hg facilitated by adsorption to secondary Fe-Mn oxides that did not occur in the other studies.

After authigenic enrichments of Hg have been confirmed in volcanism studies, often Hg MIF will be used to help apply constraints on sources of Hg. In volcanism studies variations in Δ^{199}Hg of ~ +0.1 to 0.2 are used to detect subaerial volcanism (e.g., Meixnerová et al., 2021), while submarine volcanism is expected to exhibit Δ^{199}H ≈ 0‰ as mantle Hg is emitted with no MIF (Zambardi et al., 2009). Additionally, inputs of Hg can also be constrained using MIF data. For example, Jin et al. (2023) identified Δ^{199}Hg shifts of ~ - 0.2 to suggest Hg release from organic rich deposits in the ocean by

explosive hydrothermal venting. These negative MIF shifts fall within the range of fractionation observed in this study, implying weathering could lead to erroneous indications of volcanism. I note that the Hg isotopic composition of the sediments and the local atmospheric/soil Hg isotopic composition is an important factor that is variable based on location.

Recently Hg isotope studies have detected photic zone euxinia (PZE), a condition where anoxic and H_2S-rich waters are present in the photic zone on the ocean. Ancient PZE was a potential impediment to the evolution of aerobic life and a kill mechanism for mass extinctions (Zheng et al., 2018), using MIF and MDF data. In studies focusing on PZE, Δ^{199}Hg shifts of ~ -0.1 to 0.3 ‰ and δ^{202}Hg shifts of approximately +0.4 ‰ have been identified to detect PZE in ancient oceans (Zheng et al., 2018, 2023; Sun et al., 2023; Wu et al., 2023). These isotopic shifts fall within the range of fractionation observed in the sample set, implying weathering could support erroneous indications of PZE.

4.7. Conclusions

The findings presented in this study highlight the significant impact of weathering processes on Hg isotope signals in sedimentary rocks. Investigation of black shale samples from Clay City, KY (USA) revealed substantial shifts in δ^{202}Hg, Δ^{199}Hg, and Δ^{201}Hg values, amounting to -1.09 ‰ (±0.08‰ 2SD), 0.20 ‰ (±0.05‰ 2SD), and (±0.04‰ 2SD), respectively. Δ^{202}Hg had no significant variations throughout the weathering profile. These postdepositional changes have the potential to mask or generate erroneous signatures related to volcanic or paleoredox processes, even in samples with

minimal indications of weathering. Consequently, caution is required when interpreting isotopic signatures, as altered compositions can persist in samples with minimal indications of weathering, emphasizing the need for careful evaluation.

Preservation of pyrite S content is a promising indicator for assessing the preservation of Hg isotopic signatures in weathered samples. The sample at 6.4 m with ~80% breakdown of pyrite S displays isotopic variations that are indistinguishable within error with the most well-preserved sample at 13.7 m, suggesting that early stages of oxidative weathering do not introduce detectable isotopic fractionation. However, isotopic variations were observed in all samples that lost >99% of S Pyrite, even in samples that displayed only minimal loss of total organic carbon (~15%). However, further testing is necessary to confirm the reliability of S pyrite as an indicator of how well a samples Hg isotopic composition is preserved.

The analysis of the samples revealed a combination of processes that I suggest is the most parsimonious explanation for the isotopic shifts in the weathered samples. These processes include authigenic Hg mobilization through oxidative weathering and Hg gain from soil-derived sources or remobilization from upper layers of the outcrop. Mercury gain was facilitated by adsorption onto secondary Fe-Mn oxides or organic ligands. The observed variations in MDF and MIF values can be attributed to positive MDF during authigenic Hg mobilization, incorporation of Hg in weathering fluids (with isotopic compositions that can vary based on location), and negative MDF during adsorption to Fe-Mn oxides. The adsorption of Hg to secondary Fe-Mn oxides plays a crucial role in mobility of Hg, acting as a sink for Hg in solution that could otherwise possibly be delivered to aquatic systems.

The study revealed that the Hg isotopic composition of the local soil, which is influenced by atmospheric Hg and surrounding plants, imparts a significant isotopic signature onto the rocks during weathering. Thus, regional Hg isotope ratios of atmospheric and soil Hg play a fundamental role in shaping the isotopic compositions during weathering processes. The interplay between weathering processes and Hg isotope fractionation observed in this study calls for careful examination of weathering influences when selecting samples for paleoenvironmental studies.

4.8 Acknowledgements

This work was supported by NASA Future Investigators in NASA Earth and Space Science and Technology Fellowship to Sullivan (19-PLANET20-0226) and NSF EAR – Geobiology and low temp. Geochem. (943360412).

4.9 References

Andersen, M.B., Stirling, C.H., Weyer, S. (2017) Uranium Isotope Fractionation. Reviews in Mineralogy and Geochemistry, 82, 799–850.

Barling, J. and Anbar, A.D. (2004) Molybdenum isotope fractionation during adsorption by manganese oxides. Earth and Planetary Science Letters, 217(3–4), 315–329.

Bergquist, B.A. and Blum, J.D. (2009) The Odds and Evens of Mercury Isotopes: Applications of Mass-Dependent and Mass-Independent Isotope Fractionation. Elements, 5, 353–357.

Blum, J.D. and Bergquist, B.A. (2007) Reporting of variations in the natural isotopic composition of mercury. Analytical and Bioanalytical Chemistry, 388(2), 353–359.

Blum, J.D., Sherman, L.S., Johnson, M.W. (2014) Mercury Isotopes in Earth and Environmental Sciences. Annual Review of Earth and Planetary Sciences, 42, 249–269.

Charbonnier, G., Adatte, T., Föllmi, K.B, Suan, G (2020) Effect of Intense Weathering and Postdepositional Degradation of Organic Matter on Hg/TOC Proxy in Organic-rich Sediments and its Implications for Deep-Time Investigations. Geochemistry, Geophysics, Geosystems, 21, 1–19.

Charbonnier, G. and Follmi, K.B. (2017) Mercury enrichments in lower Aptian sediments support the link between Ontong Java large igneous province activity and oceanic anoxic episode 1a. Geology, 45, 63–66.

Chen, J., Hintelmann, G., Dimock, B. (2010) Chromatographic pre-concentration of Hg from dilute aqueous solutions for isotopic measurement by MC-ICP-MS. Journal of Analytical and Atomic Spectrometry, 25, 1402–1409.

Chen, J., Hintelmann, H., Zheng, W., Feng, X., Cai, H., Wang, Z., Yuan, S., Wang, Z. (2016) Isotopic evidence for distinct sources of mercury in lake waters and sediments. Chemical Geology, 426, 33–44.

Demers, J.D., Blum, J.D., Zak, D.R. (2013) Mercury isotopes in a forested ecosystem: Implications for air-surface exchange dynamics and the global mercury cycle: Mercury isotopes in a forested ecosystem. Global Biogeochemical Cycles, 27, 222–238.

Demers, J.D., Sherman, L.S., Blum, J.D., Marsik, F.J., Dvonch, J.T. (2015) Coupling atmospheric mercury isotope ratios and meteorology to identify sources of mercury impacting a coastal urban-industrial region near Pensacola, Florida, USA. Global Biogeochemical Cycles, 29, 1689–1705.

Eglinton, T.I. (1994) Carbon isotopic evidence for the origin of macromolecular aliphatic structures in kerogen. Organic Geochemistry, 21, 721–735.

Ericksen, J.A., Gustin, M.S., Schorran, D.E., Johnson, D.W., Lindberg, S.E., Coleman, J.S. (2003) Accumulation of atmospheric mercury in forest foliage. Atmospheric Environment, 37, 1613–1622.

Estrade, N., Carignan, J., Sonke, J.E., Donard, O.F.X. (2009) Mercury isotope fractionation during liquid–vapor evaporation experiments. Geochimica et Cosmochimica Acta, 73, 2693–2711.

Frieling, J., Mather, T.A., März, C., Jenkyns, H.C., Hennekam, R., Reichart, G-J., Slomp, C.P., van Helmond, N.A.G.M. (2023) Effects of redox variability and early diagenesis on marine sedimentary Hg records. Geochimica et Cosmochimica Acta, 351, 78–95.

Ghosh, S., Schauble, E.A., Lacrampe Couloume, G., Blum, J.D., Bergquist, B.A. (2013) Estimation of nuclear volume dependent fractionation of mercury isotopes in equilibrium liquid–vapor evaporation experiments. Chemical Geology, 336, 5–12.

Grasby, S.E., Sanei, H., Beauchamp, B., and Chen, Z. (2013) Mercury deposition through the Permo-Triassic Biotic Crisis. Chemical Geology, 351, 209–216.

Gratz, L.E., Keeler, G.J., Blum, J.D., Sherman, L.S. (2010) Isotopic composition and fractionation of mercury in Great Lakes precipitation and ambient air. Environmental Science and Technology, 44, 7764–7770.

Hayes, R.A. (1993) Soil Survey of Powell and Wolfe Counties, Kentucky. US Department of Agriculture, Soil Conservation Service.

Holmes, P., James, K.A.F., Levy, L.S. (2009) Is low-level environmental mercury exposure of concern to human health? Science of the Total Environment, 408, 171–182.

Huang, Q., Liu, Y., Chen, J., Feng, X., Huang, W., Yuan, S., Cai, G., and Fu, X. (2015) An improved dual-stage protocol to pre-concentrate mercury from airborne particles for precise isotopic measurement. Journal of Analytical and Atomic Spectrometry, 30, 957–966.

Jaffe, L.A., Peucker-Ehrenbrink, B., Petsch, S.T. (2002) Mobility of rhenium, platinum group elements, and organic carbon during black shale weathering. Earth and Planetary Science Letters, 198, 339–353.

Jin, S., Kemp, D.B., Yin, R., Sun, R., Shen, J., Jolley D.W., Vieira, M., Huang, C. (2023) Mercury isotope evidence for protracted North Atlantic magmatism during the Paleocene-Eocene Thermal Maximum. Earth and Planetary Science Letters, 602, 117926.

Jiskra, M., Wiederhold, J.G., Bourdon, B., Kretzschmar, R. (2012) Solution speciation controls mercury isotope fractionation of Hg(II) sorption to goethite. Environmental Science and Technology, 46, 6654–6662.

Jiskra, M., Wiederhold, J.G., Skyllberg, U., Kronberg, R.-M., Hajdas, I., Kretzschmar, R. (2015) Mercury Deposition and Re-emission Pathways in Boreal Forest Soils Investigated with Hg Isotope Signatures. Environmental Science and Technology, 49, 7188–7196.

Kane, J.S., Arbogast, B.F., Leventhal, J.S. (1990) Characterization of Devonian Ohio Shale SDO-1 as a USGS geochemical reference sample: Geostandards Newsletter, 14, 169–196.

Kendall, B., Dahl, T.W., Anbar, A.D. (2017) The stable isotope geochemistry of molybdenum. Reviews in Mineralogy and Geochemistry, 82, 683–732.

Kritee, K., Barkay, T., Blum, J.D. (2009) Mass dependent stable isotope fractionation of mercury during *mer* mediated microbial degradation of monomethylmercury. Geochimica et Cosmochimica Acta, 73, 1285–1296.

Kritee, K., Blum, J.D., Johnson, M.W., Bergquist, B.A., Barkay, T. (2007) Mercury Stable Isotope Fractionation during Reduction of Hg(II) to Hg(0) by Mercury Resistant Microorganisms. Environmental Science and Technology, 41, 1889–1895.

Li, Y., Shao, L., Fielding, C.R., Frank, T.D., Wang, D., Mu, G., Lu, J. (2023) The chemical index of alteration in Permo-Carboniferous strata in North China as an indicator of environmental and climate change throughout the late Paleozoic Ice Age. Global and Planetary Change, 221, 104035.

Liu, H., Shao, J., Yu, B., Liang, Y., Duo, B., Fu, J., Yang, R., Shi, J. Jiang, G. (2019) Mercury isotopic compositions of mosses, conifer needles, and surface soils: Implications for mercury distribution and sources in Shergyla Mountain, Tibetan Plateau. Ecotoxicology and Environmental Safety, 172, 225–231.

Lockwood, R. and Chen, K.Y. (1973) Adsorption of mercury(II) by hydrous manganese oxides. Environmental Science and Technology, 7, 1028–1034.

Loukola-Ruskeeniemi, K., Kantola, M., Halonen, T., Seppanen, K., Henttonen, P., Kallio, E., Kurki, P., Savolainen, H. (2002) Mercury-bearing black shales and human Hg instake in eastern Finland: impact and mechanisms. Environmental Geology, 43, 283–297.

Mason, R.P., Choi, A.L., Fitzgerald, W.F., Hammerschmidt, C.R., Lamborg, C.H., Soerensen, A.L., Sunderland, E.M. (2012) Mercury biogeochemical cycling in the ocean and policy implications. Environmental Research, 119, 101–117.

Mason R.P., Fitzgerald W.F., Morel F.M.M. (1994) The biogeochemical cycling of elemental mercury: anthropogenic influences. Geochimica et Cosmochimica Acta, 58, 3191–3198.

Mason, R.P. and Sheu, G.-R. (2002) Role of the ocean in the global mercury cycle. Global Biogeochemical Cycles, 16, 1–14.

Meixnerová, J., Blum, J.D., Johnson, M.W., Stüeken, E.E., Kipp, M.A., Anbar, A.D., and Buick, R. (2021) Mercury abundance and isotopic composition indicate subaerial volcanism prior to the end-Archean “whiff” of oxygen. Proceedings of the National Academy of Sciences, 118, 1–6.

Morford, J.L., Emerson, S.R., Breckel, E.J., Kim, S.H. (2005) Diagenesis of oxyanions (V, U, Re, and Mo) in pore waters and sediments from a continental margin. Geochimica et Cosmochimica Acta, 69, 5021–5032.

Nesbitt, H.W. and Young, G.M. (1982) Early Proterozoic climates and plate motions inferred from major element chemistry of lutites. Nature, 299, 715–717.

Nriagu, J. and Becker, C. (2003) Volcanic emissions of mercury to the atmosphere: Global and regional inventories. Science of the Total Environment, 304, 3–12.

Obrist, D., Agnan, Y., Jiskra, M., Olson, C.L., Colegrove, D.P., Hueber, J., Moore, C.W., Sonke, J.E., Helmig, D. (2017) Tundra uptake of atmospheric elemental mercury drives Arctic mercury pollution. Nature, 547, 201–204.

Olson, C.L., Jiskra, M., Sonke, J.E., Obrist, D. (2019) Mercury in tundra vegetation of Alaska: Spatial and temporal dynamics and stable isotope patterns. Science of the Total Environment, 660, 1502–1512.

Park J., Stein H.J., Georgiev S.V., Hannah J.L. (2022) Degradation of Hg signals on incipient weathering: Core versus outcrop geochemistry of Upper Permian shales, East Greenland and Mid-Norwegian Shelf. Chemical Geology, 608, 121030.

Percival, L.M.E., Ruhl, M., Hesselbo, S.P., Jenkyns, H.C., Mather, T.A., Whiteside, J.H. (2017) Mercury evidence for pulsed volcanism during the end-Triassic mass extinction. Proceedings of the National Academy of Sciences, 114, 7929–7934.

Petsch, S.T., Berner, R.A., Eglinton, T.I. (2000) A field study of the chemical weathering of ancient sedimentary organic matter. Organic Geochemistry, 31, 457–475.

Petsch, S.T., Eglinton, T.I., Edwards, K.J. (2001a) ^{14}C-Dead Living Biomass: Evidence for Microbial Assimilation of Ancient Organic Carbon During Shale Weathering. Science, 292, 1127–1131.

Petsch, S.T., Smernik, R.J., Eglinton, T.I., Oades, J.M. (2001b) A solid state ^{13}C-NMR study of kerogen degradation during black shale weathering. Geochimica et Cosmochimica Acta, 65, 1867–1882.

Richardson, J.B., Aguirre, A.A., Buss, H.L., O'Geen, A.T., Gu, X., Rempe, D.M., Richter, D.B. (2018) Mercury Sourcing and Sequestration in Weathering Profiles at Six Critical Zone Observatories. Global Biogeochemical Cycles, 32, 1542–1555.

Rodríguez-González, P., Epov, V.N., Bridou, R., Tessier, E., Guyoneaud R., Monperrus., Amouroux, D. (2009) Species-Specific Stable Isotope Fractionation of Mercury

during Hg(II) Methylation by an Anaerobic Bacteria (Desulfobulbus propionicus) under Dark Conditions. Environmental Science and Technology, 43, 9183–9188.

Rudnick, R.L. and Gao, S. (2003) Composition of the Continental Crust. Treatise on Geochemistry, 3, 1−64.

Sanei, H., Grasby, S., Beauchamp, B. (2012). Latest Permian mercury anomalies. Geology, 40, 63–66.

Scaife, J.D., Ruhl, M., Dickson, A.J., Mather, T.A., Jenkyns, H.C., Percival, L.M.E., Hesselbo, S.P., Cartwright, J., Eldrett, J.S., Bergman, S.C., Minisini, D. (2017) Sedimentary Mercury Enrichments as a Marker for Submarine Large Igneous Province Volcanism? Evidence From the Mid-Cenomanian Event and Oceanic Anoxic Event 2 (Late Cretaceous). Geochemistry, Geophysics, Geosystems, 18, 4253–4275.

Schroeder, W.H. and Munthe, J. (1998) Atmospheric mercury—an overview. Atmospheric Environment, 32, 809–822.

Selin N.E. (2009) Global Biogeochemical Cycling of Mercury: A Review. Annual Review of Environmental and Resources, 34, 43–63.

Sial, A.N., Chen, J., Lacerda, L.D., Frei, R., Tewari, V.C., Pandit, M.K., Gaucher, C., Ferreira, V.P., Cirilli, S., Peralta, S., Korte, C., Barbosa, J.A., Pereira, N.S. (2016). Mercury enrichment and Hg isotopes in Cretaceous-Paleogene boundary successions: Links to volcanism and palaeoenvironmental impacts. Cretaceous Research, 66, 60–81.

Skyllberg, U., Xia, K., Bloom, P.R., Nater, E.A., Bleam, W.F. (2000) Binding of mercury (II) to reduced sulfur in soil organic matter along upland-peat soil transects. Journal of Environmental Quality, 29(3), 855–865.

Streets, D.G., Horowitz, H.M., Jacob, D.J., Lu, Z., Levin, L., ter Schure, A.F.H., Sunderland, E.M. (2017) Total mercury released to the environment by human activities. Environmental Science and Technology, 51, 5969–5977.

Sun, R., Cao, F., Dai, S., Shan, B., Qi, C., Xu, Z., Li, P., Liu, Y., Zheng, W., Chen, J. (2023) Atmospheric Mercury Isotope Shifts in Response to Mercury Emissions from Underground Coal Fires. Environmental Science Technology, 57, 8638–8649.

Sunderland, E.M. (2007) Mercury exposure from domestic and imported estuarine and marine fish in the U.S. seafood market. Environmental Health Perspectives, 115, 235–242.

Szponar, N., Su, Y., Stupple, G., McLagan, D.S., Pilote, M., Munoz, A., Mitchell, C.P.J., Steffen, A., Wania, F., Bergquist, B.A. (2023) Applying Passive Air Sampling and Isotopic Characterization to Assess Spatial Variability of Gaseous Elemental Mercury Across Ontario, Canada. Journal of Geophysical Research Atmospheres, 128, 1–19.

Thibodeau, A. T., Ritterbush, K., Yager, J. A., West, A. J., Ibarra, Y., Bottjer, D. J., Berelson, W. M., Bergquist, B. A., and Corsetti, F. A. (2016) Mercury anomalies and the timing of biotic recovery following the end-Triassic mass extinction. Nature Comm., 7, 1-8.

Tsui, M.T.K., Blum, J.D., Kwon, S.Y., Finlay, J.C., Balogh, S.J., Nollet, Y.H. (2012) Sources and Transfers of Methylmercury in Adjacent River and Forest Food Webs. Environmental Science and Technology, 46, 10957–10964.

Tuttle, M.L.W., Breit, G.N., Goldhaber, M.B. (2009) Weathering of the New Albany Shale, Kentucky: II. Redistribution of minor and trace elements. Applied Geochemistry, 24, 1565–1578.

Wiederhold, J., Cramer, C., Daniel, K., Infante, I., Bourdon, B., Kretzschmar, R. (2010) Equilibrium mercury isotope fractionation between dissolved Hg(II) species and thiol-bound Hg. Environmental Science and Technology, 44, 4191–4197.

Woerndle G., Tsz-Ki, T., Sebestyen, S., Blum, J., Nie, X., Kolka, R. (2018) New Insights on Ecosystem Mercury Cycling Revealed by Stable Isotopes of Mercury in Water Flowing from a Headwater Peatland Catchment. Environmental Science and Technology, 52, 1854–1861.

Wu, Y., Tian, H., Yin, R., Chen, D., Grasby, S. E., Shen, J., Li, T., Ji, S., Peng, P. (2023) Highly fractionated Hg isotope evidence for dynamic euxinia in shallow waters of the Mesoproterozoic ocean. Earth and Planetary Science Letters, 616, 118211.

Yamashita, Y., Takahashi, Y., Haba, H., Enomoto, S., Shimizu, H. (2007) Comparison of reductive accumulation of Re and Os in seawater-sediment systems. Geochimica et Cosmochimica Acta, 71, 3458-3475.

Yin, R., Krabbenhoft, D., Bergquist, B., Zheng, W., Lepak, R., Hurley, J. (2016) Effects of mercury and thallium concentrations on high precision determination of mercury isotopic composition by Neptune Plus multiple collector inductively coupled plasma mass spectrometry. Journal of Analytical and Atomic Spectrometry, 31, 2060-2068.

Yu, B., Fu, X., Yin, R., Zhang, H., Wang, X., Lin, C.-J., Wu, C., Zhang, Y., He, N., Fu, P., Wang, Z., Shang, L., Sommar, J., Sonke, J., Maurice L., Guinot B., Feng, X. (2016) Isotopic Composition of Atmospheric Mercury in China: New Evidence

for Sources and Transformation Processes in Air and in Vegetation. Environmental Science and Technology, 50, 9262–9269.

Yuan, W., Liu, M., Chen, D., Xing, Y-W., Spicer, R. A., Chen, J., Them, T. R., Wang, X., Li, S., Guo, C., Zheng, G., Zhang, L., Zhang, H., Feng, X. (2023) Mercury isotopes show vacular plants had colonized land extensively by the early Silurian. Science Advances, 9, 1 – 10.

Zambardi, T., Sonke, J. E., Toutain, J. P., Sortino, F., Shinohara, H. (2009) Mercury emissions and stable isotopic compositions at Vulcano Island (Italy). Earth and Planetary Science Letters, 277 (1–2), 236–243.

Zheng, W., Demers, J. D., Lu, X., Bergquist, B. A., Anbar, A. D., Blum, J. D., Gu, B. (2019) Mercury Stable Isotope Fractionation during Abiotic Dark Oxidation in the Presence of Thiols and Natural Organic Matter. Environmental Science and technology, 53, 1853-1862.

Zheng, W., Gilleaudeau, G. J., Algeo, T.J., Zhao, Y., Song, Y., Zhang, Y., Sahoo, S. K., Anbar, A. D., Carmichael, S. K., Xie, S., Liu, C-Q., Chen, J. (2023) Mercury isotope evidence for recurrent photic-zone euxinia triggered by enhanced terrestrial nutrient inputs during the Late Devonian mass extinction. Earth and Planetary Science Letters, 613, 118175.

Zheng, W., Gilleaudeau, G. J., Kah, L.C., Anbar, A. D. (2018) Mercury isotope signatures record photic zone euxinia in the Mesoproterozoic ocean. Proceedings of the National Academy of Sciences, 115, 10594−10599.

Zheng, W., Obrist, D., Weis, D., Bergquist, B. A. (2016) Mercury isotope compositions across North American forests: Mercury Isotopes Across U.S. Forests. Global Biogeochemical Cycles, 30, 1475–1492.

Zheng, W., Xie, Z., Bergquist, B. A. (2015) Mercury Stable Isotopes in Ornithogenic Deposits As Tracers of Historical Cycling of Mercury in Ross Sea, Antarctica. Environmental Science and Technology, 49, 7623 – 7632.

Zhou, J., Obrist, D., Dastoor, A., Jiskra, M., Ryjkov, A. (2021) Vegetation uptake of mercury and impacts on global cycling. Nature Reviews in Earth and Environment, 2, 269–284.

CHAPTER 5

CONCLUSIONS

Chapter 2 provides the first application of Re isotopes as a paleoredox tool throughout a time of changing environmental redox conditions. I found that the variations in Re isotope ratios coincided with other redox sensitive metals that have different removal mechanisms. For example, at the beginning of the 'whiff' interval when Re enrichment begins there is also a shift in Re to light isotope ratios. At this time, Mo and Tl isotopes shift towards heavy and light values, respectively, that is thought to be due to isotopic fraction introduced by adsorption of these elements onto Fe-Mn oxides. Re, however, is insensitive to Fe-Mn cycling. The shift in Re isotopes is potentially due to oxidative crustal weathering delivering lighter Re into the ocean, driving the isotopes lighter, or perhaps fractionation during removal to a reducing sink. Unfortunately, at this early stage in the development of Re isotopes as a geochemical tool, there is much about Re geochemical behavior that is unknown.

For paleoredox applications, an examination of modern settings is an obvious next step to take to understand Re isotopic fractionation when the redox conditions are known. Analyses of the abundance and isotopic composition of the water column, suspended particles, sediments, and sediment pore waters under reducing conditions will provide much needed constraints on Re isotopic fractionation. Commonly studied locations for this type of study are redox stratified bodies of water (e.g., the Black Sea, the Benguela Margin) which is discussed in more detail in the 'future work' section of chapter 2. An important open question is if there are any rocks that record the chemical composition of seawater. If Re is similar to Mo (which it often is), organic rich shales deposited under

highly sulfidic (i.e., euxinic) conditions are the most likely target to test if these sediments can record the isotopic composition of seawater. Another interesting open avenue of research is the Re isotopic composition of carbonates. While carbonates are not known to have Re abundances relative to black shales, they have been shown to be useful for other redox sensitive elements (e.g., U; Chen et al., 2016, 2018) and could possibly record the isotopic composition of seawater with minimal or no fractionation. Furthermore, carbonates are commonly deposited throughout Earth history, thus could be an excellent source of information from the past.

Chapter 3 provides the first application of Re isotopes as a nuclear forensics tool. The Re isotopic composition of uranium ore concentrates (UOC) showed significant isotopic fractionation of up to 2.32‰ in a small set of 12 samples. The UOCs were derived from unconformity, sandstone, and quart-pebble conglomerate U ores. For nuclear forensic applications, an examination of the isotopic composition of additional ore types and more samples from the same ore types examined in this study would be beneficial. There are 12 additional primary U deposit types that the International Atomic Energy Agency recognizes, one of which is black shales. As discussed previously, black shales deposited under euxinic conditions are one of the most likely sedimentary rocks to record the Re isotopic composition of seawater. Uranium ore concentrates derived from black shale ore will likely be enriched in Re due to the high Re abundance of black shales, which should make isotopic analyses easy with small sample sizes.

One of the challenges for the widespread use of Re isotopes as a nuclear forensics tool – without improvements to the method I developed in Chapter 3 – is that ~10 ng of

Re is required for one isotopic analysis. This can be prohibitively high for isotopic analysis of low Re abundance nuclear material. However, the sample requirement limitation can be alleviated by modifications to the running parameters for the MC-ICP-MS method. For example, using more sensitive detectors, modifying the inlet systems flow rate, and decreasing the number of cycles required for accurate isotope ratio analyses will be good future directions for research.

A current open question is if there is Re isotopic fractionation introduced during processing of ore material to create the UOCs. Put another way, it is unknown if the Re isotopic composition of a UOC sample represents the bulk Re isotopic composition of the ore material it was derived from. During UOC processing the goal is to isolate U from matrix elements. Rhenium is considered a matrix element that processing tries to remove, so it is likely that some Re is lost during processing. However, the extreme enrichment of Re in some sandstone-ore derived UOCs > 1 ppm – relative to most other ores in the 10s of ppb – is very interesting and it would be scientifically beneficial to determine the cause of these high Re abundances. Are the high Re abundances related to high Re abundance ore material, or is there a reagent used in to milling process that has a high Re blank? If the high Re abundances are related to having high Re abundances in the ore material, that would indicate that some milling methods for sandstone ore let significant abundances of Re through to the produced UOC and may indicate that geologic information from the ore material can be extrapolated if the isotopic composition of Re is largely retained through the milling process. However, if the high Re abundances are related to a reagent used in the processing of the ore, this would provide valuable nuclear forensics information that could help narrow down which milling facility a UOC could

have been produced from and what method was used. There are many interesting future directions to study in this area including examination of the original ore material, to the reagents used during processing. Thus, finding more information about Re geochemistry during ore processing will be very interesting from nuclear forensics and possibly a geologic point of view if the isotopic composition of the ore material is retained throughout processing.

Chapter 4 provides the first study of the influence of weathering on Hg isotope signatures in black shales. This data set was challenging to interpret at first. The first surprise was the relatively consistent Hg abundance throughout the weathering profile. Significant loss of Hg was expected in the heavily weathered samples based on black shale weathering studies that had shown >75% loss of Hg in heavily weathered black shales. The abundance data was double, and triple checked to make sure this was indeed the case. I was able to convince myself that the data was accurate, and that there was indeed similar Hg abundances in heavily weathered samples and the less weathered samples. In the end, I think I have a story that is probably close to what has happened to the Hg in the outcrop. One possibility is that Hg mobility within the outcrop (from upper beds above the sampled bed perhaps) is more important than soil-derived Hg. More geochemical data from other layers would be helpful to find out if this is the case.

An open question raised by this study is how exactly Hg MIF can be altered by weathering. This study was not able to differentiate between Hg gained in Clay City samples by atmospheric deposition and deposition from fluid intrusion, both of which are capable of altering MIF in black shales. Regional Hg atmospheric isotopic compositions can be much different (> 1 ‰) than the isotopic compositions of samples. Thus, small

gains in Hg from atmospheric deposition could alter the MIF signal in black shales. Further examination determining the possible impact of Hg gain via atmospheric deposition is a promising direction for future research. An additional promising future direction to take to continue the study of Hg in weathering environments is to examine the speciation of Hg. The work in this dissertation examined bulk Hg and did not distinguish between chemical species. Microbial methylation of Hg has been shown to create an isotopic fractionation. Methylmercury is an extremely toxic neurotoxin to humans, thus it would be very interesting to see if there is methylmercury production occurring in the black shales from a human health perspective, as well as a paleoredox perspective as this process is associated with a mass-dependent fractionation. Alternatively, maybe there is microbial demethylation of Hg occuring which would be just as interesting to find. This is a great next step for the Clay City Samples. It is a very easy outcrop to access.

REFERENCES

Abshire, M.L., Romaniello, S.J., Kuzminov, A.M., Cofrancesco, J., Severmann, S., Riedinger, N. (2020) Uranium isotopes as a proxy for primary depositional redox conditions in organic-rich marine systems. Earth and Planetary Science Letters, 529, 115878.

Anbar, A.D., Buick, R., Gordon, G.W., Johnson, A.C., Kendall, B., Lyons, T.W., Ostrander, C.M., Planavsky, N.J., Reinhard, C.T., Stüeken, E.E. (2023) Technical comment on "Reexamination of 2.5-Ga 'whiff' of oxygen interval points to anoxic ocean before GOE." Science Advances, 9, eabq3736.

Anbar, A.D., Creaser, R.A., Papanastassiou, D.A., Wasserburg, G.J. (1992) Rhenium in seawater: Confirmation of generally conservative behavior. Geochimica et Cosmochimica Acta, 56, 4099–4103.

Anbar, A.D., Duan, Y., Lyons, T.W., Arnold, G.L., Kendall, B., Creaser, R.A., Kaufman, A.J., Gordon, G.W., Scott, C., Garvin, J., Buick, R. (2007) A Whiff of Oxygen Before the Great Oxidation Event? Science, 317, 1903–1906.

Anbar, A.D., Knab, K.A., Barling, J. (2001) Precise Determination of Mass-Dependent Variations in the Isotopic Composition of Molybdenum Using MC-ICPMS. Analytical Chemistry, 73, 1425–1431.

Anders, E. and Grevesse, N. (1989) Abundance of the elements: Meteoritic and solar. Geochimica et Cosmochimica Acta, 53, 197–214.

Andersen, M.B., Stirling, C.H., Weyer, S. (2017) Uranium Isotope Fractionation. Reviews in Mineralogy and Geochemistry, 82, 799–850.

Andrén, H., Rodushkin, I., Stenberg, A., Malinvsky, D., Baxter, D.C. (2004) Sources of mass bias and isotope ratio variation in multi-collector ICP-MS: optimization of instrumental parameters based on experimental observations. Journal of Analytical Atomic Spectrometry, 19, 1217–1224.

Barley, M.E., Bekker, A., Krapez, B. (2005) Late Archean to Early Paleoproterozoic global tectonics, environmental change and the rise of atmospheric oxygen. Earth and Planetary Science letters, 238, 156–171.

Barling, J. and Anbar, A.D. (2004) Molybdenum isotope fractionation during adsorption by manganese oxides. Earth and Planetary Science Letters, 217(3–4), 315–329.

Bennett, G., Dressler, B.O., Roberston, J.A. (1991) The Huronian supergroup and associated intrusive rocks, in: P.C. Thurston, H.R. Williams, R.H. Sutcliffe, G.M. Stott (Eds.), Geology of Ontario, Ontario Geologic Survey, 4, 549–591.

Bergquist, B.A. and Blum, J.D. (2009) The Odds and Evens of Mercury Isotopes: Applications of Mass-Dependent and Mass-Independent Isotope Fractionation. Elements, 5, 353–357.

Blum, J.D. and Bergquist, B.A. (2007) Reporting of variations in the natural isotopic composition of mercury. Analytical and Bioanalytical Chemistry, 388(2), 353–359.

Blum, J.D., Sherman, L.S., Johnson, M.W. (2014) Mercury Isotopes in Earth and Environmental Sciences. Annual Review of Earth and Planetary Sciences, 42, 249–269.

Bopp, C.J., Lundstrom, C.C., Johnson, T.M., Glessner, J.J.G. (2009) Variations in $^{238}U/^{235}U$ in uranium ore deposits: isotopic signatures of the U reduction process? Geology, 37, 611–614.

Brennecka, G.A., Borg, L.E., Hutcheon, I.D., Sharp, M.A., Anbar, A.D. (2010) Natural variations in uranium isotope ratios of uranium ore concentrates: Understanding the $^{238}U/^{235}U$ fractionation mechanism. Earth and Planetary Science Letters, 291, 228–233.

Brennecka, G.A., Wasylenki, L.E., Bargar, J.R., Weyer, S., Anbar, A.D. (2011) Uranium Isotope Fractionation during Adsorption to Mn-Oxyhydroxides. Environmental Science and Technology, 45, 1370–1375.

Burron, I., Costa, D., Sharpe, R., Fayek, M., Gauert, C., Hofmann, A. (2018) 3.2 Ga detrital uraninite in the Witwatersrand Basin, South Africa: Evidence of a reducing Archean atmosphere. Geology, 46, 295–298.

Catling, D.C. (2013) Astrobiology: A Very Short Introduction. Oxford University Press, l, 1–161.

Charbonnier, G., Adatte, T., Föllmi, K.B, Suan, G (2020) Effect of Intense Weathering and Postdepositional Degradation of Organic Matter on Hg/TOC Proxy in Organic-rich Sediments and its Implications for Deep-Time Investigations. Geochemistry, Geophysics, Geosystems, 21, 1–19.

Charbonnier, G. and Follmi, K.B. (2017) Mercury enrichments in lower Aptian sediments support the link between Ontong Java large igneous province activity and oceanic anoxic episode 1a. Geology, 45, 63–66.

Chen, J., Hintelmann, G., Dimock, B. (2010) Chromatographic pre-concentration of Hg from dilute aqueous solutions for isotopic measurement by MC-ICP-MS. Journal of Analytical and Atomic Spectrometry, 25, 1402–1409.

Chen, J., Hintelmann, H., Zheng, W., Feng, X., Cai, H., Wang, Z., Yuan, S., Wang, Z. (2016) Isotopic evidence for distinct sources of mercury in lake waters and sediments. Chemical Geology, 426, 33–44.

Colodner, D., Edmond, J., Boyle, E. (1995) Rhenium in the Black Sea: comparison with molybdenum and uranium. Earth and Planetary Science Letters, 131, 1–15.

Colodner, D., Sachs, J., Ravizza, G., Turekian, K., Edmond, J., Boyle, E. (1993) The geochemical cycle of rhenium: a reconnaissance. Earth and Planetary Science letters, 117, 205–221.

Dellinger, M., Hilton, R.G., Nowell, G.M. (2020) Measurements of rhenium isotopic composition in low-abundance samples. Journal of Analytical Atomic Spectrometry, 35, 377–387.

Dellinger, M., Hilton, R.G., Nowell, G.M. (2021) Fractionation of rhenium isotopes in the Mackenzie River basin during oxidative weathering. Earth and Planetary Science Letters, 573, 117131.

Delwiche, C.C. and Steyn, P.L. (1970) Nitrogen Isotope Fractionation in Soils and Microbial Reactions. Environmental Science and Technology, 11, 929–935.

Demers, J.D., Blum, J.D., Zak, D.R. (2013) Mercury isotopes in a forested ecosystem: Implications for air-surface exchange dynamics and the global mercury cycle: Mercury isotopes in a forested ecosystem. Global Biogeochemical Cycles, 27, 222–238.

Demers, J.D., Sherman, L.S., Blum, J.D., Marsik, F.J., Dvonch, J.T. (2015) Coupling atmospheric mercury isotope ratios and meteorology to identify sources of mercury impacting a coastal urban-industrial region near Pensacola, Florida, USA. Global Biogeochemical Cycles, 29, 1689–1705.

Denton, J.S., Bostick, D.A., Boulyha, S.F., Cunningham, J.A., Dimayuga, I., Hexel, C.R., Hiess, J., Jovanovic, S.V., Kaye, P, et al. (2022) International interlaboratory compilation of trace element concentrations in the CUP-2 uranium ore concentrate standard. Journal of Radioanalytical and Nuclear Chemistry, 332, 2817–2832.

Devlin McLoughlin, V.E.D., Shollenberger, Q.R., Brennecka, G.A. (2023) Determining provenance of uranium ore concentrates using $^{143}Nd/^{144}Nd$. Talanta, 253, 124088.

Dickson, A.J., Hsieh, Y., Bryan, A. (2020) The rhenium isotope composition of Atlantic Ocean seawater. Geochimica et Cosmochimica Acta, 287, 221–228.

Dooley, J.R., Harshman, E.N., Rosholt, J.N. (1974) Uranium-Lead ages of the uranium deposits of gas hills and Shirley basin, Wyoming, Economic Geology, 69, 527–531.

Du Vivier, A.D.C., Selby, D., Condon, D.J., Takashima, R., Nishi, H. (2015) Pacific 187Os/188Os isotope chemistry and U–Pb geochronology: Synchroneity of global Os isotope change across OAE 2. Earth and Planetary Science Letters, 428, 204–216.

Du Vivier, A.D.C., Selby, D., Sageman, B.B., Jarvis, I., Gröcke, D.R., Voigt, S. (2014) Marine 187Os/188Os isotope stratigraphy reveals the interaction of volcanism and ocean circulation during Oceanic Anoxic Event 2. Earth and Planetary Science Letters, 389, 23–33.

Duan, Y., Anbar, A.D., Arnols, G.L., Lyons, T.W., Gordon, G.W., Kendall, B. (2010) Molybdenum isotope evidence for mild environmental oxygenation before the Great Oxidation Event. Geochimica et Cosmochimica Acta, 74, 6655–6668.

Eglinton, T.I. (1994) Carbon isotopic evidence for the origin of macromolecular aliphatic structures in kerogen. Organic Geochemistry, 21, 721–735.

Eiler, J.M., Bergquist, B., Bourg, I., Cartigny, P., Farquhar, J., Gagnon, A., Guo, W., Halevy, I., Hofmann, A., Larson, T.E., Levin, N., Schauble, E.A., Stolper, D. (2014) Frontiers of stable isotope geoscience. Chemical Geology, 372, 119–143.

Ericksen, J.A., Gustin, M.S., Schorran, D.E., Johnson, D.W., Lindberg, S.E., Coleman, J.S. (2003) Accumulation of atmospheric mercury in forest foliage. Atmospheric Environment, 37, 1613–1622.

Estrade, N., Carignan, J., Sonke, J.E., Donard, O.F.X. (2009) Mercury isotope fractionation during liquid–vapor evaporation experiments. Geochimica et Cosmochimica Acta, 73, 2693–2711.

Finlay, A.J., Selby, D., Osborne M.J. (2012) Petroleum source rock identification of United Kingdom Atlantic Margin oil fields and the Western Canadian Oil Sands using Platinum, Palladium, Osmium and Rhenium: Implications for global petroleum systems. Earth and Planetary Science Letters, 313–314, 95–104.

Frieling, J., Mather, T.A., März, C., Jenkyns, H.C., Hennekam, R., Reichart, G-J., Slomp, C.P., van Helmond, N.A.G.M. (2023) Effects of redox variability and early diagenesis on marine sedimentary Hg records. Geochimica et Cosmochimica Acta, 351, 78–95.

Garvin, J., Buick, R., Anbar, A.D., Arnold, G.L., Kaufman, A.J. (2009) Isotopic evidence for an aerobic nitrogen cycle in the latest Archean. Science, 323, 1045–1048.

Ghosh, S., Schauble, E.A., Lacrampe Couloume, G., Blum, J.D., Bergquist, B.A. (2013) Estimation of nuclear volume dependent fractionation of mercury isotopes in equilibrium liquid–vapor evaporation experiments. Chemical Geology, 336, 5–12.

Goldman, A.D. and Kacar, B. (2021) Cofactors are Remnants of Life's Origin and Early Evolution. Journal of Molecular Evolution, 89, 127–133.

Gramlich, J.W., Murphy, T.J., Garner, E.L., Shields, W.R. (1973) Absolute isotopic abundance ratio and atomic weight of a reference sample of rhenium. Journal of Research of the National Bureau of Standards, 77A, 691–698.

Grasby, S.E., Sanei, H., Beauchamp, B., and Chen, Z. (2013) Mercury deposition through the Permo-Triassic Biotic Crisis. Chemical Geology, 351, 209–216.

Gratz, L.E., Keeler, G.J., Blum, J.D., Sherman, L.S. (2010) Isotopic composition and fractionation of mercury in Great Lakes precipitation and ambient air. Environmental Science and Technology, 44, 7764–7770.

Gumsley, A.P., Chamberlain, K.R., Bleeker, W., Söderlund, U., De Kock, M.O., Larsson, E.R., Bekker, A. (2017) Timing and tempo of the Great Oxidation Event. Proceedings of the National Academy of Science, 114, 1811–1816.

Hayes, R.A. (1993) Soil Survey of Powell and Wolfe Counties, Kentucky. US Department of Agriculture, Soil Conservation Service.

Helz, G. R. (2022) The Re/Mo redox proxy reconsidered. Geochimica et Cosmochimica Acta, 317, 507–522.

Helz, G.R. and Dolor, M.K. (2012) What regulates rhenium deposition in euxinic basins? Chemical Geology, 305, 131–141.

Hoefs, J. (1997) Stable isotope geochemistry. Book (4th edition). Berlin: Springer Verlag.

Holmes, P., James, K.A.F., Levy, L.S. (2009) Is low-level environmental mercury exposure of concern to human health? Science of the Total Environment, 408, 171–182.

Huang, Q., Liu, Y., Chen, J., Feng, X., Huang, W., Yuan, S., Cai, G., and Fu, X. (2015) An improved dual-stage protocol to pre-concentrate mercury from airborne particles for precise isotopic measurement. Journal of Analytical and Atomic Spectrometry, 30, 957–966.

IAEA-TEC-DOC-328 (1985) Geological Environments of Sandstone-type Uranium Deposits. Technical document issued by the International Atomic Energy Agency, Vienna.

Irisawa, K. and Hirata, T. (2006) Tungsten isotopic analysis on six geochemical reference materials using multiple collector-ICP-mass spectrometry coupled with a rhenium-external correction technique. Journal of Analytical Atomic Spectrometry, 21, 1387–1395.

Ishikawa, A., Senda, R., Suzuki, K., Dale, C.W., Meisel, T. (2014) Re-evaluating digestion methods for highly siderophile element and 187Os isotope analysis: Evidence from geological reference materials. Chemical Geology, 384, 27–46.

Jaffe, L.A., Peucker-Ehrenbrink, B., Petsch, S.T. (2002) Mobility of rhenium, platinum group elements, and organic carbon during black shale weathering. Earth and Planetary Science Letters, 198, 339–353.

Jin, S., Kemp, D.B., Yin, R., Sun, R., Shen, J., Jolley D.W., Vieira, M., Huang, C. (2023) Mercury isotope evidence for protracted North Atlantic magmatism during the Paleocene-Eocene Thermal Maximum. Earth and Planetary Science Letters, 602, 117926.

Jiskra, M., Wiederhold, J.G., Bourdon, B., Kretzschmar, R. (2012) Solution speciation controls mercury isotope fractionation of Hg(II) sorption to goethite. Environmental Science and Technology, 46, 6654–6662.

Jiskra, M., Wiederhold, J.G., Skyllberg, U., Kronberg, R.-M., Hajdas, I., Kretzschmar, R. (2015) Mercury Deposition and Re-emission Pathways in Boreal Forest Soils Investigated with Hg Isotope Signatures. Environmental Science and Technology, 49, 7188–7196.

Johnson, A.C., Romaniello, S.J., Reinhard, C.T., Gregory, D.D., Garcia-Robledo, E., Revsbech, N.P., Canfield, D.E., Lyons, T.W., Anbar, A.D. (2019) Experimental determination of pyrite and molybdenite oxidation kinetics at nanomolar oxygen concentrations. Geochimica et Cosmochimica Acta, 249, 160–172.

Kane, J.S., Arbogast, B.F., Leventhal, J.S. (1990) Characterization of Devonian Ohio Shale SDO-1 as a USGS geochemical reference sample: Geostandards Newsletter, 14, 169–196.

Kaufman, A.J., Johnston, D.T., Farquhar, J., Masterson, A.L., Lyons, T.W., Bates, S., Anbar, A.D., Arnold, G.L., Garvin, J., Buick, R. (2007) Late Archean biospheric oxygenation and atmospheric evolution. Science, 317, 1900–1903.

Kendall, B., Brennecka, G.A., Weyer, S., Anbar, A.D. (2013) Uranium isotope fractionation suggests oxidative uranium mobilization at 2.50 Ga. Chemical Geology, 362, 105–114.

Kendall, B., Creaser, R.A., Reinhard, C.T., Lyons, T.W., Anbar, A.D. (2015) Transient episodes of mild environmental oxygenation and oxidative continental weathering during the late Archean. Science Advances, 1, 1–10.

Kendall, B., Dahl, T.W., Anbar, A.D. (2017) The stable isotope geochemistry of molybdenum. Reviews in Mineralogy and Geochemistry, 82, 683–732.

Kendall, B., Creaser, R.A., Selby, D. (2006) Re-Os geochronology of postglacial black shales in Australia: Constraints on the timing of "Sturtian" glaciation. Geology, 34, 729–732.

Kendall, B., Reinhard, C.T., Lyons, T.W., Kaufman, A.J., Poulton, S.W., Anbar, A.D. (2010) Pervasive oxygenation along late Archaean ocean margins. Nature Geoscience, 3, 647–652.

Koide, M., Hodge, V.F., Yang, J.S., Stallard, M., Goldberg, E.G., Calhoun, J., Bertine, K.K. (1986) Some comparative marine chemistries of rhenium, gold, silver and molybdenum. Applied Geochemistry, 1, 705–714.

Korzhinsky, M.A., Tkachenko, S.I., Shmulovich, K.I., Taran, Y.A., Steinberg, G.S. (1994) Discovery of a pure rhenium mineral at Kudriavy volcano. Nature, 369, 51–52.

Krajkó, J., Varga, Z., Yalcintas, E., Wallenius, M., Mayer, K. (2014) Application of neodymium isotope ratio measurements for the origin assessment of uranium ore concentrates. Talanta, 129, 499–504.

Krapež , B., Barley, M.E., Pickard, A.L. (2003) Hydrothermal and resedimented origins of the precursor sediments to banded iron formation: sedimentological evidence from the Early Palaeoproterozoic Brockman Supersequence of Western Australia: Resedimented origins of banded iron formation. Sedimentology. 50, 979–1011.

Kristo, M.J., Gaffney, A.M., Marks, N.E., Knight, K., Cassata, W.S., Hutcheon, I.D. (2016) Nuclear forensic science: analysis of nuclear material out of regulatory control. Annual Review of Earth and Planetary Science, 44, 555–579.

Kritee, K., Barkay, T., Blum, J.D. (2009) Mass dependent stable isotope fractionation of mercury during *mer* mediated microbial degradation of monomethylmercury. Geochimica et Cosmochimica Acta, 73, 1285–1296.

Kritee, K., Blum, J.D., Johnson, M.W., Bergquist, B.A., Barkay, T. (2007) Mercury Stable Isotope Fractionation during Reduction of Hg(II) to Hg(0) by Mercury Resistant Microorganisms. Environmental Science and Technology, 41, 1889–1895.

Lamborg, C.H., Fitzgerald, W.F., Damman, A.W.H., Benoit, J.M., Balcom, P.H., Engstrom D.R. (2002) Modern and historic atmospheric mercury fluxes in both hemispheres: Global and regional mercury cycling implications: Modern and historic fluxes of atmospheric mercury. Global Biogeochemical Cycles, 16, 51-1–51–11.

Lassiter, J.C. (2003) Rhenium volatility in subaerial lavas: constraints from subaerial and submarine portions of the HSDP-2 Mauna Kea drillcore. Earth and Planetary Science Letters, 214, 311–325.

Li, Y., Shao, L., Fielding, C.R., Frank, T.D., Wang, D., Mu, G., Lu, J. (2023) The chemical index of alteration in Permo-Carboniferous strata in North China as an indicator of environmental and climate change throughout the late Paleozoic Ice Age. Global and Planetary Change, 221, 104035.

Liu, R., Hu, L., Humayun, M. (2017) Natural variations in the rhenium isotopic composition of meteorites. Meteoritics and Planetary Science, 52, 479–492.

Liu, H., Shao, J., Yu, B., Liang, Y., Duo, B., Fu, J., Yang, R., Shi, J. Jiang, G. (2019) Mercury isotopic compositions of mosses, conifer needles, and surface soils: Implications for mercury distribution and sources in Shergyla Mountain, Tibetan Plateau. Ecotoxicology and Environmental Safety, 172, 225–231.

Lockwood, R. and Chen, K.Y. (1973) Adsorption of mercury(II) by hydrous manganese oxides. Environmental Science and Technology, 7, 1028–1034.

Lodders, K. (2003) Solar system abundances and condensation temperatures of the elements. The Astrophysical Journal, 591, 1220–1247.

Loukola-Ruskeeniemi, K., Kantola, M., Halonen, T., Seppanen, K., Henttonen, P., Kallio, E., Kurki, P., Savolainen, H. (2002) Mercury-bearing black shales and human Hg instake in eastern Finland: impact and mechanisms. Environmental Geology, 43, 283–297.

Lowenstein, T.K., Kendall, B., Anbar, A.D. (2013) The geologic history of seawater. In Treatise on Geochemistry: Second Edition, 8, 569–622.

Luo, G., Ono, S., Beukes, N.J., Wang, D.T., Xie, S., Summons, R.E. (2016). Rapid oxygenation of Earth's atmosphere 2.33 billion years ago. Science Advances, 2(5), e1600134.

Lyons, T.W., Reinhard, C.T., Planavsky, N.J. (2014) The rise of oxygen in Earth's early ocean and atmosphere. Nature, 506, 307–315.

Markey, R., Stein, H.J., Hannah, J.L., Zimmerman, A., Selby, D., Creaser, R.A. (2007) Standardizing Re–Os geochronology: A new molybdenite Reference Material (Henderson, USA) and the stoichiometry of Os salts. Chemical Geology, 244, 74–87.

Mason, R.P., Choi, A.L., Fitzgerald, W.F., Hammerschmidt, C.R., Lamborg, C.H., Soerensen, A.L., Sunderland, E.M. (2012) Mercury biogeochemical cycling in the ocean and policy implications. Environmental Research, 119, 101–117.

Mason, R.P., Fitzgerald, W.F., Morel, F.M.M. (1994) The biogeochemical cycling of elemental mercury: Anthropogenic influences. Geochimica et Cosmochimica Acta, 58, 3191–3198.

Mason, R.P. and Sheu, G.-R. (2002) Role of the ocean in the global mercury cycle. Global Biogeochemical Cycles, 16, 1–14.

Meisel, T. and Moser, J. (2004) Platinum-Group Element and Rhenium Concentrations in Low Abundance Reference Materials. Geostandards abd Geoanalytical Research, 28, 233–250.

Meixnerová, J., Blum, J.D., Johnson, M.W., Stüeken, E.E., Kipp, M.A., Anbar, A.D., and Buick, R. (2021) Mercury abundance and isotopic composition indicate subaerial volcanism prior to the end-Archean "whiff" of oxygen. Proceedings of the National Academy of Sciences, 118, 1–6.

Migeon, V., Fiteoussi, C., Pili, E., Bourdon, B. (2020) Molybdenum isotope fractionation in uranium oxides and during key processes of the nuclear fuel cycle: Towards a new nuclear forensic tool. Geochimica et Cosmochimica Acta, 279, 238–257.

Miller, C.A., Peucker-Ehrenbrink, B., Ball, L. (2009) Precise determination of rhenium isotope composition by multi-collector inductively-coupled plasma mass spectrometry. Journal of Analytical Atomic Spectrometry, 24, 1069–1078.

Miller, C.A., Peucker-Ehrenbrink, B., Schauble, E.A. (2015) Theoretical modeling of rhenium isotope fractionation, natural variations across a black shale weathering profile, and potential as a paleoredox proxy. Earth and Planetary Science letters, 430, 339–348.

Miller, C.A., Peucker-Ehrenbrink, B., Walker, B.D., Marcantonio, F. (2011) Re-assessing the surface cycling of molybdenum and rhenium. Geochimica et Cosmochimica Acta, 75, 7146–7179.

Morford, J.L., Emerson, S.R., Breckel, E.J., Kim, S.H. (2005) Diagenesis of oxyanions (V, U, Re, and Mo) in pore waters and sediments from a continental margin. Geochimica et Cosmochimica Acta, 69, 5021–5032.

Morford, J.L., Martin, W.R., Carney, C.M. (2012) Rhenium geochemical cycling: Insights from continental margins. Chemical Geology, 325, 73–86.

Motta, L.C., Chien, A.D., Rask, A.E., Zimmerman, P.M. (2020) Mercury Magnetic Isotope Effect: A Plausible Photochemical Mechanism. Journal of Physical Chemistry A, 124, 3711–3719.

Nesbitt, H.W. and Young, G.M. (1982) Early Proterozoic climates and plate motions inferred from major element chemistry of lutites. Nature, 299, 715–717.

Neubert, N., Nagler, T.F., Bottcher, M.E. (2008) Sulfidity controls molybdenum isotope fractionation into euxinic sediments: Evidence form the modern Black Sea. Geology, 35, 775–778.

Noddack, W., Tacke, I., Berg, O. (1925) Zwei neue Elemente der Mangangruppe. Sitzung der physikalisch-mathematischen Klasse, 11, 400–409.

Norman, M.D., Garcia, M.O., Bennett, V.C. (2004) Rhenium and chalcophile elements in basaltic glasses from Ko'olau and Moloka'I volcanoes: Magmatic outgassing and composition of the Hawaiian plume. Geochimica et Cosmochimica Acta, 68, 3761–3777.

Novo, L.A.B., Mahler, C.F., González, L. (2015) Plants to harvest rhenium: scientific and economic viability. Environmental Chemistry Letters, 13, 439–445.

Nriagu, J. and Becker, C. (2003) Volcanic emissions of mercury to the atmosphere: Global and regional inventories. Science of the Total Environment, 304, 3–12.

Obrist, D., Agnan, Y., Jiskra, M., Olson, C.L., Colegrove, D.P., Hueber, J., Moore, C.W., Sonke, J.E., Helmig, D. (2017) Tundra uptake of atmospheric elemental mercury drives Arctic mercury pollution. Nature, 547, 201–204.

Ogrič, M., Dellinger, M., Grant, K.E., Galy, V., Gu, X., Brantley, S.L., Hilton, R.G. (2023) Low rates of rock organic carbon oxidation and anthropogenic cycling of rhenium in a slowly denuding landscape. Earth Surface Processes and Landforms, 48, 1202–1218.

Olson, C.L., Jiskra, M., Sonke, J.E., Obrist, D. (2019) Mercury in tundra vegetation of Alaska: Spatial and temporal dynamics and stable isotope patterns. Science of the Total Environment, 660, 1502–1512.

Oró, J., Miller, S.L., Lazcano, A. (1990) The origin and early evolution of life on earth. Annual Review of Earth and Planetary Science, 18, 317–356.

Ostrander, C.M. (2020) Refining Earth's Ocean Oxygenation History using Molybdenum and Thallium Isotopes. Dissertation. Arizona State University. 1–275.

Ostrander C.M., Johnson A.C., Anbar A.D. (2021) Earth's First Redox Revolution. Annual Reviews in Earth and Planetary Science, 49, 337–366.

Ostrander, C.M., Nielsen, S.G., Owens, J.D., Kendall, B., Gordon, G. W., Romaniello, S.J., Anbar A.D. (2019) Fully oxygenated water columns over continental shelves before the Great Oxidation Event. Nature Geoscience, 12, 186–191.

Ostrander, C.M., Severmann, S., Gordon, G.W., Kendall, B., Lyons, T.W., Zheng, W., Roy, M., Anbar A.D. (2022) Significance of ^{56}Fe depletions in late-Archean shales and pyrite. Geochimica et Cosmochimica Acta, 316, 87–104.

Park J., Stein H.J., Georgiev S.V., Hannah J.L. (2022) Degradation of Hg signals on incipient weathering: Core versus outcrop geochemistry of Upper Permian shales, East Greenland and Mid-Norwegian Shelf. Chemical Geology, 608, 121030.

Peel, K., Weiss, D., Chapman, J., Arnold, T., Coles, B. (2008) A simple combined sample–standard bracketing and inter-element correction procedure for accurate mass bias correction and precise Zn and Cu isotope ratio measurements. Journal of Analytical Spectrometry, 23, 103–110.

Percival, L.M.E., Ruhl, M., Hesselbo, S.P., Jenkyns, H.C., Mather, T.A., Whiteside, J.H. (2017) Mercury evidence for pulsed volcanism during the end-Triassic mass extinction. Proceedings of the National Academy of Sciences, 114, 7929–7934.

Petsch, S.T., Berner, R.A., Eglinton, T.I. (2000) A field study of the chemical weathering of ancient sedimentary organic matter. Organic Geochemistry, 31, 457–475.

Petsch, S.T., Eglinton, T.I., Edwards, K.J. (2001a) ^{14}C-Dead Living Biomass: Evidence for Microbial Assimilation of Ancient Organic Carbon During Shale Weathering. Science, 292, 1127–1131.

Petsch, S.T., Smernik, R.J., Eglinton, T.I., Oades, J.M. (2001b) A solid state ^{13}C-NMR study of kerogen degradation during black shale weathering. Geochimica et Cosmochimica Acta, 65, 1867–1882.

Peucker-Ehrenbrink, B. and Ravizza, G. (2000) The marine osmium isotope record. Terra Nova, 12, 205−219.

Philippot, P., Ávila, J.N., Killingsworth, B.A., Tessalina, S., Baton, F., Caquineau, T., Muller, E., Pecoits, E., Cartigny, P., Lalonde, S.V., Ireland, T.R., Thomazo, C., Van Kranendonk, M.J., Busigny, V. (2018) Globally asynchronous sulphur isotope signals require re-definition of the Great Oxidation Event. Nature Communications, 9, 2245.

Pitcher, L., Helz, R.T., Walker, R.J., Piccoli, P. (2009) Fractionation of the platinum-group elements and Re during crystallization of basalt in Kilauea Iki Lava Lake, Hawaii. Chemical Geology, 260, 196–210.

Pourmand, A. and Dauphas, N. (2010) Distribution coefficients of 60 elements on TODGA resin: Application to Ca, Lu, Hf, U, and Th isotope geochemistry. Talanta, 81, 741–753.

Rasmussen, B., Blake, T.S., Fletcher, I.R. (2005) U–Pb zircon age constraints on the Hamersley spherule beds: evidence for a single 2.63 Ga Jeerinah–Carawine impact ejecta layer. Geology, 33(9), 725–728.

Reading, D.G. (2016) Nuclear forensics: determining the origin of uranium ores and uranium ore concentrates via radiological, elemental and isotopic signatures. Doctoral Thesis, University of Southampton, Ocean and Earth Science, 1–247.

Reinhard, C.T., Raiswell, R., Scott, C., Anbar, A.D., and Lyons, T.W. (2009) A Late Archean Sulfidic Sea Stimulated by Early Oxidative Weathering of the Continents. Science, 326, 713–716.

Richardson, J.B., Aguirre, A.A., Buss, H.L., O'Geen, A.T., Gu, X., Rempe, D.M., Richter, D.B. (2018) Mercury Sourcing and Sequestration in Weathering Profiles at Six Critical Zone Observatories. Global Biogeochemical Cycles, 32, 1542–1555.

Rodríguez-González, P., Epov, V.N., Bridou, R., Tessier, E., Guyoneaud R., Monperrus., Amouroux, D. (2009) Species-Specific Stable Isotope Fractionation of Mercury during Hg(II) Methylation by an Anaerobic Bacteria (Desulfobulbus propionicus) under Dark Conditions. Environmental Science and Technology, 43, 9183–9188.

Rolison, J.M., Druce, M., Shollenberger, Q.R., Kayzar-Boggs, T.M., Lindvall, R.E., Wimpenny, J. (2019) Molybdenum isotope composition of uranium ore concentrates by double spike MC-ICP–MS. Applied Geochemistry, 103, 97–105.

Rolison, J.M., Stirling, C.H., Middag, R., Rijkenberg, M.J.A. (2017) Uranium stable isotope fractionation in the Black Sea: Modern calibration of the $^{238}U/^{235}U$ paleo-redox proxy. Geochimica et Cosmochimica Acta, 203, 69–88.

Romaniello, S.J., Field, M.P., Smith, H.B., Gordon, G.W., Kim, M.H., Anbar, A.D. (2015) Fully automated chromatographic purification of Sr and Ca for isotopic analysis. Journal of Anaytical and Atomic Spectrometry, 30, 1906–1912.

Rooney, A.D., Macdonald, F.A., Strauss, J.V., Dudas, F.Ö., Hallmann, C., Selby, D. (2014) Re-Os geochronology and coupled Os-Sr isotope constraints on the Sturtian snowball Earth. Proceedings of the National Academy of Sciences, 111, 51−56.

Rudnick, R.L. and Gao, S. (2003) Composition of the Continental Crust. Treatise on Geochemistry, 3, 1−64.

Russell, W.A., Papanastassiou, D.A., Tombrello, T.A. (1978) Ca isotope fractionation on the Earth and other solar system materials. Geochimica et Cosmochimica Acta, 42, 1075–1090.

Sanei, H., Grasby, S., Beauchamp, B. (2012). Latest Permian mercury anomalies. Geology, 40, 63–66.

Scaife, J.D., Ruhl, M., Dickson, A.J., Mather, T.A., Jenkyns, H.C., Percival, L.M.E., Hesselbo, S.P., Cartwright, J., Eldrett, J.S., Bergman, S.C., Minisini, D. (2017) Sedimentary Mercury Enrichments as a Marker for Submarine Large Igneous Province Volcanism? Evidence From the Mid-Cenomanian Event and Oceanic Anoxic Event 2 (Late Cretaceous). Geochemistry, Geophysics, Geosystems, 18, 4253–4275.

Schauble, E.A. (2007) Role of nuclear volume in driving equilibrium stable isotope fractionation of mercury, thallium, and other very heavy elements. Geochimica et Cosmochimica Acta, 71, 2170–2189.

Schroeder, W.H. and Munthe, J. (1998) Atmospheric mercury—an overview. Atmospheric Environment, 32, 809–822.

Selby, D., Creaser, R.A., Stein, H.J., Markey, R.J., Hannah, J.L. (2007) Assessment of the ^{187}Re decay constant by cross calibration of Re–Os molybdenite and U–Pb zircon chronometers in magmatic ore systems. Geochimica et Cosmochimica Acta, 71, 1999–2013.

Selin, N.E. (2009) Global Biogeochemical Cycling of Mercury: A Review. Annual Review of Environmental and Resources, 34, 43–63.

Selin, N.E., Jacob, D.J., Yantosca, R.M., Strode, S., Jaeglé, L., Sunderland, E.M. (2008) Global 3-D land-ocean-atmosphere model for mercury: Present-day versus preindustrial cycles and anthropogenic enrichment factors for deposition. Global Biogeochemical Cycles, 22, 1–13.

Sheen, A.I., Kendall, B., Reinhard, C.T., Creaser, R.A., Lyons, T.W., Bekker, A., Poulton, S.W., Anbar, A.D. (2018) A model for the oceanic mass balance of rhenium and implications for the extent of Proterozoic ocean anoxia. Geochimica et Cosmochimica Acta, 227, 75–95.

Shollenberger, Q.R., Borg, L.E., Ramon, E.C., Sharp, M.A., Brennecka, G.A. (2021) Samarium isotope compositions of uranium ore concentrates: A novel nuclear forensic signature. Talanta, 221, 121431.

Sial, A.N., Chen, J., Lacerda, L.D., Frei, R., Tewari, V.C., Pandit, M.K., Gaucher, C., Ferreira, V.P., Cirilli, S., Peralta, S., Korte, C., Barbosa, J.A., Pereira, N.S. (2016). Mercury enrichment and Hg isotopes in Cretaceous-Paleogene boundary successions: Links to volcanism and palaeoenvironmental impacts. Cretaceous Research, 66, 60–81.

Skyllberg, U., Xia, K., Bloom, P.R., Nater, E.A., Bleam, W.F. (2000) Binding of mercury (II) to reduced sulfur in soil organic matter along upland-peat soil transects. Journal of Environmental Quality, 29(3), 855–865.

Slotznick, S.P., Johnson, J.E., Rasmussen, B., Raub, T.D., Webb, S.M., Zi, J.-W., Kirschvink, J.L., Fischer, W.W. (2022) Reexamination of 2.5-Ga "whiff" of oxygen interval points to anoxic ocean before GOE. Science Advances, 8, 1–10.

Smoliar, M.I., Walker, R.J., Morgan, J.W. (1996) Re-Os Ages of Group IIA, IIIA, IVA, and IVB Iron Meteorites. Science, 271, 1099–1102.

Stirling, C.H., Anderson, M.B., Potter, E.-K., Halliday, A. (2007) Low-temperature isotopic fractionation of uranium. Earth and Planetary Science Letters, 264, 208–225.

Stolper, D.A., Revsbech, N.,P., Canfield, D.E. (2010) Aerobic growth at nanomolar oxygen concentrations. Proceedings of the National Academy of Science, 107, 18755–18760.

Streets, D.G., Horowitz, H.M., Jacob, D.J., Lu, Z., Levin, L., ter Schure, A.F.H., Sunderland, E.M. (2017) Total mercury released to the environment by human activities. Environmental Science and Technology, 51, 5969–5977.

Stüeken, E.E., Buick, R., Anbar, A.D. (2015) Selenium isotopes support free O2 in the latest Archean. Geology, 43, 259–262.

Sullivan, D.L., Brandon, A.D., Eldrett, J., Bergman, S.C., Wright, S., Minisini, D. (2020) High resolution osmium data record three distinct pulses of magmatic activity

during cretaceous Oceanic Anoxic Event 2 (OAE-2). Geochimica et Cosmochimica Acta, 285, 257–273.

Sun, W., Bennett, V.C., Eggins, S.M., Kamenetsky, V.S., Arculus, R.J. (2003) Enhanced mantle-to-crust rhenium transfer in undegassed arc magmas. Nature, 422, 294–297.

Sun, R., Liu, Y., Sonke, J.E., Feifei, Z., Zhao, Y., Zhang, Y., Chen, J., Liu, C.-Q., Shen, S., Anbar, A.D., Zheng, W. (2023) Mercury isotope evidence for marine photic zone euxinia across the end-Permian mass extinction. Communications Earth and Environment, 4, 1–11.

Sunderland, E.M. (2007) Mercury exposure from domestic and imported estuarine and marine fish in the U.S. seafood market. Environmental Health Perspectives, 115, 235–242.

Sunderland, E.M. and Mason, R.P. (2007) Human impacts on open ocean mercury concentrations. Global Biogeochemical Cycles, 21, 1–15.

Szponar, N., Su, Y., Stupple, G., McLagan, D.S., Pilote, M., Munoz, A., Mitchell, C.P.J., Steffen, A., Wania, F., Bergquist, B.A. (2023) Applying Passive Air Sampling and Isotopic Characterization to Assess Spatial Variability of Gaseous Elemental Mercury Across Ontario, Canada. Journal of Geophysical Research Atmospheres, 128, 1–19.

Teng, F-Z., Dauphas, N., Watking, J.M. (2017) Non-Traditional Stable Isotopes: Retrospective and Prospective. Reviews in Mineralogy & Geochemistry book, 82, 1–26.

Tessalina. S.G., Yudovskaya. M.A., Chaplygin. I.V., Birck. J.L., Capmas. F. (2008) Sources of unique rhenium enrichment in fumaroles and sulphides at Kudryavy volcano. Geochimica et Cosmochimica Acta, 72, 889–909.

Thibodeau, A.T., Ritterbush, K., Yager, J.A., West, A.J., Ibarra, Y., Bottjer, D.J., Berelson, W. M., Bergquist, B. A., and Corsetti, F. A. (2016) Mercury anomalies and the timing of biotic recovery following the end-Triassic mass extinction. Nature Comm., 7, 1-8.

Trendall, A.F., Compston, W., Nelson, D.R., De Laeter, J.R., Bennett, V.C. (2004) SHRIMP zircon ages constraining the depositional chronology of the Hamersley Group, Western Australia*. Australian Journal of Earth Science, 51, 621–644.

Tsui, M.T.K., Blum, J.D., Kwon, S.Y., Finlay, J.C., Balogh, S.J., Nollet, Y.H. (2012) Sources and Transfers of Methylmercury in Adjacent River and Forest Food Webs. Environmental Science and Technology, 46, 10957–10964.

Tuttle, M.L.W., Breit, G.N., Goldhaber, M.B. (2009) Weathering of the New Albany Shale, Kentucky: II. Redistribution of minor and trace elements. Applied Geochemistry, 24, 1565–1578.

Tzvetkova, C., Novo, L.A.B., Atanasova-Vladimirova, S., Vassiliv, T. (2021) On the uptake of rhenium by plants: Accumulation and recovery from plant tissue. Journal of Cleaner Production, 328, 129534.

Urey, H.C. (1947) The Thermodynamic Properties of Isotopic Substances, Liverside lecture, delivered before the Chemical Society in the Royal Institution on December 18th, 1946. Journal of the Chemical Society (Resumed), 562–581.

U.S. Geological Survey (USGS) (2021) Mineral commodity summaries 2021: U.S. Geological Survey, 200 p., doi.org/10.3133/mcs2021.

Van Kranendonk M.J. (2010) Two types of Archean continental crust: Plume and plate tectonics on early Earth. American Journal of Science, 310, 1187–1209.

Varga, Z., Krajkó, J., Peńkin, M., Novák, M., Eke, Z., Wallenius, M., Mayer, K. (2017) Identification of uranium signatures relevant for nuclear safeguards and forensics. Journal of Radioanalytical and Nuclear Chemistry, 312, 639–654.

Varga, Z., Nicholl, A., Wallenius, M., Mayer, K., Mock, T. (2023) Propagation and variation of material characteristics during the uranium ore concentrate production at Dolní Rožinka, Czech Republic. Journal of Radioanalytical and Nuclear Chemistry, 332, 2863–2873.

Varga, Z., Wallenius, M., Mayer, K., Keegan, E., Millet, S. (2009) Application of Lead and Strontium Isotope Ratio Measurements for the Origin Assessment of Uranium Ore Concentrates. Analytical Chemistry, 81, 8327–8334.

Von Pechmann, E. (1986) Mineralogy, age dating, and genesis of the kylie and spring creek uranium prospects, waterhouse complex, Mineral Paragenesis, Theophrastus Publications S.A., Athens, 303–343.

Weyer, S., Anbar, A.D., Gerdes, A., Gordon, G.W., Algeo, T.J., Boyle, E.A. (2008) Natural fractionation of $^{238}U/^{235}U$. Geochimica et Cosmochimica Acta, 72, 345–359.

Wiederhold, J., Cramer, C., Daniel, K., Infante, I., Bourdon, B., Kretzschmar, R. (2010) Equilibrium mercury isotope fractionation between dissolved Hg(II) species and thiol-bound Hg. Environmental Science and Technology, 44, 4191–4197.

Woerndle G., Tsz-Ki, T., Sebestyen, S., Blum, J., Nie, X., Kolka, R. (2018) New Insights on Ecosystem Mercury Cycling Revealed by Stable Isotopes of Mercury in Water Flowing from a Headwater Peatland Catchment. Environmental Science and Technology, 52, 1854–1861.

Wu, Y., Tian, H., Yin, R., Chen, D., Grasby, S. E., Shen, J., Li, T., Ji, S., Peng, P. (2023) Highly fractionated Hg isotope evidence for dynamic euxinia in shallow waters of the Mesoproterozoic ocean. Earth and Planetary Science Letters, 616, 118211.

Yamashita, Y., Takahashi, Y., Haba, H., Enomoto, S., Shimizu, H. (2007) Comparison of reductive accumulation of Re and Os in seawater-sediment systems. Geochimica et Cosmochimica Acta, 71, 3458–3475.

Yin, R., Krabbenhoft, D., Bergquist, B., Zheng, W., Lepak, R., Hurley, J. (2016) Effects of mercury and thallium concentrations on high precision determination of mercury isotopic composition by Neptune Plus multiple collector inductively coupled plasma mass spectrometry. Journal of Analytical and Atomic Spectrometry, 31, 2060–2068.

Yu, B., Fu, X., Yin, R., Zhang, H., Wang, X., Lin, C.-J., Wu, C., Zhang, Y., He, N., Fu, P., Wang, Z., Shang, L., Sommar, J., Sonke, J., Maurice L., Guinot B., Feng, X. (2016) Isotopic Composition of Atmospheric Mercury in China: New Evidence for Sources and Transformation Processes in Air and in Vegetation. Environmental Science and Technology, 50, 9262–9269.

Yuan, W., Liu, M., Chen, D., Xing, Y-W., Spicer, R. A., Chen, J., Them, T. R., Wang, X., Li, S., Guo, C., Zheng, G., Zhang, L., Zhang, H., Feng, X. (2023) Mercury isotopes show vacular plants had colonized land extensively by the early Silurian. Science Advances, 9, 1–10.

Yudovskaya, M., Tessalina, S., Distler, V., Chaplygin, I., Chugaev, A., Dikov Y. (2008) Behavior of highly-siderophile elements during magma degassing: A case study at the Kudryavy volcano. Chemical Geology, 248, 318–341.

Zambardi, T., Sonke, J. E., Toutain, J. P., Sortino, F., Shinohara, H. (2009) Mercury emissions and stable isotopic compositions at Vulcano Island (Italy). Earth and Planetary Science Letters, 277 (1–2), 236–243.

Zheng, W., Demers, J. D., Lu, X., Bergquist, B. A., Anbar, A. D., Blum, J. D., Gu, B. (2019) Mercury Stable Isotope Fractionation during Abiotic Dark Oxidation in the Presence of Thiols and Natural Organic Matter. Environmental Science and technology, 53, 1853–1862.

Zheng, W., Gilleaudeau, G. J., Algeo, T.J., Zhao, Y., Song, Y., Zhang, Y., Sahoo, S. K., Anbar, A. D., Carmichael, S. K., Xie, S., Liu, C-Q., Chen, J. (2023) Mercury

isotope evidence for recurrent photic-zone euxinia triggered by enhanced terrestrial nutrient inputs during the Late Devonian mass extinction. Earth and Planetary Science Letters, 613, 118175.

Zheng, W., Gilleaudeau, G. J., Kah, L.C., Anbar, A. D. (2018) Mercury isotope signatures record photic zone euxinia in the Mesoproterozoic ocean. Proceedings of the National Academy of Sciences, 115, 10594−10599.

Zheng, W., Obrist, D., Weis, D., Bergquist, B. A. (2016) Mercury isotope compositions across North American forests: Mercury Isotopes Across U.S. Forests. Global Biogeochemical Cycles, 30, 1475–1492.

Zheng, W., Xie, Z., Bergquist, B. A. (2015) Mercury Stable Isotopes in Ornithogenic Deposits As Tracers of Historical Cycling of Mercury in Ross Sea, Antarctica. Environmental Science and Technology, 49, 7623 – 7632.

Zhou, J., Obrist, D., Dastoor, A., Jiskra, M., Ryjkov, A. (2021) Vegetation uptake of mercury and impacts on global cycling. Nature Reviews in Earth and Environment, 2, 269–284.

APPENDIX A

CO-AUTHOR PERMISSION TO USE THE WORKS IN PREPARATION

All co-authors for each chapter have granted permission to use works in preparation for this dissertation.